Proton-antiproton annihilation and meson spectroscopy with the Crystal Barrel

Claude Amsler

Physik-Institut der Universität Zürich, CH-8057 Zürich, Switzerland

This report reviews the achievements of the Crystal Barrel experiment at the Low-Energy Antiproton Ring (LEAR) at CERN. During seven years of operation Crystal Barrel has collected very large statistical samples in $\bar{p}p$ annihilation, especially at rest and with emphasis on final states with high neutral multiplicity. The measured rates for annihilation into various two-body channels and for electromagnetic processes have been used to test simple models for the annihilation mechanism based on the internal quark structure of hadrons. The production of ϕ mesons is larger than predicted in several annihilation channels. Important contributions to the spectroscopy of light mesons have been made. The exotic $\hat{\rho}(1405)$ meson with quantum numbers $J^{PC}=1^{-+}$ has been observed in its $\eta\pi$ decay mode. Two 2^{-+} isoscalar mesons $\eta_2(1645)$ and $\eta_2(1870)$, and the 0^{-+} isoscalar meson $\eta(1410)$ have been observed in the $\eta\pi\pi$ decay channel. From three-body annihilations three 0^{++} mesons, $a_0(1450)$, $f_0(1370)$, and $f_0(1500)$ have been established in various decay modes. One of them, $f_0(1500)$, may be identified with the expected ground-state scalar glueball. [S0034-6861(98)00404-8]

CONTENTS

I.	Introduction	1293
II.	Proton-Antiproton Annihilation at Rest; S and P Waves	1294
III.	The Crystal Barrel Experiment	1296
	A. Detector	1296
	B. Photon reconstruction	1297
	C. Available data	1298
IV.	Annihilation into Two Mesons	1298
	A. Annihilation into two neutral mesons	1299
	B. Test of the quark line rule	1300
V.	Electromagnetic Processes	1303
	A. Radiative annihilation	1303
	B. Radiative ω decays	1304
	C. $\eta'\rightarrow\pi^+\pi^-\gamma$	1306
	D. Search for light gauge bosons in pseudoscalar meson decays	1306
	E. $\eta\rightarrow 3\pi$	1307
VI.	Production of ϕ Mesons	1308
	A. Annihilation into $\pi^0\phi$, $\eta\phi$, and $\gamma\phi$	1308
	B. ϕ/ω ratio	1309
VII.	Meson Spectroscopy	1311
	A. Introduction	1311
	B. Spin-parity analysis	1312
	C. K-matrix analysis	1314
VIII.	Annihilation at Rest into Three Pseudoscalar Mesons	1316
	A. $\bar{p}p\rightarrow\pi^0\eta\eta$	1316
	B. $\bar{p}p\rightarrow\pi^0\pi^0\eta$	1318
	C. $\bar{p}p\rightarrow\pi^0\pi^0\pi^0$	1319
	D. Coupled-channel analysis	1321
	E. $\bar{p}p\rightarrow\pi^0\eta\eta'$	1322
	F. $\bar{p}p\rightarrow\pi^0\pi^0\eta'$	1322
	G. $\bar{p}p\rightarrow\pi^0K_LK_L$	1323
	H. $\bar{p}p\rightarrow\pi^{\pm}K^{\mp}K_L$	1324
	I. Summary	1326
IX.	Annihilation at Rest into Five Pions	1326
X.	The New Mesons	1327
	A. $a_0(1450)$	1327
	B. $f_0(1370)$ and $f_0(1500)$	1329
	C. $f_2(1565)$	1331
XI.	Search for Hybrids	1332
	A. $\hat{\rho}(1405)$	1332
	B. $\eta_2(1870)$	1333
XII.	E/ι Decay to $\eta\pi\pi$	1333
XIII.	Summary and Outlook	1335
	Acknowledgments	1336
	References	1337

I. INTRODUCTION

Low-energy antiproton-proton annihilation at rest is a valuable tool to investigate phenomena in the low-energy regime of quantum chromodynamics (QCD). Due to the absence of Pauli blocking, the antiproton and proton wave functions overlap, and one expects the interactions between constituent quarks and antiquarks (annihilation, pair creation, or rearrangement) to play an important role in the annihilation process. From bubble-chamber experiments performed in the sixties (Armenteros and French, 1969) one knows that annihilation proceeds through $q\bar{q}$ intermediate meson resonances. The $\omega(782)$, $f_1(1285)$, $E/\eta(1440)$, and $K_1(1270)$ mesons were discovered and numerous properties of other mesons [$a_0(980)$, $K^*(892)$, $\phi(1020)$, $a_2(1320)$] were studied in low-energy $\bar{p}p$ annihilation.[1] With the advent of QCD one now also predicts states made exclusively of gluons (glueballs), of a mixture of quarks and gluons (hybrids), and multiquark states, all of which can be produced in $\bar{p}p$ annihilation.

With the invention of stochastic cooling and the operation of the Low-Energy Antiproton Ring (LEAR) from 1983 to 1996, intense and pure accelerator beams of low-momentum antiprotons between 60 and 1940

[1]Throughout this review mesons are labeled with the names adopted in the 1996 issue of the Review of Particle Physics (Barnett, 1996).

MeV/s were available at CERN. It is impressive to compare the high flux of today's antiproton beams ($>10^6 \bar{p}/\mathrm{s}$) with the rate of about 1$\bar{p}$ every 15 minutes in the early work when the antiproton was discovered, back in 1955 (Chamberlain, 1955).

The author was asked by Reviews of Modern Physics to write a report on Crystal Barrel results. A general review on light-quark spectroscopy or a detailed survey of the $\bar{p}p$ annihilation mechanism are beyond the scope of this review and can be found elsewhere in the literature (Amsler and Myhrer, 1991; Dover *et al.*, 1992; Blüm, 1996; Landua, 1996). The topics emphasized in this review reflect the personal taste and scientific interest of the author. Some of the results on $\bar{p}d$ annihilation will not be reviewed here. They include the observation of the channels $\bar{p}d \to \pi^0 n, \eta n, \omega n$ (Amsler *et al.*, 1995a), and $\bar{p}d \to \Delta(1232)\pi^0$ (Amsler *et al.*, 1995b), which involve both nucleons in the annihilation process.

Alternative analyses of Crystal Barrel data have been performed by other groups or by individuals from within the collaboration. I shall not describe them in detail since they basically lead to the same results. However, small differences, e.g., in masses and widths of broad resonances, are reported. They can be traced to the use of a more flexible parametrization involving additional parameters (Bugg *et al.*, 1994), and, most importantly, to the inclusion of data from previous experiments studying different reactions like central collision or inelastic πp scattering (e.g., Abele *et al.*, 1996a, Bugg, Sarantsev, and Zou, 1996; Anisovich, Anisovich, and Sarantsev, 1997). In order not to confuse with foreign data and unknown biases the contributions that Crystal Barrel has made to spectroscopy, I shall only deal with experimental results published by the Crystal Barrel Collaboration or submitted for publication until 1997, but will provide a comparison with previous data, whenever appropriate.

The experiment started data taking in late 1989 and was completed in autumn 1996 with the closure of LEAR. The Crystal Barrel was designed to study low-energy $\bar{p}p$ annihilation with very high statistics, in particular annihilation into n charged particles (n-prong) and m neutrals (π^0, η, η' or ω) with $m \geq 2$, leading to final states with several photons. These annihilation channels occur with a probability of about 50% and had not been investigated previously. They are often simpler to analyze due to C-parity conservation, which limits the range of possible quantum numbers for the intermediate resonances and the $\bar{p}p$ initial states.

Most of the data analyzed were taken by stopping antiprotons in liquid hydrogen, on which I shall therefore concentrate. This article is organized as follows: After a brief reminder of the physical processes involved when antiprotons are stopped in liquid hydrogen (Sec. II), I shall describe in Sec. III the Crystal Barrel apparatus and its performance. The review then covers results relevant to the annihilation mechanism and the roles of quarks in the annihilation process (Sec. IV). Electromagnetic processes are covered in Sec. V. The observation of a strangeness enhancement may possibly be related to the presence of strange quarks in the nucleon (Sec. VI). After describing the mathematical tools for extracting masses and spins of intermediate resonances (Sec. VII), I shall review in Secs. VIII to X what is considered to be the main achievement, the discovery of several new mesons, in particular a scalar ($J^P = 0^+$) state around 1500 MeV, which is generally interpreted as the ground-state glueball. Section XI reports on the status of hybrid mesons. Section XII finally describes the status of pseudoscalar mesons in the 1400-MeV region.

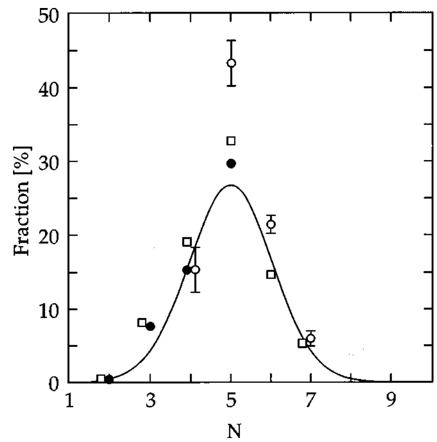

FIG. 1. Pion multiplicity distribution for $\bar{p}p$ annihilation at rest in liquid hydrogen: □, statistical distribution; ●, data; ○, estimates from Ghesquière (1974). The curve is a Gaussian fit assuming $\langle N \rangle = 5$.

II. PROTON-ANTIPROTON ANNIHILATION AT REST; S AND P WAVES

Earlier investigations of low-energy $\bar{p}p$ annihilation dealt mainly with final states involving charged mesons ($\pi^\pm, K^\pm$) or $K_S \to \pi^+\pi^-$, with at most one missing (undetected) π^0, due to the lack of a good γ detection facility [for reviews, see Armenteros and French (1969), Sedlák and Šimák (1988), and Amsler and Myhrer (1991)].

The average charged pion multiplicity is 3.0 ± 0.2 for annihilation at rest and the average π^0 multiplicity is 2.0 ± 0.2. The fraction of purely neutral annihilations (mainly from channels like $3\pi^0$, $5\pi^0$, $2\pi^0\eta$, and $4\pi^0\eta$ decaying to photons only) is $(3.9 \pm 0.3)\,\%$ (Amsler *et al.*, 1993a). This number is in good agreement with an earlier estimate from bubble chambers, $4.1^{+0.2}_{-0.6}\%$ (Ghesquière, 1974). In addition to pions, η mesons are produced with a rate of about 7% (Chiba *et al.*, 1987) and kaons with a rate of about 6% of all annihilations (Sedlák and Šimák, 1988).

In fireball models the pion multiplicity $N = N_+ + N_- + N_0$, where the subscripts stand for positive, negative, and neutral pions, respectively, follows a Gaussian distribution (Orfanidis and Rittenberg, 1973). The pion multiplicity distribution at rest in liquid hydrogen is shown in Fig. 1. Following the model of Pais (1960) one expects on statistical grounds the branching ratios to be distributed according to $1/(N_+!N_-!N_0!)$ for a given multiplicity N. The open squares show the predictions normalized to the measured branching ratios from channels with charged pions and $N_0 \leqslant 1$ (Armenteros and French, 1969). The full circles show the data from bubble chambers, together with Crystal Barrel results for $N_0 > 1$. The fit to the data (curve) leads to $\sigma = 1$ for a Gaussian distribution assuming $\langle N \rangle = 5$. The open circles show an estimate from bubble-chamber experiments, which appears to overestimate the contribution from $N=5$ (Ghesquière, 1974).

Stopping antiprotons in hydrogen are captured to form antiprotonic hydrogen atoms (protonium). The probability of forming a $\bar{p}p$ atom is highest for states with principal quantum number $n \sim 30$, corresponding to the binding energy (13.6 eV) of the K-shell electron ejected during the capture process. Two competing de-excitation mechanisms occur: (i) the cascade to lower levels by x-ray or external Auger emission of electrons from neighboring H_2 molecules and (ii) Stark mixing between the various angular momentum states due to collisions with neighboring H_2 molecules. Details on the cascade process can be found in Batty (1989). In liquid hydrogen, Stark mixing dominates (Day, Snow, and Sucher 1960) and the $\bar{p}p$ system annihilates with the angular momentum $\ell = 0$ from high S levels (S-wave annihilation) due to the absence of angular momentum barrier. The initial states are the spin-singlet $(s=0)\,^1S_0$ and the spin-triplet $(s=1)\,^3S_1$ levels with parity $P = (-1)^{\ell+1}$ and C-parity $C = (-1)^{\ell+s}$, hence with quantum numbers

$$J^{PC}(^1S_0) = 0^{-+} \quad \text{and} \quad J^{PC}(^3S_1) = 1^{--}. \tag{1}$$

The cascade, important in low-density hydrogen (e.g., in gas), populates mainly the $n=2$ level (2P) from which the $\bar{p}p$ atom annihilates due to its small size. The K_α transition from 2P to 1S has been observed at LEAR in gaseous hydrogen (Ahmad *et al.,* 1985; Baker *et al.*, 1988). Compared to annihilation, it is suppressed with a probability of $(98 \pm 1)\%$ at atmospheric pressure. Annihilation with relative angular momentum $\ell = 1$ (P-wave annihilation) can therefore be selected by detecting the L x-rays to the 2P levels, in coincidence with the annihilation products. This procedure permits the spectroscopy of intermediate meson resonances produced from the P states

$$J^{PC}(^1P_1) = 1^{+-}, \quad J^{PC}(^3P_0) = 0^{++},$$
$$J^{PC}(^3P_1) = 1^{++}, \quad J^{PC}(^3P_2) = 2^{++}. \tag{2}$$

Annihilation from P states has led to the discovery of the $f_2(1565)$ meson (May *et al.,* 1989).

The much reduced Stark mixing in low-density hydrogen also allows annihilation from higher P levels. At a target pressure of 1 bar, S and P waves each contribute about 50% to annihilation (Doser *et al.,* 1988). Annihilation from D waves is negligible due to the very small overlap of the p and $\bar{p}$ wave functions.

The assumption of S-wave dominance in liquid hydrogen is often a crucial ingredient in amplitude analysis when determining the spin and parity of an intermediate resonance in the annihilation process, since the quantum numbers of the initial state must be known. The precise fraction of P-wave annihilation in liquid has been the subject of a longstanding controversy. The reaction $\bar{p}p \to \pi^0\pi^0$ can only proceed through the P states 0^{++} or 2^{++} (see Sec. IV.A), while $\pi^+\pi^-$ also proceeds from S states (1^{--}). The annihilation rate $B(\pi^0\pi^0)$ for this channel in liquid was measured earlier by several groups but with inconsistent results (Devons *et al.,* 1971; Adiels *et al.,* 1987; Chiba *et al.,* 1988; see also Chiba *et al.,* 1989).

Crystal Barrel determined the branching ratio for $\bar{p}p \to \pi^0\pi^0$ in liquid by measuring the angles and energies of the four decay photons (Amsler *et al.*, 1992a). The main difficulties in selecting this channel are annihilation into $3\pi^0$, which occurs with a much higher rate and, most importantly, P-wave annihilation in flight. The former background source could be reduced with the good γ-detection efficiency and large solid angle of Crystal Barrel, while the latter could be eliminated thanks to the very narrow stop distribution from cooled low-energy antiprotons from LEAR (0.5 mm at 200 MeV/c). The small contamination from annihilation in flight could be subtracted from the stopping distribution by measuring the annihilation vertex. The latter was determined by performing a five-constraint fit to $\bar{p}p \to \pi^0\pi^0$, assuming energy conservation, two invariant 2γ masses consistent with $2\pi^0$, and momentum conservation perpendicular to the beam axis. The branching ratio for $\pi^0\pi^0$ is

$$B(\pi^0\pi^0) = (6.93 \pm 0.43) \times 10^{-4}, \tag{3}$$

in agreement with Devons *et al.* (1971) but much larger than Adiels *et al.* (1987) and Chiba *et al.* (1988). From the annihilation rate $B(\pi^+\pi^-)_{2P}$ into $\pi^+\pi^-$ from atomic 2P states (Doser *et al.,* 1988) one can, in principle, extract the fraction f_p of P-wave annihilation in liquid:[2]

$$f_p = 2\frac{B(\pi^0\pi^0)}{B(\pi^+\pi^-)_{2P}} = (28.8 \pm 3.5)\,\%. \tag{4}$$

This is a surprisingly large contribution. However, Eq. (4) assumes that the population of the fine and hyperfine structure states is the same for the 2P as for the higher P levels, which is in general not true. In liquid, strong Stark mixing constantly repopulates the levels. A P state with large hadronic width, for instance, $^3P_0$ (Carbonell, Ihle, and Richard, 1989), will therefore contribute more to annihilation than expected from a pure statistical population. On the other hand, in low-pressure gas or for states with low principal quantum numbers the levels are populated according to their statistical weights. The branching ratio for annihilation into a given final state is

[2]In Doser *et al.* (1988) f_p was found to be $(8.6 \pm 1.1)\,\%$, when using the most precise measurement for $\pi^0\pi^0$ available at that time (Adiels *et al.,* 1987).

given in terms of the branching ratios B_i^S and B_i^P from the two S and four P-states, respectively (Batty, 1996):

$$B=[1-f_P(\rho)]\sum_{i=1}^{2} w_i^S E_i^S(\rho) B_i^S$$
$$+f_P(\rho)\sum_{i=1}^{4} w_i^P E_i^P(\rho) B_i^P, \tag{5}$$

where ρ is the target density. The purely statistical weights are

$$w_i^S=\frac{2J_i+1}{4}, \quad w_i^P=\frac{2J_i+1}{12}. \tag{6}$$

The enhancement factors E_i describe the departure from a pure statistical population ($E_i=1$). For $\pi^0\pi^0$ in liquid one obtains

$$B(\pi^0\pi^0)=f_P(\text{liq})\left[\frac{1}{12}E_{^3P_0}(\text{liq})B_{^3P_0}(\pi^0\pi^0)\right.$$
$$\left.+\frac{5}{12}E_{^3P_2}(\text{liq})B_{^3P_2}(\pi^0\pi^0)\right], \tag{7}$$

and for $\pi^+\pi^-$ from 2P states

$$B(\pi^+\pi^-)_{2P}=2\left[\frac{1}{12}B_{^3P_0}(\pi^0\pi^0)+\frac{5}{12}B_{^3P_2}(\pi^0\pi^0)\right]. \tag{8}$$

It is obviously not possible to determine $f_P(\text{liq})$ unless the enhancement factors are unity [and hence Eq. (4) follows]. The enhancement factors were determined with an x-ray cascade calculation (Batty, 1996) using the observed yields of K and L x-rays in antiprotonic atoms and the predicted hadronic widths from optical potential models of the $\overline{p}p$ interaction (Carbonell, Ihle, and Richard, 1989). Batty (1996) finds $E_{^3P_0}(\text{liq})=2.1-2.6$ and $E_{^3P_2}(\text{liq})=0.96-1.06$, depending on the potential model. The branching ratios B_i and $f_P(\rho)$ were then fitted to the measured two-body branching ratios for $\overline{p}p \to \pi^0\pi^0, \pi^+\pi^-$, K^+K^-, K_SK_S, and K_SK_L at various target densities, with and without L x-ray coincidence. The fraction of P-wave annihilation is shown in Fig. 2 as a function of density. Except at very low density one obtains a good agreement between data and cascade calculations. In liquid hydrogen one finds

$$f_P(\text{liq})=(13\pm4)\,\%, \tag{9}$$

a more realistic value when compared to Eq. (4). For meson spectroscopy using liquid hydrogen, one therefore assumes annihilation from S waves and neglects P waves, unless a significantly better and stable fit can be achieved by adding P waves. However, depending on the complexity of the final state, the inclusion of P waves becomes prohibitive due to the large number of fit parameters.

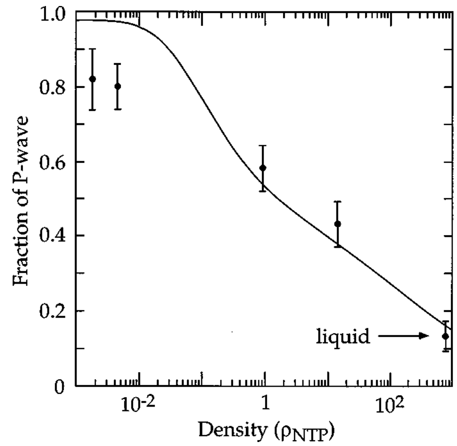

FIG. 2. Fraction f_P of P-wave annihilation as a function of hydrogen density (curve). The dots with error bars give the results from the optical model of Dover and Richard (1980) using two-body branching ratios (adapted from Batty, 1996).

III. THE CRYSTAL BARREL EXPERIMENT

A. Detector

Figure 3 shows a sketch of the Crystal Barrel detector (Aker *et al.,* 1992). The incoming antiprotons entered a 1.5 T solenoidal magnet along its axis and interacted in a liquid-hydrogen target, 44 mm long and 17 mm in diameter. A segmented silicon counter in front of the target defined the incoming beam. The final-state charge multiplicity was determined online with two cylindrical proportional wire chambers. The charged-particle momentum was measured by a jet drift chamber, which also provided π/K separation below 500 MeV/c by ionization sampling.

Photons were detected in a barrel-shaped assembly of 1,380 CsI(Tl) crystals, 16.1 radiation lengths long (30 cm), with photodiode readout. The crystals were oriented towards the interaction point and covered a solid

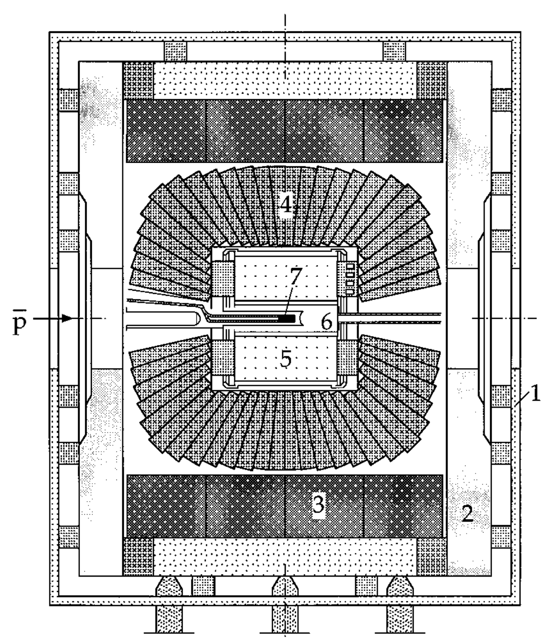

FIG. 3. The Crystal Barrel detector: 1,2, yoke; 3, coil; 4, CsI(Tl) barrel; 5, Jet drift chamber; 6, proportional wire chambers; 7, LH_2 target.

angle of $0.97\times4\pi$. Each crystal, wrapped in teflon and aluminized mylar, was enclosed in a 100-μm-thick titanium container. The light (peaking at 550 nm) was collected at the rear end by a wavelength shifter and the reemitted light was detected by a photodiode glued on the edge of the wavelength shifter. With the low electronic noise of typically 220 keV the energy resolution was

$$\frac{\sigma}{E}=\frac{0.025}{E[\mathrm{GeV}]^{1/4}} \tag{10}$$

and photons could be detected efficiently down to 4 MeV. The angular resolution was typically $\sigma=20$ mrad for both polar and azimuthal angles. The mass resolution was $\sigma=10$ MeV for π^0 and 17 MeV for $\eta\to2\gamma$.

A rough calibration of the electromagnetic calorimeter was first obtained with traversing minimum ionizing pions which deposit 170 MeV in the crystals. The final calibration was achieved with zero-prong events using 2γ invariant masses from π^0 decays. An energy-dependent correction was applied to take into account shower leakage at the rear end of the crystals. The stability of the calibration was monitored with a light pulser system.

The jet drift chamber had 30 sectors, each with 23 sense wires at radial distances between 63 mm and 239 mm, read out on both ends by 100-MHz flash analog-to-digital convertors (ADC's). The position resolution in the plane transverse to the beam axis ($r\phi$ coordinates) was $\sigma=125$ μm using slow gas, a 90:10% CO_2/isobutane mixture. The coordinate z along the wire was determined by charge division with a resolution of $\sigma=8$ mm. This led to a momentum resolution for pions of $\sigma/p\simeq2\%$ at 200 MeV/c, rising to $\simeq7\%$ at 1 GeV/c for those tracks that traversed all jet drift-chamber layers.

The z coordinates were calibrated by fitting straight tracks from four-prong events without magnetic field. The momentum calibration was performed with monoenergetic pions and kaons from the two-body final states $\pi^+\pi^-$ and K^+K^-. Pressure- and temperature-dependent drift time tables were generated and fitted to the measured momentum distribution.

In 1994 the jet drift chamber was replaced by one with only 15 sectors for the six innermost layers. In 1995 the proportional wire chambers were also replaced by a microstrip vertex detector consisting of 15 single-sided silicon detectors arranged in a windmill configuration at a radial distance of 13 mm around the target (Fig. 4). Each detector had 128 strips with a pitch of 50 μm running parallel to the beam axis. The increase of charge multiplicity between the microstrip vertex detector and the inner layers of the jet drift chamber made it possible to trigger on $K_S\to\pi^+\pi^-$. The microstrip vertex detector also provided an improved vertex resolution in $r\phi$ and a better momentum resolution.

For annihilation at rest in liquid hydrogen the $\bar{p}$ incident momentum was 200 MeV/c with typically 10^4 incident $\bar{p}$/s to minimize pileup in the crystals. For annihilation in gaseous hydrogen the liquid target was replaced by a hydrogen flask at 13 bar. The incident momentum was 105 MeV/c. Since the annihilation rate was higher than the maximum possible data acquisition speed, a multilevel trigger could be used. The two proportional wire chambers and the inner layers (2–5) of the jet drift chamber determined the charged multiplicity of the final state. Events with long tracks could be selected for optimum momentum resolution by counting the charged multiplicity in the outer layers (20 and 21) of the jet drift chamber. A hardwired processor determined the cluster multiplicity in the barrel. A processor then fetched the digitized energy deposits in the barrel and computed all two-photon invariant masses, thus providing a trigger on the π^0 or η multiplicity (Urner, 1995).

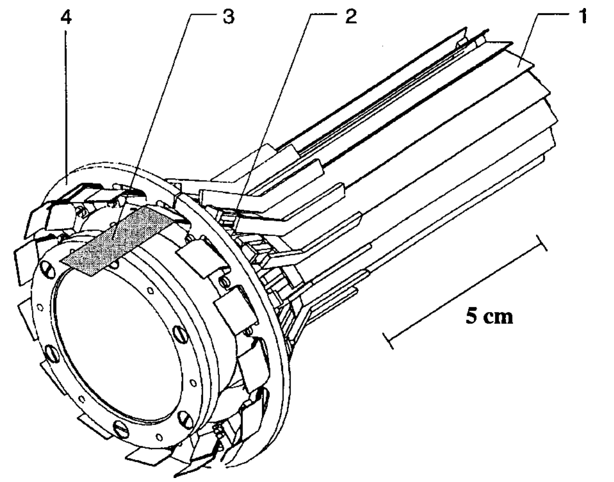

FIG. 4. The silicon vertex detector: 1, microstrip detectors; 2, hybrids; 3, readout electronics; 4, cooling ring (from Regenfus 1997).

B. Photon reconstruction

We now briefly describe the photon reconstruction, which is particularly relevant to the results reviewed in this article. Photon-induced electromagnetic showers spread out over several crystals. The size of a cluster depends on the photon energy and varies from 1 to about 20 crystals. The reconstruction of photons is done by searching for clusters of neighboring crystals with energy deposits of at least 1 MeV. The threshold for cluster identification (typically between 4 and 20 MeV) depends on the annihilation channel being studied. Local maxima with a predefined threshold (typically between 10 and 20 MeV) are then searched for within clusters. When only one local maximum is found, the photon energy is defined as the cluster energy and the direction is given by the center of gravity of the crystals, weighted by their energies. When n local maxima are found within a cluster, the latter is assumed to contain showers from n photons. In this case the cluster energy E_C is shared between the n subclusters of nine crystals with energies E_i around the local maxima. Hence the photon energies are given by

$$E_{\gamma,i}=\frac{E_i}{\sum_{j=1}^{n} E_j} E_C . \tag{11}$$

Additional clusters mocking photons are due to shower fluctuations, which may develop small but well separated satellites in the vicinity of the main shower. These ''splitoffs'' can be removed by requiring a minimum separation between the showers. However, this cut may reduce the detection efficiency for high-energy π^0's since photons from π^0 decay cluster around the minimum opening angle. The opening angle between two photons with energies $E_1 \leqslant E_2$ from π^0 decay is given by

$$\cos\phi=1-\frac{(1+R)^2}{2\gamma^2 R} \text{ with } R=\frac{E_1}{E_2}, \tag{12}$$

where $\gamma=E_{\pi^0}/m_{\pi^0}$. Hence for all pairs of neighboring clusters one calculates R and removes the low-energy clusters whenever $\cos\phi$ is larger than given by Eq. (12), assuming the maximum possible value of γ in the annihilation channel under consideration (Pietra, 1996).

Clusters generated by ionizing particles can be removed by matching the impact points extrapolated from the reconstructed tracks in the jet drift chamber. However, splitoffs from charged particles are more cumbersome to eliminate. They are initiated, for example, from neutrons which travel long distances before being absorbed. These splitoffs can be suppressed by requiring momentum and energy conservation in the annihilation process (kinematic fits).

C. Available data

The bulk of the Crystal Barrel data consists in $\bar{p}p$ annihilation at rest and in flight in liquid hydrogen. As discussed above, annihilation from initial P states is enhanced when using a gaseous target. Annihilation in deuterium at rest allows the formation of $\bar{N}N$ bound states (baryonium) below $2m_N$, the spectator neutron (or proton) removing the excess energy (for a review on baryonium states, see Amsler, 1987). With a spectator proton one gains access to $\bar{p}n$ annihilation, a pure isospin $I=1$ initial state.

The data collected by Crystal Barrel are shown in Table I. Data were taken in liquid hydrogen, gaseous hydrogen (13 bar), and liquid deuterium with a minimum bias trigger (requiring only an incident antiproton) or with the multiplicity trigger requiring zero-prong or n-prong with long tracks in the jet drift chamber. In addition, data were collected with specialized triggers enhancing specific final states. As a comparison, the largest earlier sample of annihilations at rest in liquid was obtained by the CERN-Collège de France Collaboration with about 100 000 pionic events and 80 000 events containing at least one $K_S \to \pi^+\pi^-$ (Armenteros and French, 1969). The Asterix Collaboration collected some 10^7 pionic events in gaseous hydrogen at 1 bar [for a review and references see Amsler and Myhrer (1991)].

TABLE I. Summary of data (in millions of events) with a minimum bias trigger (MB), for zero-prong, two-prong, four-prong, and more specialized triggers at rest (first three rows) and in liquid hydrogen at high $\bar{p}$ momenta (in MeV/c). LH_2, liquid hydrogen; LD_2, liquid deuterium; GH_2, gaseous hydrogen.

	MB	0	2	4	Triggers			
LH_2	16.8	24.7	19.3	10.4	16.9 [a]	8.5 [b]	4.0 [c]	0.4 [g]
LD_2	3.2	6.0	0.5	0.5	11.9 [a]	8.1 [d]	11.7 [e]	
GH_2	8.6	18.0	14.3	8.2	6.4 [a]			
600	1.3	5.9	2.2		1.2 [a]			
900		20.0	19.4					
1050	0.3	7.2						
1200	1.6	10.4	6.0		2.0 [f]			
1350	1.0	11.5						
1525	20.6	10.2	4.5					
1642	0.1	11.1	12.5					
1800		6.8	3.6					
1900	13.6	14.5	15.7					

[a] $K_S(\to\pi^+\pi^-)X$.
[b] $\pi^+\pi^-\pi^0\pi^0\eta$.
[c] $\pi^0\eta\eta$.
[d] One-prong.
[e] Three-prong.
[f] $\pi^+\pi^-\pi^0\eta$.
[g] $\pi^+\pi^-\eta$.

The total number of annihilations at rest in liquid hydrogen collected by Crystal Barrel is 10^8. The triggered zero-prong sample at rest (24.7×10^6 events) corresponds, with a neutral branching ratio of 3.9% (Amsler *et al.,* 1993a), to 6.3×10^8 annihilations.

IV. ANNIHILATION INTO TWO MESONS

The mechanism through which the $\bar{p}p$ system annihilates into two or more mesons is not understood in detail. This is not surprising, since annihilation occurs in the nonperturbative regime of QCD and therefore models must be used. A substantial theoretical effort has been invested to predict the branching ratios for annihilation at rest into two or even three mesons from initial S and P states. For a review of annihilation models and references, see Kerbikov, Kondratyuk, and Sapozhnikov (1989) and Amsler and Myhrer (1991).

Since the proton and the antiproton wave functions overlap, one expects quarks to play an important role in the annihilation dynamics. For instance, $\bar{p}p$ annihilation into two mesons can be described by the annihilation of two $q\bar{q}$ pairs and the creation of a new pair (see Fig. 5, annihilation graph A) or by the annihilation of one $q\bar{q}$ pair and the rearrangement of the other two pairs (rearrangement graph R). At low energies there is, however, no consensus as to which operator should be used to describe the emission and absorption of gluons. Single gluons are emitted and absorbed from $^3S_1 q\bar{q}$ vertices, while for several gluons one assumes $^3P_0$. Predictions

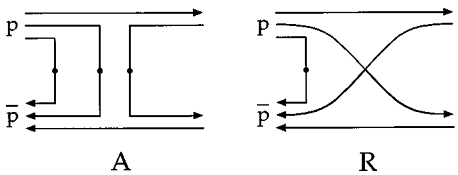

FIG. 5. Annihilation graph A and rearrangement graph R for $\bar{p}p$ annihilation into two mesons.

for the annihilation branching ratios based on these assumptions have been made by Green and Niskanen (1987), and the dependence on angular momentum, spin, and isospin has been studied in detail by Dover *et al.* (1992).

In a naive approach, one assumes that only the flavor flow between initial and final states is important (Genz, 1983; Hartmann, Klempt, and Körner 1988). The quark line rule states that annihilation into $u\bar{u}$ and $d\bar{d}$ is excluded if the A graph dominates, while annihilation into two $d\bar{d}$ mesons is forbidden if R dominates (see Fig. 5). The Okubo-Zweig-Iizuka (OZI) rule (Okubo, 1963) is a special case of the quark line rule: Annihilation into one or more $s\bar{s}$ mesons is forbidden. We shall confront these simple rules below with Crystal Barrel data on two-meson annihilation.

Another approach, which we shall use, is the nearest threshold dominance model, which describes reasonably well the observed final-state multiplicity as a function of $\bar{p}$ momentum (Vandermeulen, 1988). The branching ratio for annihilation into two mesons with masses m_a und m_b is given by

$$W = pC_0C_{ab}\exp(-A\sqrt{s-(m_a+m_b)^2}), \tag{13}$$

where p is the meson momentum in the $\bar{p}p$ center-of-mass system with total energy $\sqrt{s}$, C_0 a normalization constant, and C_{ab} a multiplicity factor depending on spin and isospin. The constant $A=1.2\,\mathrm{GeV}^{-1}$ has been fitted to the cross section for $\bar{p}p$ annihilation into $\pi^+\pi^-$ as a function of $\bar{p}$ momentum. For annihilation into kaons, the fit to kaonic channels requires the additional normalization factor $C_1/C_0=0.15$. Thus annihilation into the heaviest possible meson pair is enhanced with respect to phase space p by the exponential form factor in Eq. (13). This is natural in the framework of baryon exchange models which prefer small momentum transfers at the baryon-meson vertices.

In more refined models the branching ratios for annihilation at rest depend on the atomic wave function distorted by strong interaction at short distances (Carbonell, Ihle, and Richard, 1989). Predictions for the branching ratios therefore depend on models for the meson exchange potential, which are uncertain below 1 fm. Also, the quark description has to be complemented by baryon and meson exchanges to take the finite size of the emitted mesons into account.

In the absence of strong interaction the $\bar{p}p$ atomic state is an equal superposition of isospin $I=0$ and $I=1$ states. Naively one would therefore expect half the protonium states to annihilate into a final state of given isospin. However, $\bar{p}p$ to $\bar{n}n$ transitions occuring at short distances may modify the population of $I=0$ and $I=1$ states and therefore enhance or reduce the annihilation rate to a final state of given isospin (Klempt, 1990; Jaenicke, Kerbikov, and Pirner 1991). Nonetheless, one expects that predictions for ratios of branching ratios of channels with the same isospin and proceeding from the same atomic states are less sensitive to model dependence.

We now turn to the phenomenology of annihilation into two mesons, in particular two neutral mesons, for which new data from Crystal Barrel are available.

A. Annihilation into two neutral mesons

Consider a pair $M\bar{M}$ of charge-conjugated mesons in the eigenstate of isospin I. The P, C, and G parities are

$$P(M\bar{M})=(-1)^L, \tag{14}$$

$$C(M\bar{M})=(-1)^{L+S}, \tag{15}$$

$$G(M\bar{M})=(-1)^{L+S+I}, \tag{16}$$

where L is the relative angular momentum and S the total spin. For a $\bar{p}p$ system with angular momentum ℓ and spin s, one has

$$P(\bar{p}p)=(-1)^{\ell+1}, \tag{17}$$

$$C(\bar{p}p)=(-1)^{\ell+s}, \tag{18}$$

$$G(\bar{p}p)=(-1)^{\ell+s+I}. \tag{19}$$

For annihilation into two mesons the two sets of equations relate the quantum numbers of the initial state to those of the final state, since P, C, G, and I are conserved. In addition, L, S, ℓ, and s must be chosen so that the total angular momentum J is conserved:

$$|L-S|\leqslant J\leqslant L+S, \quad |\ell-s|\leqslant J\leqslant \ell+s. \tag{20}$$

The relations (14)–(16) can be used to determine L, S, and I from P, C, and G. For example, for a pair of nonstrange charge-conjugated mesons G is +1. For two identical neutral nonstrange pseudoscalar mesons (e.g., $\pi^0\pi^0$) with $S=0$, $C=+1$ implies that L is even and then Eq. (17) requires ℓ to be odd (annihilation from P states only). Equation (16) further requires with $G=+1$ that $I=0$ and hence with Eq. (19) annihilation from the ($I=0$) 0^{++} or 2^{++} atomic states.

For a pair of nonidentical neutral pseudoscalar mesons (e.g., $\pi^0\eta$) L may be odd and hence the possible quantum numbers are 0^{++}, 1^{-+}, 2^{++}, 3^{-+}, etc. However, 1^{-+} and 3^{-+} do not couple to $\bar{p}p$ since Eqs. (17) and (18) require ℓ to be even and $s=0$, hence J is even. Annihilation into two neutral nonstrange pseudoscalar mesons is therefore forbidden from atomic S states.

Crystal Barrel has measured the branching ratios for $\bar{p}p$ annihilation into two neutral light mesons from about 10^7 annihilations into zero-prong events (Amsler *et al.*, 1993b). These data have been collected by vetoing

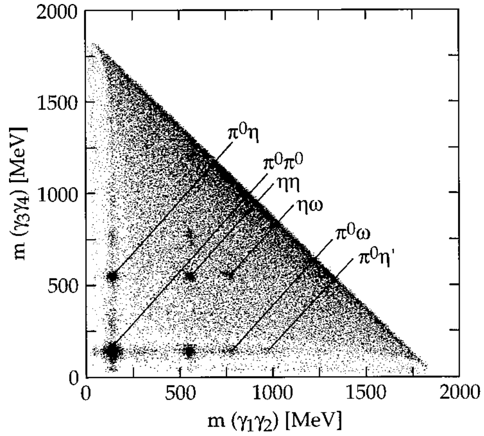

FIG. 6. 2γ invariant-mass distribution for a sample of 4γ events (six entries/event).

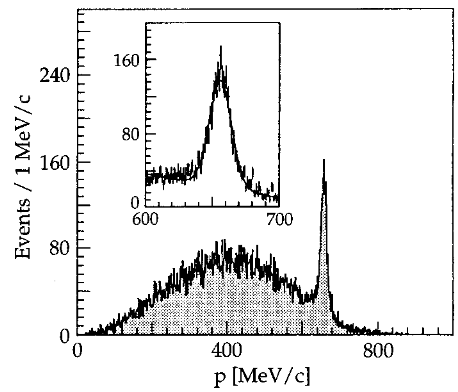

FIG. 7. $\pi^0\gamma$ momentum distribution in $\overline{p}p\to 4\pi^0\gamma$ (four entries/event). The peak is due to $\overline{p}p\to\omega\eta$. The inset shows the ω region and a fit (Gaussian and polynomial background).

charged particles with the proportional wire chambers and the internal layers of the jet drift chamber. The lowest γ multiplicity was four (e.g., $\pi^0\pi^0,\pi^0\eta$) and the highest nine (e.g., $\eta\omega$, with $\eta\to 3\pi^0$ and $\omega\to\pi^0\gamma$). To control systematic errors in the detection efficiency, some of these branching ratios were determined from different final-state multiplicities. For example, η decays to 2γ and $3\pi^0$ and hence $\eta\eta$ is accessible from 4γ and 8γ events.

Figure 6 shows a scatterplot of 2γ-invariant masses for events with 4γ. Events were selected by requiring four clusters in the barrel and applying momentum and energy conservation (a four-constraint, or 4C, fit). Signals from $\pi^0\pi^0$, $\pi^0\eta$, $\eta\eta$, and even $\pi^0\eta'$ are clearly visible. The dark diagonal band at the edge is due to wrong combinations. The detection and reconstruction efficiency was typically 40% for 4γ events, obtained by Monte Carlo simulation with GEANT. As discussed above, two neutral pseudoscalars couple only to atomic P states and are therefore suppressed in liquid hydrogen. On the other hand, the channels $\pi^0\omega$ and $\eta\omega$ couple to $^3S_1$ and hence have a larger branching ratio. In spite of the good detection efficiency of the detector, one therefore observes the background signals from $\pi^0\omega$ and $\eta\omega$, where ω decays to $\pi^0\gamma$ with a missing (undetected) photon.

Figure 7 shows the $\pi^0\gamma$ momentum distribution for $\overline{p}p\to 4\pi^0\gamma$ events (8C fit requiring $4\pi^0$). The peak at 657 MeV/c is due to the channel $\overline{p}p\to\eta\omega$ ($\eta\to 3\pi^0$, $\omega\to\pi^0\gamma$). For these 9γ events the detection efficiency was 10%.

The branching ratios are given in Table II. They are always corrected for the unobserved (but known) decay modes of the final-state mesons (Barnett *et al.,* 1996). For Crystal Barrel data the absolute normalization was provided by comparison with $\pi^0\pi^0$, which was measured with minimum-bias data [Eq. (3)]. For completeness, we also include in Table II the branching ratios for annihilation into two charged light mesons.

Signals for $\omega\pi^0$ and $\omega\eta$ were also observed for ω decaying to $\pi^+\pi^-\pi^0$, leading to $\pi^+\pi^-4\gamma$ (Schmid, 1991). Figure 8 shows the $\pi^+\pi^-\pi^0$ invariant-mass spectrum for $\pi^+\pi^-\pi^0\eta$ events. The branching ratio for $\omega\pi^0$ and $\omega\eta$ are in excellent agreement with the ones from zero-prong events (Table II).

The angular distribution in the ω rest frame contains information on the initial atomic state. The distribution of the angle between the normal to the plane spanned by the three pions and the direction of the recoiling η is plotted in the inset of Fig. 8. Using the method described in Sec. VII.B, one predicts the distribution to behave like $\sin^2\theta$ for annihilation from $^3S_1$ while the distribution should be isotropic for annihilation from $^1P_1$. The fit (curve) allow for a (12 ± 4)% P wave. Figure 9 shows the angular distribution of the γ in the ω rest frame for $\omega\eta(\omega\to\pi^0\gamma)$. The predicted distribution is $(1+\cos^2\theta)$ from $^3S_1$ and is again isotropic for $^1P_1$. The fit (curve) allow for a (9 ± 3)% P wave. However, these results assume that the relative angular momentum between η and ω is $L=0$ from $^1P_1$, thus neglecting $L=2$. Without this assumption, the fraction of P wave cannot be determined from the angular distributions due to the unknown interference between the $L=0$ and $L=2$ amplitudes.

Some of the branching ratios for two neutral mesons were measured earlier (Adiels *et al.,* 1989; Chiba *et al.,* 1988; see also Chiba *et al.,* 1989) by detecting and reconstructing π^0's or η's with small solid-angle detectors and observing peaks in the π^0 or η inclusive momentum spectra. Since the branching ratios are small, these early data are often statistically weak or subject to uncertainties in the baseline subtraction from the inclusive spectra. In fact, most of the Crystal Barrel results disagree with these measurements, which should not be used anymore. Table II therefore updates Table I in Amsler and Myhrer (1991).

B. Test of the quark line rule

We now compare the measured two-meson branching ratios in Table II with predictions from the quark line rule. The flavor content of the η and η' mesons is given by

TABLE II. Branching ratios B for $\overline{p}p$ annihilation at rest in liquid. See Amsler and Myhrer (1991) for annihilation in gaseous hydrogen. Further branching ratios from Dalitz plot analyses are listed in Table XIII below.

Channel			B		Reference
e^+e^-	3.2	±	0.9	10^{-7}	Bassompierre *et al.* (1976)
$\pi^0\pi^0$	6.93	±	0.43	10^{-4}	Amsler *et al.* (1992a)‡
	4.8	±	1.0	10^{-4}	Devons *et al.* (1971)
$\pi^+\pi^-$	3.33	±	0.17	10^{-3}	Armenteros and French (1969)
$\pi^+\pi^-$	3.07	±	0.13	10^{-3}	Amsler *et al.* (1993b)‡
$\pi^0\eta$	2.12	±	0.12	10^{-4}	Amsler *et al.* (1993b)‡
$\pi^0\eta'$	1.23	±	0.13	10^{-4}	Amsler *et al.* (1993b)‡
$\pi^0\rho^0$	1.72	±	0.27	10^{-2}	Armenteros and French (1969)
$\pi^\pm\rho^\mp$	3.44	±	0.54	10^{-2}	Armenteros and French (1969)
$\eta\eta$	1.64	±	0.10	10^{-4}	Amsler *et al.* (1993b)‡
$\eta\eta'$	2.16	±	0.25	10^{-4}	Amsler *et al.* (1993b)‡
$\omega\pi^0$	5.73	±	0.47	10^{-3}	Amsler *et al.* (1993b) [a]‡
	6.16	±	0.44	10^{-3}	Schmid (1991) [b]‡
$\omega\eta$	1.51	±	0.12	10^{-2}	Amsler *et al.* (1993b) [a]‡
	1.63	±	0.12	10^{-2}	Schmid (1991) [b]‡
$\omega\eta'$	0.78	±	0.08	10^{-2}	Amsler *et al.* (1993b)‡
$\omega\omega$	3.32	±	0.34	10^{-2}	Amsler *et al.* (1993b)‡
$\eta\rho^0$	4.81	±	0.85	10^{-3}	[c]
	3.87	±	0.29	10^{-3}	Abele *et al.* (1997a)‡
$\eta'\rho^0$	1.29	±	0.81	10^{-3}	Foster *et al.* (1968a)
	1.46	±	0.42	10^{-3}	Urner (1995)‡
$\rho^0\rho^0$	1.2	±	1.2	10^{-3}	Armenteros and French (1969)
$\rho^0\omega$	2.26	±	0.23	10^{-2}	Bizzarri *et al.* (1969)
K^+K^-	1.01	±	0.05	10^{-3}	Armenteros and French (1969)
K^+K^-	0.99	±	0.05	10^{-3}	Amsler *et al.* (1993b)‡
K_SK_L	7.6	±	0.4	10^{-4}	Armenteros and French (1969)
K_SK_L	9.0	±	0.6	10^{-4}	Amsler *et al.* (1995c)‡

[a]From $\omega\rightarrow\pi^0\gamma$.
[b]From $\omega\rightarrow\pi^+\pi^-\pi^0$.
[c]Average between Baltay *et al.* (1966), Espigat *et al.* (1972) and Foster *et al.* (1968a).
‡Crystal Barrel experiment.

$$|\eta\rangle=\frac{1}{\sqrt{2}}(|u\overline{u}\rangle+|d\overline{d}\rangle)\sin(\theta_i-\theta_p)-|s\overline{s}\rangle\cos(\theta_i-\theta_p),$$

$$|\eta'\rangle=\frac{1}{\sqrt{2}}(|u\overline{u}\rangle+|d\overline{d}\rangle)\cos(\theta_i-\theta_p)+|s\overline{s}\rangle\sin(\theta_i-\theta_p), \tag{21}$$

where $\theta_i=35.3°$ is the ideal mixing angle. The flavor wave functions of the π^0 and ρ^0 are

$$|\pi^0\rangle,|\rho^0\rangle=\frac{1}{\sqrt{2}}(|d\overline{d}\rangle-|u\overline{u}\rangle), \tag{22}$$

and those of ω and ϕ, assuming ideal mixing in the vector nonet,

$$|\omega\rangle=\frac{1}{\sqrt{2}}(|u\overline{u}\rangle+|d\overline{d}\rangle), \quad |\phi\rangle=-|s\overline{s}\rangle. \tag{23}$$

The branching ratio for annihilation into two neutral mesons is then given by $B=\widetilde{B}\cdot W$ with

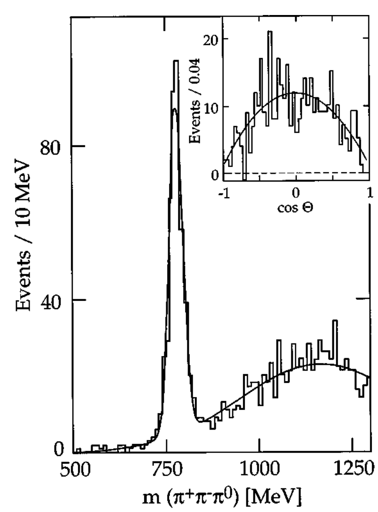

FIG. 8. $\pi^+\pi^-\pi^0$ invariant-mass distribution for $\pi^+\pi^-\pi^0\eta$ events. The peak is due to $\overline{p}p\rightarrow\omega\eta$. The inset shows the background-subtracted angular distribution in the ω rest frame (see text).

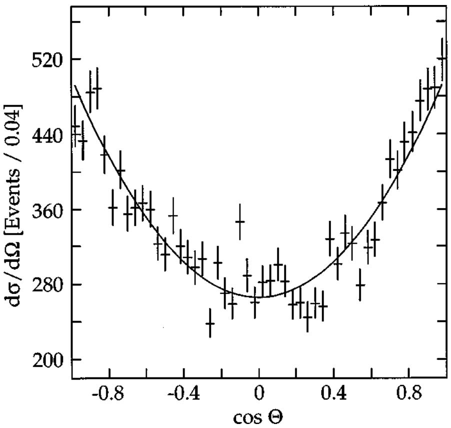

FIG. 9. γ angular distribution in the ω rest frame for $\omega\eta(\omega\to\pi^0\gamma)$ (see text).

$$\tilde{B}=|\langle\overline{p}p|T|M_1M_2\rangle|^2=|\sum_{i,j} T([q_i\overline{q_i}]_1,[q_j\overline{q_j}]_2)$$
$$\times\langle q_i\overline{q_i}|M_1\rangle\langle q_j\overline{q_j}|M_2\rangle|^2, \tag{24}$$

and[3] $q_i=u$ or d (Genz, 1985). In the absence of $s\overline{s}$ pairs in the nucleon, the quark line rule forbids the production of $s\overline{s}$ mesons, and therefore the $s\overline{s}$ components in M_1 and M_2 can be ignored in Eq. (24). The predicted ratios of branching ratios are given by the first four rows in Table III for various channels from the same atomic states. They depend only on the pseudoscalar mixing angle θ_p. To extract θ_p the measured branching ratios from Table II must be first divided by W [Eq. (13)], ignoring C_0 and C_{ab}, which cancel in the ratio.

The pseudoscalar mixing angle has been measured in various meson decays (e.g., η and η' radiative decays, J/ψ radiative decays to η and η') and is known to be close to $-20°$ (Gilman and Kauffmann, 1987). The agreement with our simple model of annihilation is amazing (third column of Table III). We emphasize that the predictions in the upper four rows of Table III are valid independently of the relative contributions from the A and R graphs.

Conversely, one can assume the validity of the model and extract from the first four rows in Table III the average

$$\theta_p=(-19.4\pm0.9)°. \tag{25}$$

Leaving the constant A in Eq. (13) as a free fit parameter one obtains $\theta_p=(-17.3\pm1.8)°$ from early Crystal Barrel data (Amsler *et al.,* 1992b). This result is in excellent agreement with a reanalysis (Bramon, Escribano, and Scadron, 1997) of J/ψ decay into a vector and a pseudoscalar: $\theta_p=(-16.9\pm1.7)°$. Assuming now dominance of the planar graph A, the amplitudes $T([u\overline{u}]_1,[d\overline{d}]_2)$ and $T([d\overline{d}]_1,[u\overline{u}]_2)$ vanish, and one obtains the predictions in the lower part of Table III.

[3]The theoretical prediction $\tilde{B}$ has to be multiplied by two for a pair of nonidentical mesons.

TABLE III. Pseudoscalar mixing angle θ_p derived from the measured ratios of two-body branching ratios ($\theta_i=35.3°$). The first four rows assume only the quark line rule in the annihilation process. The last six rows assume in addition the dominance of the annihilation graph A.

Ratio	Prediction	θ_p (deg)
$\tilde{B}(\pi^0\eta)/\tilde{B}(\pi^0\eta')$	$\tan^2(\theta_i-\theta_p)$	-18.1 ± 1.6
$\tilde{B}(\eta\eta)/\tilde{B}(\eta\eta')$	$\frac{1}{2}\tan^2(\theta_i-\theta_p)$	-17.7 ± 1.9
$\tilde{B}(\omega\eta)/\tilde{B}(\omega\eta')$	$\tan^2(\theta_i-\theta_p)$	-21.1 ± 1.5
$\tilde{B}(\eta\rho^0)/\tilde{B}(\eta'\rho^0)$	$\tan^2(\theta_i-\theta_p)$	$-25.4\pm^{5.0}_{2.9}$
$\tilde{B}(\eta\rho^0)/\tilde{B}(\omega\pi^0)$	$\sin^2(\theta_i-\theta_p)$	-11.9 ± 3.2
$\tilde{B}(\eta'\rho^0)/\tilde{B}(\omega\pi^0)$	$\cos^2(\theta_i-\theta_p)$	-30.5 ± 3.5
$\tilde{B}(\eta\eta)/\tilde{B}(\pi^0\pi^0)$	$\sin^4(\theta_i-\theta_p)$	$-6.2\pm^{0.6}_{1.1}$
$\tilde{B}(\eta\eta')/\tilde{B}(\pi^0\pi^0)$	$2\sin^2(\theta_i-\theta_p)$ $\times\cos^2(\theta_i-\theta_p)$	14.6 ± 1.8 or -34.0 ± 1.8
$\tilde{B}(\omega\eta)/\tilde{B}(\pi^0\rho^0)$	$\sin^2(\theta_i-\theta_p)$	$-23.7\pm^{7.6}_{8.9}$
$\tilde{B}(\omega\eta')/\tilde{B}(\pi^0\rho^0)$	$\cos^2(\theta_i-\theta_p)$	-20.1 ± 3.7

The measurements lead, in general, to incorrect values for θ_p, presumably due to the contribution of the R graph. Also, for $\rho^0\rho^0$ and $\omega\omega$ one expects from A dominance:

$$\tilde{B}(\rho^0\rho^0)=\tilde{B}(\omega\omega), \tag{26}$$

in violent disagreement with the data (Table II). On the other hand, if R dominates, the amplitude $T([d\overline{d}]_1,[d\overline{d}]_2)$ vanishes and one predicts from Eq. (24) with $a^2\equiv\sin^2(\theta_i-\theta_p)$ the inequality (Genz, Martinis, and Tatur, 1990)

$$|a^2\sqrt{2\tilde{B}(\pi^0\pi^0)}-\sqrt{2\tilde{B}(\eta\eta)}|^2$$
$$\leqslant 4a^2\tilde{B}(\pi^0\eta)\leqslant|a^2\sqrt{2\tilde{B}(\pi^0\pi^0)}+\sqrt{2\tilde{B}(\eta\eta)}|^2, \tag{27}$$

which is fulfilled by data.

There is, however, a caveat: the predictions of Eq. (24) have been compared to the measured branching ratios corrected by W. As pointed out earlier, Eq. (13) provides a good fit to the mutiplicity distribution in low-energy $\overline{p}p$ annihilation as a function of $\overline{p}$ momentum. Other correcting factors can, however, be found in the literature. In Sec. VII we shall use the phase space factor

$$W=pF_L^2(p), \tag{28}$$

where $F_L(p)$ is the Blatt-Weisskopf damping factor, which suppresses high angular momenta L for small p.

TABLE IV. Damping factors $F_L(p)$ where z stands for $(p/p_R)^2$ and p_R is usually taken as 197 MeV/c. After Hippel and Quigg (1972; see also Blatt and Weisskopf, 1952).

L	$F_L(p)$
0	1
1	$\sqrt{2z/z+1}$
2	$\sqrt{13z^2/(z-3)^2+9z}$
3	$\sqrt{277z^3/z(z-15)^2+9(2z-5)^2}$
4	$\sqrt{12\,746z^4/(z^2-45z+105)^2+25z(2z-21)^2}$

This factor is determined by the range of the interaction, usually chosen as 1 fm ($p_R=197\,\mathrm{MeV}/c$). Convenient expressions for $F_L(p)$ are given in Table IV. For p much larger than p_R, $F_L(p)\propto 1$ and for p much smaller than p_R

$$F_L(p)\propto p^L. \tag{29}$$

This last prescription provides a reasonable agreement when comparing the measured decay branching ratios of mesons, especially tensors, with predictions from SU(3), as we shall discuss in Sec. X.A. These alternative phase-space factors may also be used to determine the pseudoscalar mixing angle. However, they do not lead to consistent values for θ_p (Amsler *et al.,* 1992b). Agreement is achieved with prescription (13), which we shall also employ in the next section.

In conclusion, the naive quark model assuming only the quark line rule and two-body threshold dominance reproduces the correct pseudoscalar mixing angle from the measured two-meson final states. This is a clear indication of quark dynamics in the annihilation process. The relative contributions from R and A cannot be extracted, but the nonplanar graph R must contribute substantially to the annihilation process.

V. ELECTROMAGNETIC PROCESSES

We now turn to annihilation channels involving the electromagnetic interaction. The direct emission of photons is expected to occur from quark-antiquark pairs annihilating in the $^3S_1(q\bar{q})$ state. The rates for these processes can be compared with predictions from the vector dominance model, as shown in Sec. V.A. The main contribution to annihilation final states with unpaired photons stems from radiative decay of intermediate mesons, the rate of which can be compared with SU(3) predictions (Secs. V.B and V.C). The search for monochromatic photons may lead to the observation of new bosons (Sec. V.D). Proton-antiproton annihilation is also a copious source of η mesons, and the $\eta\to 3\pi$ decay may be studied to test current ideas on chiral perturbation (Sec. V.E).

A. Radiative annihilation

Radiative annihilation $\bar{p}p\to\gamma X$, where X stands for any neutral meson, involves the annihilation of a $q\bar{q}$ pair into a photon. The branching ratios can be calculated from the vector dominance model, which relates γ emission to the emission of ρ, ω, and ϕ mesons (Delcourt, Layssac, and Pelaquier, 1984). Assuming ideal mixing in the vector nonet, one may actually neglect ϕ production, which is forbidden by the quark line rule. The isospin $I=0$ and $I=1$ amplitudes from the same $\bar{p}p$ atomic state interfere, since isospin is not conserved in electromagnetic processes. The amplitude for $\bar{p}p\to\gamma X$ is then given by the coherent sum of the two $I=0$ and $I=1$ amplitudes with unknown relative phase β (Fig. 10). According to the vector dominance model, the $\gamma\rho$ coupling $g_{\rho\gamma}$ is a factor of three stronger than the $\gamma\omega$ coupling. The branching ratio is then[4]

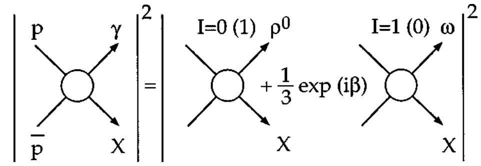

FIG. 10. Following the vector dominance model, radiative annihilation is described by a superposition of two isospin amplitudes with unknown relative phase β. The quantity X stands for any neutral meson.

$$\tilde{B}(\gamma X)=A^2\left[\tilde{B}(\rho X)+\frac{1}{9}\tilde{B}(\omega X)+\frac{2}{3}\sqrt{\tilde{B}(\rho X)\tilde{B}(\omega X)}\cos\beta\right], \tag{30}$$

with

$$A=\frac{e g_{\rho\gamma}}{m_\rho^2}=0.055. \tag{31}$$

Equation (30) provides lower and upper limits ($\cos\beta=\pm 1$) for branching ratios.

Radiative annihilation has not been observed so far, with the exception of $\pi^0\gamma$ (Adiels *et al.,* 1987). Crystal Barrel measured the rates for $\pi^0\gamma$, $\eta\gamma$, $\omega\gamma$, and obtained upper limits for $\eta'\gamma$ and $\gamma\gamma$ (Amsler *et al.*, 1993c). Annihilation into $\phi\gamma$ (Amsler *et al.,* 1995c) is treated in Sec. VI.A.

The starting data sample consisted of 4.5×10^6 zero-prong events, i.e., only neutral events (no charged particles detected in the final state). Figure 11 shows a typical $\pi^0\gamma$ event leading to three detected photons. The main background to $\pi^0\gamma$ stems from annihilations into $\pi^0\pi^0$ for which one of the photons from π^0 decay has not been detected, mainly because its energy lies below detection threshold (10 MeV). The π^0 momentum for $\pi^0\gamma$ is slightly higher (5 MeV/c) than for $\pi^0\pi^0$. The small downward shift of the π^0 momentum peak due to $\pi^0\pi^0$ contamination could be observed, thanks to the

[4]For two identical particles, e.g., $\rho^0\rho^0$ or $\omega\omega$, the measured branching ratios $\tilde{B}$ divided by phase space have to be multiplied by two.

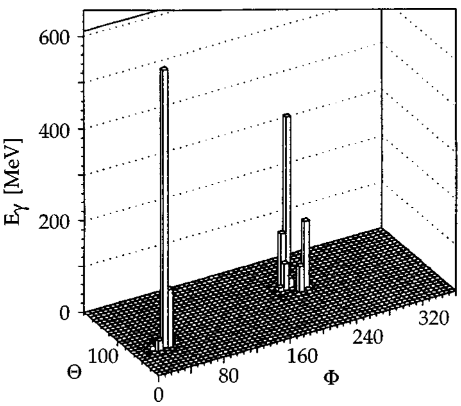

FIG. 11. Energy deposits in the barrel vs polar angle Θ and azimuthal angle Φ for a $\pi^0\gamma$ event. The two γ's from π^0 decay cluster near the minimum opening angle (16.5°).

good energy resolution of the detector, and could be used to estimate the feedthrough from $\pi^0\pi^0$: (29 $\pm$8)%, in agreement with Monte Carlo simulations. The result for the $\pi^0\gamma$ branching ratio is given in Table V. It disagrees with the one obtained earlier from the π^0 inclusive momentum spectrum: $(1.74\pm0.22)\times10^{-5}$ (Adiels *et al.,* 1987).

Results for $\eta\gamma$, $\omega\gamma$ and $\eta'\gamma$ are also given in Table V. The ω was detected in its $\pi^0\gamma$ and the η' searched for in its 2γ decay mode. The main contaminants were $\eta\pi^0$, $\omega\pi^0$, and $\eta'\pi^0$, respectively, with one photon escaping detection. For $\bar{p}p\to\gamma\gamma$, 98$\pm$10 events were observed, of which 70$\pm$8 were expected feedthrough from $\pi^0\gamma$ and $\pi^0\pi^0$. This corresponds to a branching ratio of $(3.3\pm1.5)\times10^{-7}$, which the collaboration prefers to quote as an upper limit (Table V).

The branching ratios, divided by W [Eq. (13)], are compared in Table V with the range allowed by Eq. (30). Apart from $\phi\gamma$, to which we shall return later, the results agree with predictions from the vector dominance model. For $\pi^0\gamma$ and $\eta\gamma$ (from $^3S_1$) the isospin amplitudes interfere destructively ($\cos\beta\sim-0.3$), while for $\omega\gamma$ (from $^1S_0$) they interfere constructively ($\cos\beta\sim0.13$). We emphasize that these conclusions depend on the prescription for the phase-space correction. With a phase-space factor of the form p^3 one finds strongly destructive amplitudes (Amsler *et al.,* 1993c; see also Locher, Lu, and Zou, 1994 and Markushin, 1997).

No prediction can be made from the vector dominance model for $\gamma\gamma$ due to the contribution of three amplitudes with unknown relative phases: $\rho^0\omega$ from $I=1$, $\rho^0\rho^0$ and $\omega\omega$ from $I=0$. Also, the branching ratio for $\rho^0\rho^0$ is poorly known (Table II).

TABLE V. Branching ratios B for radiative $\bar{p}p$ annihilation at rest in liquid from Crystal Barrel (Amsler *et al.,* 1993c, 1995c). The lower and upper limits L and U, calculated from the vector dominance model, are given in the third and fourth column, respectively.

Channel	B	L	U
$\pi^0\gamma$	$4.4\pm0.4\times10^{-5}$	3.1×10^{-5}	6.8×10^{-5}
$\eta\gamma$	$9.3\pm1.4\times10^{-6}$	1.0×10^{-6}	2.5×10^{-5}
$\omega\gamma$	$6.8\pm1.8\times10^{-5}$	8.5×10^{-6}	1.1×10^{-4}
$\eta'\gamma$	$<1.2\times10^{-5}$ [a]	2.7×10^{-7}	10^{-5}
$\gamma\gamma$	$<6.3\times10^{-7}$ [a]		
$\phi\gamma$	$2.0\pm0.4\times10^{-5}$	2.1×10^{-7}	1.5×10^{-6}

[a]Upper limit (95% confidence).

B. Radiative ω decays

The rates for radiative meson decays can be calculated from the naive quark model using SU(3) and the OZI rule (O'Donnell, 1981). Assuming ideal mixing in the vector nonet, one finds, neglecting the small difference between u and d quark masses,

$$\frac{B(\omega\to\eta\gamma)}{B(\omega\to\pi^0\gamma)}=\frac{1}{9}\frac{p_\eta^3}{p_{\pi^0}^3}\cos^2(54.7°+\theta_p)=0.010, \qquad (32)$$

where $p_\pi=379\mathrm{MeV}/c$ and $p_\eta=199\ \mathrm{MeV}/c$ are the decay momenta in the ω rest frame and θ_p is the pseudoscalar mixing angle (Amsler *et al.,* 1992b). However, the production and decay of the ω and ρ mesons are coupled by the isospin-breaking ω to ρ transition, since these mesons overlap (for references on $\rho-\omega$ mixing, see O'Connell *et al.,* 1995). Since the width of ρ is much larger than the width of ω, the effect of $\rho-\omega$ mixing is essential in processes where ρ production is larger than ω production, for example, in e^+e^- annihilation where ω and ρ are produced with a relative rate of 1/9. The determination of the branching ratio for $\omega\to\eta\gamma$ varies by a factor of 5 depending on whether the interference between $\omega\to\eta\gamma$ and $\rho^0\to\eta\gamma$ is constructive or destructive (Dolinsky *et al.,* 1989). A similar effect is observed in photoproduction (Andrews *et al.,* 1977). The GAMS Collaboration has determined the $\omega\to\eta\gamma$ decay branching ratio, $(8.3\pm2.1)\times10^{-4}$, using the reaction $\pi^-p\to\omega n$ at large momentum transfers, thus suppressing ρ production (Alde *et al.,* 1994).

In $\bar{p}p$ annihilation at rest the branching ratio for $\pi^0\omega$ is much smaller than the branching ratio for $\pi^0\rho^0$, while the converse is true for $\eta\omega$ and $\eta\rho^0$ (Table II). We therefore expect that a determination of the $\omega\to\eta\gamma$ branching ratio from $\pi^0\omega$, neglecting $\rho-\omega$ mixing, will lead to a larger value than from $\eta\omega$. However, a simultaneous analysis of both branching ratios, including $\rho-\omega$ mixing, should lead to consistent results and allow a determination of the relative phase between the two amplitudes.

In Abele *et al.* (1997b) the channels $\pi^0\omega$ and $\eta\omega$ ($\omega\to\eta\gamma$) were reconstructed from 15.5 million zero-prong events with five detected γ's. The events were submitted to a six-constraint kinematic fit assuming total energy and total momentum conservation, at least one $\pi^0\to2\gamma$ (or one $\eta\to2\gamma$), and $\omega\to3\gamma$. The $\omega\to3\gamma$ Dalitz plots for $\pi^0\omega$ and $\eta\omega$ are shown in Fig. 12, using the variables

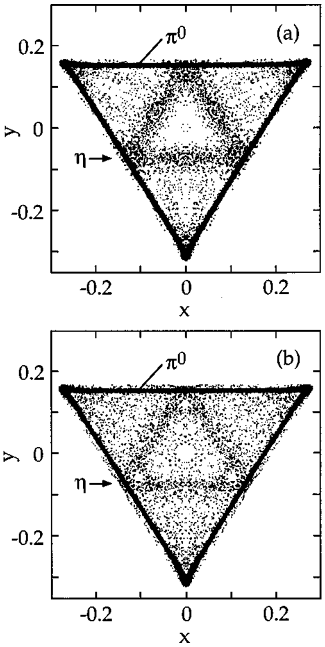

FIG. 12. $\omega\to 3\gamma$ Dalitz plots (a) for $\pi^0\omega$ events (62 853 events, six entries/event); (b) for $\eta\omega$ events (54 865 events, six entries/event).

$$x=\frac{T_2-T_1}{\sqrt{3}Q},\quad y=\frac{T_3}{Q}-\frac{1}{3}, \tag{33}$$

where T_1, T_2, and T_3 are the kinetic energies of the γ's in the ω rest frame and $Q=T_1+T_2+T_3$. The prominent bands along the boundaries are due to $\omega\to\pi^0\gamma$ and the weaker bands around the center to $\omega\to\eta\gamma$.

The main background contributions arose from 6γ events ($\bar{p}p\to 3\pi^0, 2\pi^0\eta, 2\eta\pi^0$) with a missing photon. This background (10% in the $\pi^0\omega$ and 5% in the $\eta\omega$ Dalitz plots) was simulated using the three pseudoscalar distributions discussed in Sec. VIII and could be reduced with appropriate cuts (Pietra, 1996). After removal of the π^0 bands, $147\pm 25\omega\to\eta\gamma$ events were found in the η bands, of Fig. 12(a) and 123 ± 19 events in the η bands of Fig. 12(b).

The branching ratio for $\omega\to\eta\gamma$ was derived by normalizing on the known branching ratio for $\omega\to\pi^0\gamma$, (8.5 ± 0.5)% (Barnett *et al.,* 1996). Correcting for the reconstruction efficiency, Abele *et al.* (1997b) found a branching ratio of $(13.1\pm 2.4)\times 10^{-4}$ from $\pi^0\omega$ and $(6.5\pm 1.1)\times 10^{-4}$ from $\eta\omega$, hence a much larger signal from $\pi^0\omega$.

Consider now the isospin-breaking electromagnetic $\rho-\omega$ transition. The amplitude S for the reaction $\bar{p}p\to X(\rho-\omega)\to X\eta\gamma$ is, up to an arbitrary phase factor (Goldhaber, Fox, and Quigg, 1969),

$$S=\frac{|A_\rho||T_\rho|}{P_\rho}\left(1-\frac{|A_\omega|}{|A_\rho|}\frac{e^{i\alpha}\delta}{P_\omega}\right)+e^{i(\alpha+\phi)}\frac{|A_\omega||T_\omega|}{P_\omega}\left(1-\frac{|A_\rho|}{|A_\omega|}\frac{e^{-i\alpha}\delta}{P_\rho}\right), \tag{34}$$

where A is the production and T the decay amplitude of the two mesons and $P_\rho\equiv m-m_\rho+i\Gamma_\rho/2$, $P_\omega\equiv m-m_\omega+i\Gamma_\omega/2$. The parameter δ was determined from $\omega,\rho\to\pi^+\pi^-$: $\delta=(2.48\pm 0.17)$ MeV (Weidenauer *et al.,* 1993). The relative phase between the production amplitudes A_ρ and A_ω is α, while the relative phase between the decay amplitudes T_ρ and T_ω is ϕ. In the absence of $\rho-\omega$ interference ($\delta=0$), Eq. (34) reduces to a sum of two Breit-Wigner functions with relative phase $\alpha+\phi$. The magnitudes of the amplitudes A and T are proportional to the production branching ratios and the partial decay widths, respectively.

The production phase α can be determined from $\rho,\omega\to\pi^+\pi^-$ since the isospin-violating decay amplitude $T(\omega\to\pi^+\pi^-)$ may be neglected, leaving only the first term in Eq. (34). A value for α consistent with zero, $(-5.4\pm 4.3)°$, was measured by Crystal Barrel, using the channel $\bar{p}p\to\eta\pi^+\pi^-$ where $\rho-\omega$ interference was observed directly (Abele *et al.,* 1997a). This phase is indeed predicted to be zero in e^+e^- annihilation, in photoproduction, and also in $\bar{p}p$ annihilation (Achasov and Shestakov, 1978).

With the branching ratios for $\omega\pi^0$, $\omega\eta$, $\pi^0\rho^0$, and $\eta\rho^0$ given in Table II the intensity $|S|^2$ was fitted to the number of observed $\omega\to\eta\gamma$ events in $\omega\pi^0$ and $\omega\eta$, using Monte Carlo simulation. Both channels led to consistent results for

$$B(\omega\to\eta\gamma)=(6.6\pm 1.7)\times 10^{-4}, \tag{35}$$

in agreement with the branching ratio from $\omega\eta$, obtained by neglecting $\rho-\omega$ interference. The phase $\phi=(-20^{+70}_{-50})°$ leads to constructive interference. The result of Eq. (35) is in excellent agreement with Alde *et al.* (1994) and with the constructive interference solution in e^+e^-, $(7.3\pm 2.9)\times 10^{-4}$ (Dolinsky *et al.,* 1989). This then solves the longstanding ambiguity in e^+e^- annihilation between the constructive ($\phi=0$) and destructive ($\phi=\pi$) interference solutions. The branching ratio for $\rho^0\to\eta\gamma$, $(12.2\pm 10.6)\times 10^{-4}$, is not competitive but agrees with results from e^+e^-, $(3.8\pm 0.7)\times 10^{-4}$ for constructive interference (Andrews *et al.,* 1977 and Dolinsky *et al.,* 1989). Using Eq. (32) one then finds

$$\frac{B(\omega\to\eta\gamma)}{B(\omega\to\pi^0\gamma)}=(7.8\pm 2.1)\times 10^{-3}, \tag{36}$$

in agreement with the SU(3) prediction.

The $\omega\to 3\gamma$ Dalitz plot is also useful to search for the direct process $\omega\to 3\gamma$, which is similar to the decay of ($^3S_1$) orthopositronium into 3γ and has not been observed so far. By analogy, the population in the $\omega\to 3\gamma$ Dalitz plot is expected to be almost homogeneous except for a slight increase close to its boundaries (Ore and Powell, 1949). Using the central region in Fig. 12(a), which contains only one event (6 entries), one obtains the upper limit $B(\omega\to 3\gamma)=1.9\times 10^{-4}$ at 95% confidence level. This is somewhat more precise that the previous upper limit, 2×10^{-4} at 90% confidence level (Prokoshkin and Samoilenko, 1995).

C. $\eta' \to \pi^+\pi^-\gamma$

The $\pi^+\pi^-\gamma$ decay mode of the η' is generally believed to proceed through the $\rho(770)\gamma$ intermediate state (Barnett *et al.,* 1996). However, the ρ mass extracted from a fit to the $\pi^+\pi^-$ mass spectrum appears to lie some 20 MeV higher than for ρ production in e^+e^- annihilations. This effect is due to the contribution of the direct decay into $\pi^+\pi^-\gamma$ (Bityukov *et al.,* 1991) through the so-called box anomaly (Benayoun *et al.,* 1993). Crystal Barrel studied the $\eta' \to \pi^+\pi^-\gamma$ channel where the η' was produced from the annihilation channels $\pi^0\pi^0\eta'$, $\pi^+\pi^-\eta'$, and $\omega\eta'$ (Abele *et al.,* 1997g). Evidence for the direct decay was confirmed at the 4σ level by fitting the $\pi^+\pi^-$ mass spectrum from a sample of 7,392 η' decays. Including contributions from the box anomaly, the ρ mass turned out to be consistent with the standard value from e^+e^- annihilation. Using the known two-photon decay widths of η and η' and the $\eta \to \pi^+\pi^-\gamma$ decay spectrum from Layter *et al.* (1973), the collaboration derived the pseudoscalar nonet parameters $f_\pi/f_1 = 0.91 \pm 0.02$, $f_8/f_\pi = 0.90 \pm 0.05$. This result is in accord with nonet symmetry ($f_1 = f_8$). The pseudoscalar mixing angle $\theta_p = (-16.44 \pm 1.20)^\circ$ agrees with the Crystal Barrel result $\theta_p = (-17.3 \pm 1.8)^\circ$ (Amsler *et al.,* 1992b).

D. Search for light gauge bosons in pseudoscalar meson decays

Extensions of the standard model allow additional gauge bosons, some of which could be light enough to be produced in the decay of pseudoscalar mesons (Dobroliubov and Ignatiev, 1988). Radiative decays $\pi^0, \eta, \eta' \to \gamma X$ are particularly suitable since they are sensitive only to gauge bosons X with quantum numbers $J^P = 1^-$. Branching ratios are predicted to lie in the range 10^{-7} to 10^{-3} (Dobroliubov, 1990). Experimental upper limits for $\pi^0 \to \gamma X$ are of the order 5×10^{-4} for long-lived gauge bosons with lifetime $\tau > 10^{-7}$ s (Atiya *et al.,* 1992). Short-lived gauge bosons decaying subsequently to e^+e^- are not observed with an upper limit of 4×10^{-6} (Meijer Drees *et al.,* 1992).

Crystal Barrel searched for radiative decays where X was a long-lived weakly interacting gauge boson escaping from the detector without interaction, or decaying to $\nu\bar{\nu}$. The search was performed using the reactions $\bar{p}p \to 3\pi^0$, $\pi^0\pi^0\eta$, and $\pi^0\pi^0\eta'$ at rest (Amsler *et al.,* 1994a, 1996a), which occur with a sufficiently high probability (see Table IX below) and are kinematically well constrained. Events with five photons were selected from a sample of 15 million annihilations into neutral final states (18 million for η' decays). Since the branching ratio for zero-prong annihilation (i.e., only into neutral particles in the final state) is about 4%, the data sample corresponds to some 400 million $\bar{p}p$ annihilations in liquid hydrogen.

Events consistent with $\pi^0\pi^0$ decays and a single (unpaired) γ were then selected by requiring energy and momentum conservation for $\bar{p}p$ annihilation into $\pi^0\pi^0\pi^0$, $\pi^0\pi^0\eta$, or $\pi^0\pi^0\eta'$ with a missing π^0, η, or η'. Thus three-constraint kinematic fits were applied, ignoring the remaining fifth photon. The measured energy of the latter was then transformed into the rest frame of the missing pseudoscalar. In this frame a missing state X with mass m_X would produce a peak in the γ-energy distribution at

$$E^*_\gamma = \frac{m}{2}\left(1 - \frac{m_X^2}{m^2}\right), \tag{37}$$

with width determined by the experimental resolution, where m is the mass of the missing pseudoscalar. Thus, if X is simply a missing (undetected) γ from π^0, η, or η' decay, one finds with $m_X = 0$ that $E^*_\gamma = m/2$, as expected.

The main source of background is annihilation into three pseudoscalars, for which one of the photons escaped detection. This occurs for (i) photons with energies below detection threshold ($E < 20$ MeV) or (ii) for photons emitted into insensitive areas of the detector. The latter background can be reduced by rejecting events for which the missing γ could have been emitted, e.g., in the holes along the beam pipe. The high efficiency and large angular coverage of the Crystal Barrel are therefore crucial in this analysis. For the $3\pi^0$ channel an important background also arose from $\bar{p}p \to \pi^0\omega$ with $\omega \to \pi^0\gamma$, leading to 5γ. This background could be reduced by rejecting events that satisfied the $\pi^0\omega(\to \pi^0\gamma)$ kinematics. For $\pi^0\pi^0\eta$, the background channel $K_S(\to 2\pi^0)K_L$ with an interacting K_L faking a missing η could be eliminated with appropriate kinematic cuts.

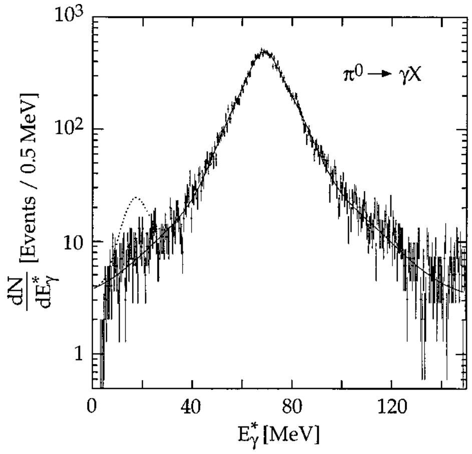

FIG. 13. Energy distribution (24 503 events) of the single γ in the missing π^0 rest frame for events satisfying the kinematics $\bar{p}p \to 2\pi^0$ and a missing π^0. The solid line is a fit. The dotted curve shows the expected signal for a branching ratio of 5×10^{-4}.

The E^*_γ energy distribution for π^0 decay is shown in Fig. 13. The broad peak around 70 MeV is due to π^0 decays into 2γ, where one γ has escaped detection, or from residual $\pi^0\omega$ events. The fit to the distribution (solid line) agrees with the simulated rate of background

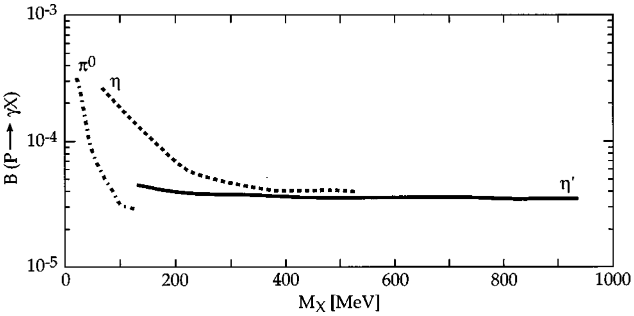

FIG. 14. Upper limits (90% confidence level) for radiative pseudoscalar decays as a function of missing mass.

from $3\pi^0$ and $\pi^0\omega$. The dotted line shows the expected signal for a state with mass $m_X=120$ MeV, produced in π^0 decay with a branching ratio of 5×10^{-4}. The corresponding distributions for η and η' decays can be found in Amsler *et al.* (1996a).

Upper limits for radiative decays are given in Fig. 14 as a function of m_X. The upper limit for π^0 decay is an order of magnitude lower than from previous experiments (Atiya *et al.,* 1992). For η and η' decays no limits were available previously. Light gauge bosons were therefore not observed in radiative pseudoscalar decays at a level of 10^{-4} to 10^{-5}.

E. $\eta\to3\pi$

The 3π decay of the η plays an important role in testing low-energy QCD predictions. This isospin-breaking decay is mainly due to the mass difference between u and d quarks. Crystal Barrel measured the relative branching ratios for $\eta\to\pi^+\pi^-\pi^0$, $\eta\to3\pi^0$, and $\eta\to2\gamma$ from samples of annihilations into $2\pi^+2\pi^-\pi^0$, $\pi^+\pi^-3\pi^0$, and $\pi^+\pi^-2\gamma$, respectively (Amsler *et al.,* 1995d). The ratios of partial widths are

$$r_1\equiv\frac{\Gamma(\eta\to3\pi^0)}{\Gamma(\eta\to\pi^+\pi^-\pi^0)}=1.44\pm0.13,$$

$$r_2\equiv\frac{\Gamma(\eta\to2\gamma)}{\Gamma(\eta\to\pi^+\pi^-\pi^0)}=1.78\pm0.16. \tag{38}$$

The result for r_1 is in good agreement with chiral perturbation theory: 1.43 ± 0.03 (Gasser and Leutwyler, 1985) and 1.40 ± 0.03 when taking unitarity corrections into account (Kambor, Wiesendanger, and Wyler, 1996). With the known 2γ partial width (Barnett *et al.,* 1996) one can calculate from r_2 the partial width $\Gamma(\pi^+\pi^-\pi^0)=258\pm32$ eV, in accord with chiral perturbation theory ($\Gamma=230$ eV), taking into account corrections to the $u-d$ mass difference (Donoghue, Holstein, and Wyler, 1992). In good approximation, the $\eta\to\pi^+\pi^-\pi^0$ Dalitz plot may be described by the matrix element squared,

$$|M(x,y)|^2\propto1+ay+by^2, \tag{39}$$

with

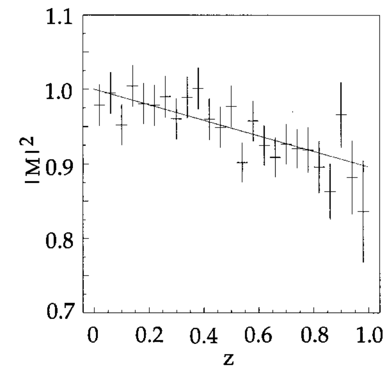

FIG. 15. Squared matrix element for $\eta\to3\pi^0$. The straight line shows the fit according to Eq. (42).

$$y\equiv\frac{3T_0}{m(\eta)-m(\pi^0)-2m(\pi^\pm)}-1, \tag{40}$$

where T_0 is the kinetic energy of the neutral pion. The parameters a and b were determined by Amsler *et al.* (1995d), but more accurate values are now available from the annihilation channel $\bar{p}p\to\pi^0\pi^0\eta$. Abele *et al.* (1998b) find

$$a=-1.19\pm0.07,\quad b=0.19\pm0.11, \tag{41}$$

in reasonable agreement with chiral perturbation calculations which predict $a=-1.3$ and $b=0.38$ (Gasser and Leutwyler, 1985).

The matrix element for η decay to $3\pi^0$ is directly connected to the matrix element for the charged mode because $3\pi^0$ is an $I=1$ state. The matrix element squared for η decay to $3\pi^0$ is given by

$$|M(z)|^2=1+2\alpha z, \tag{42}$$

where z is the distance from the center of the $\eta\to3\pi^0$ Dalitz plot,

$$z=\frac{2}{3}\sum_{i=1}^{3}\left[\frac{3E_i-m(\eta)}{m(\eta)-3m(\pi^0)}\right]^2, \tag{43}$$

and where E_i are the total energies of the pions. Experiments have so far reported values for α compatible with zero, e.g., Alde *et al.* (1984) find -0.022 ± 0.023.

Crystal Barrel analyzed the $3\pi^0$ Dalitz plot with 98 000 η decays from the annihilation channel $\pi^0\pi^0\eta$, leading to ten detected photons (Abele *et al.,* 1998c). The background and acceptance corrected matrix element is shown in Fig. 15 as a function of z. The slope is

$$\alpha=-0.052\pm0.020. \tag{44}$$

Chiral perturbation theory up to next-to-leading order predicts α to be zero (Gasser and Leutwyler, 1985), leading to a homogeneously populated Dalitz plot. Taking unitarity corrections into account, Kambor, Wiesendanger, and Wyler (1996) predict a negative value, $\alpha=-0.014$. The Crystal Barrel result is somewhat at variance with the value advocated by theory. Given the large experimental error, a more accurate value would be useful to measure the quark masses as well. Unlike a

and b in Eq. (41), the slope α provides a rather sensitive probe of chiral perturbation theory (Wyler, 1998).

VI. PRODUCTION OF ϕ MESONS

It has been known for some time that ϕ production is enhanced beyond expectation from the OZI rule in various hadronic reactions (Cooper *et al.,* 1978). Let us return to Eq. (21) and replace η by ϕ and η' by ω. The mixing angle becomes the mixing angle θ_v in the vector nonet. According to the OZI rule, ϕ and ω can only be produced through their $u\bar{u}+d\bar{d}$ components. Hence ϕ production should vanish for an ideally mixed vector nonet ($\theta_v=\theta_i$) in which ϕ is purely $s\bar{s}$. Since ϕ also decays to 3π, this is not quite the case, and we find for the ratio of branching ratios, with a recoiling meson X and apart from phase-space corrections,

$$\tilde{R}_X=\frac{\tilde{B}(X\phi)}{\tilde{B}(X\omega)}=\tan^2(\theta_i-\theta_v)=4.2\times10^{-3}\quad\text{or}\quad 1.5\times10^{-4}, \tag{45}$$

for the quadratic ($\theta_v=39°$) or linear ($\theta_v=36°$) Gell-Mann-Okubo mass formula (Barnett *et al.*, 1996).

The branching ratios for $\bar{p}n$ annihilation into $\pi^-\phi$ and $\pi^-\omega$ have been measured in deuterium bubble chambers. The ratio $\tilde{R}_{\pi^-}$ lies in the range 0.07 to 0.22, indicating a strong violation of the OZI rule (for a review, see Dover and Fishbane, 1989). The Asterix experiment at LEAR measured ϕ production in $\bar{p}p$ annihilation into $\pi^0\phi$, $\eta\phi$, $\rho^0\phi$, and $\omega\phi$ in gaseous hydrogen at standard temperature and pressure (STP) (50% P-wave annihilation) and in coincidence with atomic L x-rays (P-wave annihilation). The branching ratios for pure S wave were then obtained indirectly by linear extrapolation (Reifenröther *et al.,* 1991). With the corresponding ω branching ratios, then available from literature, the authors reported a strong violation of the OZI rule, especially for $\pi^0\phi$. Some of the branching ratios from Crystal Barrel were, however, in disagreement with previous results. We shall therefore review the direct measurement of ϕ production in liquid from Crystal Barrel and then reexamine the evidence for OZI violation with the two-body branching ratios listed in Table II.

A. Annihilation into $\pi^0\phi$, $\eta\phi$, and $\gamma\phi$

Crystal Barrel studied the channels

$$\bar{p}p\to K_SK_L\pi^0\quad\text{and}\quad K_SK_L\eta, \tag{46}$$

where K_S decays to $\pi^0\pi^0$ and η to $\gamma\gamma$, leading to six photons and a missing (undetected) K_L (Amsler *et al.,* 1993d). The starting data sample consisted of 4.5×10^6 zero-prong annihilations. By imposing energy and momentum conservation, it was possible to apply a five-constraint kinematic fit to the masses of the three reconstructed pseudoscalar mesons and the K_S mass, leading to 2834 $K_SK_L\pi^0$ and 72 $K_SK_L\eta$ events with an estimated background of 4% and 36%, respectively.

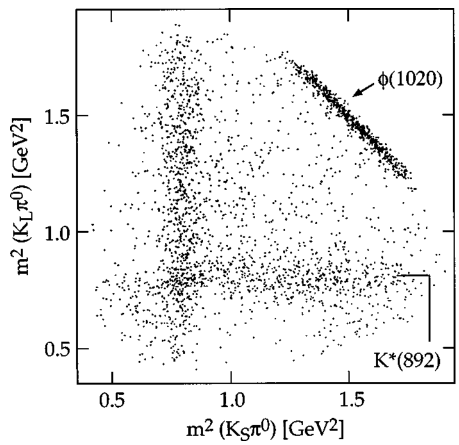

FIG. 16. Dalitz plot of the final state $K_SK_L\pi^0$ (2834 events).

The $K_SK_L\pi^0$ Dalitz plot is shown in Fig. 16. One observes the production of $K^*(892)$ ($\to K\pi$) and $\phi(\to K_SK_L)$. A Dalitz plot analysis was performed with the method described in Sec. VII.B. Since the C parity of K_SK_L is negative[5] the contributing initial atomic S state is $^3S_1$. One obtains a good fit to the Dalitz plot with only two amplitudes, one for $K^*\bar{K}$ (and its charge-conjugated $K\bar{K}^*$, which interferes constructively) and one for $\pi^0\phi$ with a relative contribution to the $K_SK_L\pi^0$ channel of

$$\frac{K^*\bar{K}+K\bar{K}^*}{\pi^0\phi}=2.04\pm0.21. \tag{47}$$

The final state $K_SK_L\eta$ is much simpler, since only $\eta\phi$ contributes (Amsler *et al.,* 1993d). One obtains by comparing the intensities for $\pi^0\phi$ and $\eta\phi$

$$\frac{B(\pi^0\phi)}{B(\eta\phi)}=8.3\pm2.1, \tag{48}$$

taking into account the unobserved decay modes of the η meson.

Events with a K_L interacting in the CsI crystals were removed by the selection procedure, which required exactly six clusters in the barrel. The last two results therefore assume that the interaction probability for K_L in CsI does not vary significantly with K_L momentum. Therefore this interaction probability needs to be determined to derive absolute branching ratios for $\pi^0\phi$ and $\eta\phi$. This number cannot be obtained directly by Monte Carlo simulation due to the lack of data for low-energy K_L interacting with nuclear matter. With monoenergetic (795 MeV/c) K_L from the channel $\bar{p}p\to K_SK_L$, Amsler *et al.* (1995c) found an interaction probability of (57 ± 3)% in the CsI barrel. This led to a branching ratio

[5]Note that $K^0\overline{K^0}$ recoiling against π^0 appears as $K_SK_S + K_LK_L$ (J^{PC} = even^{++}) from $^1S_0$ and as K_SK_L (J^{PC} = odd^{--}) from $^3S_1$.

TABLE VI. Branching ratios for ϕ production at rest in liquid.

Channel					Reference
$\pi^0\phi$	6.5	±	0.6	10^{-4}	[a]‡
$\pi^0\phi$	3.0	±	1.5	10^{-4}	Chiba *et al.* (1988)
$\pi^0\phi$	4.0	±	0.8	10^{-4}	Reifenröther *et al.* (1991) [b, c]
$\eta\phi$	7.8	±	2.1	10^{-5}	Amsler *et al.* (1995c)‡
$\eta\phi$	3.0	±	3.9	10^{-5}	Reifenröther *et al.* (1991) [b]
$\eta\phi$	7.6	±	3.1	10^{-5}	Albernico *et al.* (1998)
$\omega\phi$	6.3	±	2.3	10^{-4}	Bizzarri *et al.* (1971)
$\omega\phi$	5.3	±	2.2	10^{-4}	Reifenröther *et al.* (1991) [b, d]
$\rho^0\phi$	3.4	±	1.0	10^{-4}	Reifenröther *et al.* (1991) [b]
$\gamma\phi$	2.0	±	0.4	10^{-5}	[a]‡

Header: B spans the value columns.

[a]Updates Amsler *et al.* (1995c).
[b]Annihilation in gas extrapolated to pure S-wave annihilation.
[c]Using Chiba *et al.* (1988) in liquid.
[d]Using Bizzarri *et al.* (1971) in liquid.
‡Crystal Barrel experiment.

of $(9.0\pm0.6)\times10^{-4}$ for K_SK_L, in agreement with bubble-chamber data (Table II).

An average interaction probability of (54 ± 4)% was measured with the kinematically well-constrained annihilation channel $K_S(\rightarrow\pi^+\pi^-)K_L\pi^0$ (Abele *et al.,* 1998d). However, Amsler *et al.* (1995c) used a somewhat lower probability. Updating their $\pi^0\phi$ branching ratio one finds, together with their compatible result from $\pi^0(\phi\rightarrow K^+K^-)$,

$$B(\bar{p}p\rightarrow\pi^0\phi)=(6.5\pm0.6)\times10^{-4}. \tag{49}$$

From Eq. (48) one then obtains

$$B(\bar{p}p\rightarrow\eta\phi)=(7.8\pm2.1)\times10^{-5}. \tag{50}$$

Both numbers are slightly higher than those from indirect data in gaseous hydrogen, which were extrapolated to pure S-wave annihilation (Reifenröther *et al.,* 1991), but $\eta\phi$ agrees with a recent measurement in liquid (Alberico *et al.*, 1998); see Table VI.

Radiative annihilation into ϕ mesons should be suppressed by both the OZI rule and the electromagnetic coupling. Crystal Barrel studied the channel $\gamma\phi$ with the reactions (Amsler *et al.,* 1995c)

$$\bar{p}p\rightarrow K_SK_L\gamma \text{ and } K^+K^-\gamma. \tag{51}$$

In the first reaction K_S decays to $\pi^0\pi^0$, K_L is not detected, and thus the final state consists of five photons. The $K_SK_L\gamma$ final state was selected from 8.7×10^6 zero-prong annihilations by performing a four-constraint fit, imposing energy and momentum conservation, the masses of the two pions, and the K_S mass. The background reaction $\bar{p}p\rightarrow K_SK_L$ with an interacting K_L faking the fifth photon could easily be suppressed, since K_L and K_S are emitted back-to-back. The experimental $K_SK_L\gamma$ Dalitz plot is dominated by background from $K_SK_L\pi^0$ with a missing (undetected) low-energy γ from π^0 decay and is therefore similar to the one shown in Fig. 16. The background contribution to $\gamma\phi$, mainly from $\pi^0\phi$ with a missing photon, was estimated by Monte Carlo simulation and by varying the photon detection threshold. This led to 211 ± 41 $\gamma\phi$ events corresponding to a branching ratio $B(\gamma\phi)=(2.0\pm0.5)\times10^{-5}$, after correcting for the (updated) K_L interaction probability.

A sample of 1.6×10^6 two-prong annihilations was used to select the second reaction in Eq. (51). After a cut on energy and momentum conservation (assuming kaons), the measured ionization loss in the jet drift chamber was used to separate kaons from pions. Again, the dominating background to $\gamma\phi$ arose from $\pi^0\phi$ with a missing γ. This background was subtracted by varying the γ detection threshold and by keeping only γ's with energies around 661 MeV, as required by two-body kinematics. The signal of 29 events led to a branching ratio $B(\gamma\phi)=(1.9\pm0.7)\times10^{-5}$, which is less precise but in good agreement with data from the neutral mode. The average is then

$$B(\bar{p}p\rightarrow\phi\gamma)=(2.0\pm0.4)\times10^{-5}, \tag{52}$$

which updates the result from Amsler *et al.* (1995c).

TABLE VII. Ratio of ϕ to ω production in low-energy annihilation in liquid.

X	$\tilde{R}_X[10^{-2}]$		
γ	29.4	±	9.7
π^0	10.6	±	1.2
η	0.46	±	0.13
ω	1.02	±	0.39
ρ^0	1.57	±	0.49
π^-	13.0	±	2.5
π^+	10.8	±	1.5
σ	1.75	±	0.25
$\pi^+\pi^-$	1.65	±	0.35

B. ϕ/ω ratio

Table VII and Fig. 17 show the phase-space-corrected ratios $\tilde{R}_X$ [Eq. (45)]. The nearest threshold dominance

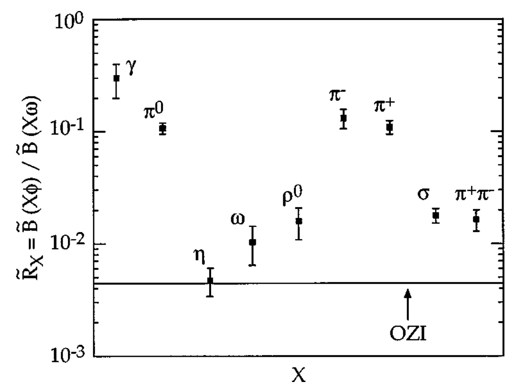

FIG. 17. Ratio of ϕ to ω production in low-energy annihilation. The measured branching ratios have been divided by the factor W, Eq. (13). The expectation from the OZI rule using the quadratic mass formula (4.2×10^{-3}) is shown by the horizontal line.

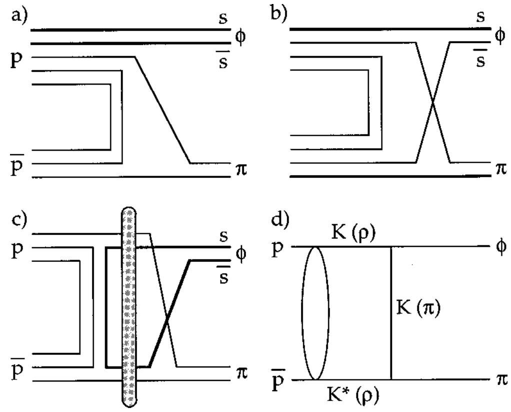

FIG. 18. OZI-allowed ϕ production with $s\bar{s}$ pairs in the nucleon: (a) shakeout mechanism; (b) OZI-allowed rearrangement process; (c) an intermediate four-quark state excited below threshold. The production of ϕ mesons can also be enhanced by final-state rescattering, $K^*\bar{K}\to\pi\phi$ or $\rho\rho\to\pi\phi$ (d).

factors [Eq. (13)] have been used, but the measured ratios do not differ significantly from $\tilde{R}_X$. Phase-space factors of the type (28) lead to even larger ratios. For $X=\gamma,\pi^0,\eta$ we used Crystal Barrel data. For $X=\omega$ we used for $\omega\omega$ the branching ratio from Crystal Barrel (multiplied by two for identical particles), and for $\omega\phi$ the branching ratio from Bizzarri *et al.* (1971) (Table VI). For completeness we also list the result for $X=\rho$ from Reifenröther *et al.* (1991) and Bizzarri *et al.* (1969), as well as the recent Obelix data for R_{π^-} (Ableev *et al.,* 1995) and R_{π^+} (Ableev *et al.,* 1994) in $\bar{p}n$ and $\bar{n}p$ annihilation.

Annihilation into $\omega\pi^0\pi^0$ and $\phi(\to K_LK_S)\pi^0\pi^0$ can be used to extract the ratio $\tilde{R}_\sigma$ (Spanier, 1997), where σ stands for the low-energy $(\pi\pi)$ S wave up to 900 MeV (Sec. VIII.D). Finally, the ratio $R_{\pi^+\pi^-}$ was also measured in $\bar{p}p$ at rest (Bertin *et al.,* 1996). Table VII and Fig. 17 show their result for $\pi^+\pi^-$ masses between 300 and 500 MeV.

The production of ϕ mesons is enhanced in all channels except $\eta\phi$ and is especially dramatic in $\gamma\phi$ (from $^1S_0$) and $\pi^0\phi$ (from $^3S_1$). Several explanations for this effect have been proposed:

(i) High-energy reactions reveal the presence of sea $s\bar{s}$ quark pairs in the nucleon at high momentum transfers but valence $s\bar{s}$ pairs could enhance the production of ϕ mesons already at small momentum transfers. Figure 18 shows the OZI-allowed production of $s\bar{s}$ mesons through the shakeout mechanism (a) and through the OZI-allowed rearrangement process (b) (Ellis *et al.,* 1995). The fraction of $s\bar{s}$ pairs in the nucleon required to explain the measured $\pi^0\phi$ rate lies between 1% and 19%. Deep-inelastic muon scattering data indicate an $s\bar{s}$ polarization opposite to the spin of the nucleon (Ellis *et al.,* 1995). For annihilation from the $^3S_1$ state the wave function of the $(^3S_1)$ $s\bar{s}$ would match the wave function of the ϕ in the rearrangement process of Fig. 18(b), leading to an enhanced production of ϕ mesons. The absence of enhancement in $\eta\phi$ could be due to destructive interference between additional graphs arising from the $s\bar{s}$ content of η. However, this model does not explain the large branching ratios for the two-vector channels $\rho^0\phi$, $\omega\phi$, and especially $\gamma\phi$, which proceed from the $^1S_0$ atomic state.

In the tensor nonet, the mainly $s\bar{s}$ meson is $f_2'(1525)$, while $f_2(1270)$ is the one mainly composed of $u\bar{u}+d\bar{d}$ quarks. Using annihilation into $K_LK_L\pi^0$ and $3\pi^0$ (Sec. VIII), Crystal Barrel measured the ratio of $f_2'(1525)\pi^0$ to $f_2(1270)\pi^0$ from $^1S_0$. After dividing by W [Eq. (13)] one finds, with the most recent branching ratio for $f_2'(1525)$ decay to $K\bar{K}$ from Barnett *et al.* (1996), see Table XIII below,

$$\frac{\tilde{B}(\bar{p}p\to f_2'(1525)\pi^0)}{\tilde{B}(\bar{p}p\to f_2(1270)\pi^0)}=\tan^2(\theta_i-\theta_t)$$
$$=(2.6\pm1.0)\times10^{-2}. \tag{53}$$

The mixing angle θ_t in the 2^{++} nonet is found to be $(26.1^{+2.0}_{-1.6})^\circ$, in good agreement with the linear (26°) or quadratic (28°) mass formulae (Barnett *et al.,* 1996). There is therefore no OZI-violating $s\bar{s}$ enhancement from $f_2'(1525)\pi^0$ in liquid hydrogen.

(ii) Dover and Fishbane (1989) suggest that the $\pi^0\phi$ enhancement is due to mixing with a four-quark state $(s\bar{s}q\bar{q})$ with mass below $2m_p$ [Fig. 18(c)]. This exotic meson would then have the quantum numbers of the $\bar{p}p$ initial state ($^3S_1=1^{--}$ with $I=1$), which would also explain why $\eta\phi$ $(I=0)$ is not enhanced and why $\pi^0\phi$ is weak from $^1P_1$ (Reifenröther *et al.,* 1991). A 1^{--} state, $C(1480)\to\pi\phi$, has in fact been reported in $\pi^-p\to\pi^0\phi n$ (Bityukov *et al.*, 1987). This isovector state cannot be of $q\bar{q}$ structure since it would decay mostly to $\pi\omega$, which is not observed. Indeed, Crystal Barrel did not find any $\pi^0\omega$ signal in this mass region in $\bar{p}p\to\pi^0\pi^0\omega$ at rest (Amsler *et al.,* 1993a). Moreover, $C(1480)$ has not been observed in $\bar{p}p$ annihilation at rest into $\pi^+\pi^-\phi$ (Reifenröther *et al.,* 1991) or into $\pi^0\pi^0\phi$ (Abele *et al.,* 1997c). In any case, the large $\gamma\phi$ signal with the "wrong" quantum numbers $^1S_0$ remains unexplained by this model.

(iii) We have seen in Eq. (47) that the $K\bar{K}\pi$ final state is dominated by $K^*\bar{K}$ production which proceeds dominantly from the $I=1$ $^3S_1$ state (see Sec. VIII.H). The ϕ enhancement could then be due to $K^*\bar{K}$ and $\rho\rho$ rescattering [Fig. 18(d)]. In Gortchakov *et al.* (1996) $K^*\bar{K}$ and $\rho\rho$ interfere constructively to produce a $\pi^0\phi$ branching ratio as high as 4.6×10^{-4}, nearly in agreement with experimental data. In the model of Locher, Lu, and Zou (1994) and Markushin (1997) the large $\gamma\phi$ branching ratio simply arises from the vector dominance model: The channels $\rho^0\omega$ and $\omega\omega$ interfere destructively in Eq. (30), thereby lowering the branching ratio for $\gamma\omega$, while $\rho^0\phi$ and $\omega\phi$ interfere constructively, thus increasing the branching ratio for $\gamma\phi$. This conclusion, however, depends strongly on the phase-space correction: Prescription (13) leads to a $\gamma\phi$ branching ratio that exceeds the OZI prediction by a factor of 10 (Table V). Also, as pointed out by Markushin (1997), the large $\rho^0\phi$ and $\omega\phi$ rates remain unexplained but could perhaps be accommodated within a two-step mechanism similar to the one shown in Fig. 18(d).

The origin of the ϕ enhancement is therefore not clear. If $I=1$ also dominates $\overline{p}p$ annihilation into $K^*\overline{K}$ from P states in gaseous hydrogen, then the rescattering model would presumably conflict with the weak $\pi\phi$ production observed from $^1P_1$ states (Reifenröther *et al.,* 1991). With strange quarks in the nucleon, the $^3S_1$ contribution and hence the contribution from $s\overline{s}$ pairs in the nucleon will be diluted by the large number of partial waves at higher $\overline{p}$ momenta. Hence ϕ production should decrease with increasing momentum. Also, the small $\eta\phi$ rate, possibly due to destructive interference, implies that $\eta'\phi$ should be abnormally large (Ellis *et al.,* 1995). Finally, since $f_2'(1525)$ is a spin-triplet meson, one would expect a strong production of $f_2'(1525)\pi^0$ from triplet $\overline{p}p$ states at rest, hence $^3P_1$ (Ellis *et al.,* 1995). The analysis of Crystal Barrel data in gaseous hydrogen and in flight will hopefully contribute to a better understanding of the ϕ enhancement in hadronic reactions.

VII. MESON SPECTROSCOPY

A. Introduction

Mesons made of light quarks u,d,s are classified within the $q\overline{q}$ nonets of SU(3) flavor. The ground states (angular momentum $L=0$), pseudoscalar (0^{-+}) and vector (1^{--}) mesons are well established. Among the first orbital excitations $(L=1)$, consisting of the four nonets 0^{++}, 1^{++}, 2^{++}, 1^{+-}, only the tensor (2^{++}) nonet is complete and unambiguous with the well-established $a_2(1320)$, $f_2(1270)$, $f_2'(1525)$, and $K_2^*(1430)$ mesons, but another tensor meson, $f_2(1565)$, was discovered at LEAR in the 1500-MeV mass range (May *et al.,* 1989).

Before Crystal Barrel, three scalar (0^{++}) states were already well established: $a_0(980)$, $f_0(980)$, and $K_0^*(1430)$. Further candidates have been reported, and we shall discuss the scalar states in more detail below. In the 1^{++} nonet two states compete for the $s\overline{s}$ assignment, $f_1(1420)$ and $f_1(1510)$. In the 1^{+-} nonet the $s\overline{s}$ meson is not established, although a candidate, $h_1(1380)$, has been reported (Aston *et al.,* 1988a; Abele *et al.,* 1997c, 1997d). Many of the radial and higher orbital excitations are still missing. Recent experimental reviews on light-quark mesons have been written by Blüm (1996) and Landua (1996) and theoretical predictions for the mass spectrum can be found in Godfrey and Isgur (1985).

Only overall color-neutral $q\overline{q}$ configurations are allowed by QCD, but additional colorless states are possible, among them multiquark mesons ($\overline{q}^2q^2$, $\overline{q}^3q^3$) and mesons made of $q\overline{q}$ pairs bound by an excited gluon g, the hybrid states (Barnes, Close, and deViron, 1983; Isgur and Paton, 1985; Close and Page, 1995). According to flux tube models, hybrid states cluster around 1.9 GeV (Isgur and Paton, 1985). Lattice QCD also predicts the lightest hybrid, a 1^{-+}, around 1.9 GeV (Lacock, Boyle, and Rowland, 1997). We shall show below (Sec. XI) that mesons with the quantum numbers 1^{-+} do not couple to $q\overline{q}$ and are therefore exotic. There are so far three prime candidates for hybrid mesons: the $\hat{\rho}(1405)$ with quantum numbers 1^{-+}, $\pi(1800)$, and $\eta_2(1870)$.

A striking prediction of QCD is the existence of isoscalar mesons that contain only gluons, the glueballs (for a recent experimental review, see Spanier, 1996). They are a consequence of the non-Abelian structure of QCD, which requires that gluons couple and hence may bind. The models predict low-mass glueballs with quantum numbers 0^{++}, 2^{++}, and 0^{-+} (Szczepaniak *et al.,* 1996). The ground-state glueball, a 0^{++} meson, is expected by lattice gauge theories to lie in the mass range 1500 to 1700 MeV. The mass of the pure gluonium state is calculated at 1550 ± 50 MeV by Bali *et al.* (1993), while Sexton, Vaccarino, and Weingarten (1995) predict a slightly higher mass of 1707 ± 64 MeV. The first excited state, a 2^{++}, is expected around 2300 MeV (Bali *et al.,* 1993).

Since the mass spectra of $q\overline{q}$, hybrids, and glueballs overlap, hybrids and glueballs are easily confused with ordinary $q\overline{q}$ states. This is presumably the reason why they have not yet been identified unambiguously. For pure gluonium one expects couplings of similar strengths to $s\overline{s}$ and $u\overline{u}+d\overline{d}$ mesons, since gluons are flavor blind. In contrast, $s\overline{s}$ mesons decay mainly to kaons and $u\overline{u}+d\overline{d}$ mesons mainly to pions. Hence decay rates to $\pi\pi$, $K\overline{K}$, $\eta\eta$, and $\eta\eta'$ can be used to distinguish glueballs from ordinary mesons. However, mixing with nearby $q\overline{q}$ states may modify the decay branching ratios (Amsler and Close, 1996; see also Amsler and Close, 1995) and obscure the nature of the observed state. Nevertheless, the existence of a scalar gluonium state, whether pure or mixed with $q\overline{q}$, is signaled by a third isoscalar meson in the 0^{++} nonet. It is therefore essential to complete the SU(3) nonets in the 1500–2000 MeV region and to identify supernumerary states. The most pressing questions to be addressed are as follows:

(1) What are the ground-state scalar mesons? In particular, is $f_0(980)$ the $s\overline{s}$ state and is $a_0(980)$ the isovector state or are these states $K\overline{K}$ molecules (Weinstein and Isgur, 1990; Close, Isgur, and Kumano, 1993), in which case the nonet members still need to be identified? Where are the first radial excitations and is there a supernumerary $I=0$ scalar meson in the 1500-MeV region? Is the $f_J(1710)$ a scalar or a tensor meson?

(2) Where are the hybrid states? Is the $\eta_2(1870)$ a hybrid and does the $\hat{\rho}(1405)$ really exist?

(3) In the 0^{-+} sector, are the $\eta(1295)$ and $\eta(1440)$ the two isoscalar radial excitations of η and η' or is

$\eta(1440)$ a structure containing several states (Bai *et al.*, 1990; Bertin *et al.*, 1995), in particular a non-$q\bar{q}$ state around 1400 MeV?

Before reviewing the new mesons discovered by Crystal Barrel and providing clues to some of these issues, we shall review the mathematical tools used to extract the mass, width, spin, and parity of intermediate resonances in $\bar{p}p$ annihilation at rest.

B. Spin-parity analysis

The Crystal Barrel data were analyzed using the isobar model, in which the $\bar{p}p$ system annihilates into N "stable" particles ($\pi^{\pm},K^{\pm},K^0,\pi^0,\eta,\eta'$) through intermediate resonances. The decay chain is assumed to be a succession of two-body decays $a\to bc$ followed by $b\to b_1b_2$ and $c\to c_1c_2$, etc. Final-state rescattering is ignored. We shall calculate from the N momentum vectors the probability w_D that the final state proceeds through a given cascade of resonances. The final state may be from real data or from phase-space distributed Monte Carlo events to be weighted by w_D.

The spins and parities of intermediate resonances are determined using the helicity formalism developed by Jacob and Wick (1959) or the equivalent method of Zemach tensors (Zemach, 1964, 1965). Here we describe briefly the helicity formalism. Suppose that a mother resonance with mass m_0 and spin J decays into two daughters (spins S_1 and S_2) with total spin S and relative angular momentum L. As quantization axis we choose the flight direction of the mother. The decay amplitude is given by the matrix (Amsler and Bizot, 1983)

$$A_{\lambda_1,\lambda_2;M}=D^J_{\lambda M}(\theta,\phi)\langle J\lambda|LS0\lambda\rangle \times\langle S\lambda|S_1S_2\lambda_1,-\lambda_2\rangle\times BW_L(m), \tag{54}$$

where the row index $\lambda=\lambda_1-\lambda_2$ runs over the $(2S_1+1)(2S_2+1)$ helicity states and the column index M over the $2J+1$ magnetic substates; θ and ϕ refer to the decay angles in the mother rest frame. The quantity $BW_L(m)$ is the Breit-Wigner amplitude[6]

$$BW_L(m)=\frac{m_0\Gamma_0}{m_0^2-m^2-im_0\Gamma(m)}F_L(p)\sqrt{\rho}, \tag{55}$$

where

$$\Gamma(m)=\Gamma_0\frac{m_0}{m}\frac{p}{p_0}\frac{F_L^2(p)}{F_L^2(p_0)}. \tag{56}$$

The mass and width of the resonance are m_0 and Γ_0, p is the two-body decay momentum, and p_0 is the decay momentum for $m=m_0$. The damping factors $F_L(p)$ are given in Table IV. The matrix D is given by

[6]The phase-space factor $\sqrt{\rho}=\sqrt{2p/m}$ should be dropped in Eq. (55) when events are drawn by Monte Carlo simulation, already assuming phase-space distribution.

$$D^J_{\lambda M}(\theta,\phi)=e^{iM\phi}d^J_{\lambda M}(\theta) \tag{57}$$

where the matrix $d^J_{\lambda M}(\theta)$ is the usual representation of a rotation around the y axis; see, for example, Barnett *et al.* (1996).

We shall describe the annihilation to the observed final state by a product of matrices A for successive decays in the cascade. Hence we first calculate from the N final-state momentum vectors the angles θ and ϕ for all resonances through a series of Lorentz boosts, apply Eq. (54) to each decay, and obtain the total amplitude through matrix multiplications, for example,

$$A=[A(c\to c_1c_2)\otimes A(b\to b_1b_2)]A(\bar{p}p\to bc), \tag{58}$$

where $\otimes$ denotes a tensor product. The matrix A has as many rows as the total final-state spin multiplicity and has $2J+1$ columns, where J is the total spin of the $\bar{p}p$ system. We define the quantization axis as the direction of one of the daughters in the first decay (the annihilating $\bar{p}p$ atom) for which we choose $\theta=0$, $\phi=0$, and $BW_L(2m_p)=F_L(p)\sqrt{p}$.

Several decay chains of intermediate resonances may lead to the same observed final state of N stable particles. The transition probability w_D for chains starting from the *same* atomic state is given by the coherent sum

$$\begin{aligned} w_D&=w\times\epsilon\times\mathrm{Tr}\left[\left(\sum_j \alpha_jA_j\right)\tilde{\rho}\left(\sum_k \alpha_k^*A_k^\dagger\right)\right]\\ &=w\times\epsilon\times\mathrm{Tr}\left|\sum_j \alpha_jA_j\right|^2, \end{aligned} \tag{59}$$

where the sums extend over all decay chains labeled by the matrices A_j. We have assumed that the initial spin-density matrix $\tilde{\rho}$ is unity, since the $\bar{p}p$ system is unpolarized. The phase space w and the detection probability ϵ will be ignored for Monte Carlo events drawn according to phase space and submitted to the detector simulation, since $w=1$ and $\epsilon=1$ or 0 for every Monte Carlo event. The parameters $\alpha_j=a_j\exp(-i\phi_j)$ are unknown constants to be fitted, and one phase, say ϕ_0, is arbitrary and set to zero. For chains decaying into the same resonances but with different electric charges (e.g., $\rho^+\pi^-,\rho^-\pi^+,\rho^0\pi^0\to\pi^+\pi^-\pi^0$) these constants are given by isospin relations. The contributions from *different* atomic states are given by incoherent sums, i.e., by summing weights w_D of the form (59).

As an example, let us derive the weight w_D for the annihilation channel $\bar{p}p\to\rho^0\rho^0\to2\pi^+2\pi^-$ from the atomic state $^1S_0$ ($J^{PC}=0^{-+}$). Parity, C parity, and total angular momentum conservation require for $\rho^0\rho^0$ that $L=1$ and $S=1$ (see Sec. IV.A). The first Clebsch-Gordan coefficient in Eq. (54) is, apart from a constant,

$$\langle 0\lambda|110\lambda\rangle\langle 1\lambda|11\lambda_1,-\lambda_2\rangle=\lambda_1\delta_{\lambda_1\lambda_2}, \tag{60}$$

and hence the amplitude vanishes unless the ρ's are emitted with the same helicity $\lambda_1=\lambda_2\neq0$. With $J=0$, the matrices (57) are unity and therefore $A(\bar{p}p)$ is a column vector with 9 rows:

$$A(\overline{p}p)=\begin{pmatrix}1\\0\\.\\.\\.\\0\\-1\end{pmatrix}F_1(p)\sqrt{p}. \tag{61}$$

For $\rho\to\pi^+\pi^-$ one finds with $S=0$ and $J=1$ that $L=1$ and the Clebsch-Gordan coefficients are unity. Hence we get with $\lambda=0$ the three-dimensional row vector

$$A(\rho)=[D^1_{01}(\theta,\phi),D^1_{00}(\theta,\phi),D^1_{0-1}(\theta,\phi)]BW_1(m). \tag{62}$$

With Eq. (58) one then obtains

$$\begin{aligned}A&=[A(\rho_1)\otimes A(\rho_2)]A(\overline{p}p)\\&=[D^1_{01}(\theta_1,\phi_1)D^1_{01}(\theta_2,\phi_2)\\&\quad -D^1_{0-1}(\theta_1,\phi_1)D^1_{0-1}(\theta_2,\phi_2)]\\&\quad \times BW_1(m_1)BW_1(m_2)F_1(p)\sqrt{p},\\&=i\sin\theta_1\sin\theta_2\sin(\phi_1+\phi_2)\\&\quad \times BW_1(m_1)BW_1(m_2)F_1(p)\sqrt{p},\end{aligned} \tag{63}$$

and therefore

$$\begin{aligned}w_D&=\sin^2\theta_1\sin^2\theta_2\sin^2\\&\quad\times(\phi_1+\phi_2)|BW_1(m_1)BW_1(m_2)|^2F_1^2(p)p.\end{aligned} \tag{64}$$

The angles refer to the directions of the pions in the ρ rest frames, with respect to the flight direction of the $\rho's$. Therefore the most probable angle between the planes spanned by the two dipions is 90°. This angular dependence is familiar in parapositronium (0^{-+}) annihilation or π^0 decay where the γ polarizations are preferably orthogonal ($\phi_1+\phi_2=90°$). However, there are two ways to combine four pions into $\rho^0\rho^0$ and therefore the final weight is actually given by the coherent sum (59) of two decay chains with $\alpha_1=\alpha_2$.

As another example of symmetrization let us consider $\overline{p}p$ annihilation into $\pi K\overline{K}$, which will be discussed in detail below. The amplitudes for annihilation through the intermediate K^* are related through isospin Clebsch-Gordan coefficients [see, for example, Conforto *et al.* (1967) or Barash *et al.* (1965)]. In general, annihilation may occur from $^1S_0$ or $^3S_1$ with isospin $I=0$ or 1. For example, $\pi^0K^+K^-$ proceeds through $K^{*+}\to\pi^0K^+$ or $K^{*-}\to\pi^0K^-$ with coefficients α_1 and α_2 equal in absolute magnitude, and the two chains interfere. Table VIII gives the relative sign between α_1 and α_2. Note that for $^3S_1$ the matrix (57) flips the sign so that the *observed* interference pattern is the same for $^1S_0$ or $^3S_1$, namely, constructive in $\pi^0K^+K^-$, $\pi^0K^0\overline{K^0}$, and ($I=0$) $\pi^\pm K^\mp K^0$, and destructive in ($I=1$) $\pi^\pm K^\mp K^0$. The signs given in Table VIII also apply to $K\overline{K}$ intermediate states with isospin $i=1$ from $I(\overline{p}p)=0$ and $I(\overline{p}p)=1$ (the latter only contributing to $\pi^\pm K^\mp K^0$) and for states with isospin $i=0$ from $I(\overline{p}p)=1$ (to which $\pi^\pm K^\mp K^0$ does not contribute).

TABLE VIII. Relative sign of α_1 and α_2 for $\overline{p}p$ annihilation into $\pi K\overline{K}$ (see text).

	$^1S_0(\overline{p}p)$		$^3S_1(\overline{p}p)$	
Channel	$I=0$	$I=1$	$I=0$	$I=1$
$\pi^\pm K^\mp K^0$	+	−	−	+
$\pi^0K^+K^-$	+	+	−	−
$\pi^0K^0\overline{K^0}$	+	+	−	−

The procedure for analyzing data is as follows: Phase-space-distributed Monte Carlo events are generated, tracked through the detector simulation, and submitted to the reconstruction program. As already mentioned, this procedure automatically takes care of the factors ρ, w, and ϵ. For $\overline{p}p$ annihilation into three stable particles, there are only two independent kinematic variables. One usually chooses the invariant masses squared, m^2_{12} and m^2_{13}. The two-dimensional distribution (Dalitz plot) is then uniformly populated for phase-space-distributed events. The procedure consists in calculating w_D for each Monte Carlo event and varying the constants α_i, the widths, masses, and spin-parity assignments of the resonances until a good fit to the observed Dalitz plot density is achieved. Resonances with spins larger than 2 are too heavy to be produced in $\overline{p}p$ annihilation at rest and are therefore ignored.

For the Dalitz plot fits it is convenient to factorize w_D in terms of the real constants a_j and ϕ_j,

$$\begin{aligned}w_D&=\sum_i a_i^2Q_{ii}+2\sum_{i<j}a_ia_j\mathrm{Re}[Q_{ij}]\cos(\phi_i-\phi_j)\\&\quad+2\sum_{i<j}a_ia_j\mathrm{Im}[Q_{ij}]\sin(\phi_i-\phi_j),\end{aligned} \tag{65}$$

where

$$Q_{ij}=\mathrm{Tr}[A_iA_j^\dagger]. \tag{66}$$

Dalitz plots weighted by Q_{ii}, Re$[Q_{ij}]$, and Im$[Q_{ij}]$ are then produced for each pair of chains i,j ($i\leq j$). The Q_{ij}, and correspondingly the weights w_D, are normalized to the total number of real events N_T,

$$Q_{ij}\to Q_{ij}/\sqrt{f_if_j}, \tag{67}$$

with

$$f_i=\sum Q_{ii}/N_T, \tag{68}$$

where the sum runs over all Monte Carlo events. One then divides the Dalitz plots into cells, adds them according to Eq. (65), and builds the χ^2,

$$\chi^2=\sum\frac{(n-w_D)^2}{n+w_D^2/n_{MC}}, \tag{69}$$

where the sum extends over all cells. The number of real events in each cell is denoted by n and the number of Monte Carlo events by n_{MC}.

With limited statistics or for more than two degrees of freedom (final states with more than three stable particles) the χ^2 minimization may be replaced by a likelihood maximization. One minimizes the quantity $S=-2\ln L$ or

$$S=2N_T\ln\left(\sum_{i=1}^{M_T} w_i[MC]\right)-2\sum_{i=1}^{N_T}\ln w_i[DAT], \quad (70)$$

where $w_i[MC]$ and $w_i[DAT]$ are weights w_D calculated for Monte Carlo and data events, respectively. The sums run over N_T data events and M_T Monte Carlo events.

From the best fit the fractional contributions of the resonances in chain i are given by

$$r_i\equiv\frac{a_i^2}{\sum_i a_i^2}, \quad (71)$$

where, obviously, $\Sigma r_i=1$. This is a somewhat arbitrary definition, which may not agree with the directly visible Dalitz plot densities, because interferences beween the chains are neglected in Eq. (71). One may define alternatively

$$r_i\equiv a_i^2, \quad (72)$$

but then Σr_i may differ significantly from unity in the presence of strong interference. Hence decay branching fractions for broad interfering resonances are not measurable unambiguously. This is an unavoidable caveat to keep in mind when extracting the internal structure of broad states from their decay branching ratios.

C. *K*-matrix analysis

The Breit-Wigner factors given by Eq. (55) violate unitarity when two resonances with the same quantum numbers overlap and decay into the same final state. Moreover, they do not describe distortions in the mass spectrum that occur around kinematical thresholds. For example, the $f_0(980)\to\pi\pi$ appears as a dip rather than a peak in the $\pi\pi$ mass spectrum of elastic $\pi\pi$ scattering, due to the opening of the decay channel $f_0(980)\to K\bar{K}$ (Au, Morgan, and Pennington 1987).

This behavior can be described with the K-matrix formalism. A detailed description can be found in Chung *et al.* (1995), and I shall only recall the formulae used in the analysis of Crystal Barrel data. Consider, for instance, the four scattering reactions

$$\begin{pmatrix} \pi\pi\to\pi\pi & \pi\pi\to K\bar{K} \\ K\bar{K}\to\pi\pi & K\bar{K}\to K\bar{K} \end{pmatrix}. \quad (73)$$

The transition amplitude T for a given partial wave is described by the 2×2 K matrix

$$T=(1-iK\rho)^{-1}K \quad (74)$$

with the real and symmetric matrix

$$K_{ij}(m)=\sum_\alpha \frac{\gamma_{\alpha_i}\gamma_{\alpha_j}m_\alpha\Gamma'_\alpha}{m_\alpha^2-m^2}B_{\alpha_i}(m)B_{\alpha_j}(m)+c_{ij}. \quad (75)$$

The sum runs over all resonances with K-matrix poles m_α decaying to $\pi\pi$ and $K\bar{K}$ with (real) coupling constants γ_{α_1} and γ_{α_2}, respectively, where

$$\gamma_{\alpha_1}^2+\gamma_{\alpha_2}^2=1. \quad (76)$$

The factors B_{α_i} are ratios of Blatt-Weisskopf damping factors (Table IV),

$$B_{\alpha_i}(m)=\frac{F_L(p_i)}{F_L(p_{\alpha_i})}, \quad (77)$$

where L is the decay angular momentum, p the π or K momenta, and p_{α_i} their momenta at the pole mass m_α. The optional real constants c_{ij} allow for a background (nonresonating) amplitude.[7] In Eq. (74) the matrix $\rho(m)$ describes the two-body phase space and is diagonal with $\rho_{11}\equiv\rho_1=2p_\pi/m$ and $\rho_{22}\equiv\rho_2=2p_K/m$. For masses far above the kinematical threshold $\rho_i\sim 1$ and below $K\bar{K}$ threshold ρ_2 becomes imaginary.

The (K-matrix) partial width of resonance α to decay into channel i is defined as

$$\Gamma_{\alpha_i}(m_\alpha)=\gamma_{\alpha_i}^2\Gamma'_\alpha\rho_i(m_\alpha), \quad (78)$$

and the (K-matrix) total width as

$$\Gamma_\alpha=\sum_i \Gamma_{\alpha_i}. \quad (79)$$

For a resonance with mass far above kinematic thresholds one obtains the partial and total widths

$$\Gamma_{\alpha_i}=\gamma_{\alpha_i}^2\Gamma'_\alpha, \quad \Gamma_\alpha=\Gamma'_\alpha, \quad (80)$$

respectively. For one resonance and one channel (elastic scattering) the K matrix reduces to

$$K=\frac{m_0\Gamma'_0B^2(m)}{m_0^2-m^2}, \quad (81)$$

and T [Eq. (74)] reduces to the relativistic Breit-Wigner formula,

$$T=\frac{m_0\Gamma_0B^2(m)/\rho(m_0)}{m_0^2-m^2-im_0\Gamma(m)}, \quad (82)$$

with

$$\Gamma(m)=\Gamma_0\frac{\rho(m)}{\rho(m_0)}B^2(m). \quad (83)$$

For a resonance far above threshold and with $\Gamma_0\ll m_0$ we get the familiar expression

$$T=\frac{\Gamma_0/2}{m_0-m-i\Gamma_0/2}. \quad (84)$$

[7]For the $\pi\pi$ S wave, the K matrix is multiplied by a factor $(m^2-2m_\pi^2)/m^2$ to ensure a smooth behavior near threshold.

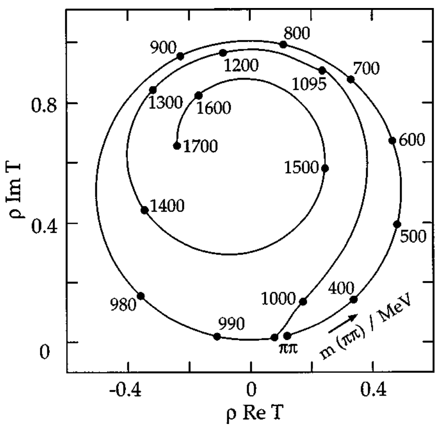

FIG. 19. Argand diagram of the $\pi\pi$ scattering amplitude T obtained from a common fit to production and scattering data (from Spanier, 1994).

Normally, the mass m_R and width Γ_R of a resonance are obtained from the poles of the T matrix. Extending the mass m to complex values, we find from Eq. (84) the poles at

$$m_P = m_R - i\frac{\Gamma_R}{2}, \tag{85}$$

with $m_R = m_0$ and $\Gamma_R = \Gamma_0$. In general, however, m_R does not coincide with the pole of the K matrix and Γ_R is different from the K-matrix width. For example, for two nonoverlapping resonances far above threshold, the K-matrix, T-matrix, and Breit-Wigner poles coincide. As the resonance tails begin to overlap the two T-matrix poles move towards one another (for an example, see Chung *et al.,* 1995).

The $\pi\pi$ S-wave scattering amplitude is related to the $\pi\pi$ phase shift δ and inelasticity η through the relation

$$\rho_1(m) T_{11}(m) = \frac{\eta(m)\exp[2i\delta(m)] - 1}{2i}. \tag{86}$$

According to Eq. (74) the corresponding K matrix then reads for pure elastic $\pi\pi$ scattering ($\eta \equiv 1$)

$$K_{11}(m) = \frac{\tan\delta(m)}{\rho_1(m)} \tag{87}$$

and becomes infinite at $m = m_0$, when δ passes through 90°. However, the amplitude T does not, in general, reach a resonance when $\delta = \pi/2$. As an example, consider the $\pi\pi$ S-wave scattering amplitude described by Eq. (86) in the complex plane (Argand diagram): The intensity $|T|^2$ reaches its maximum value around 850 MeV ($\delta = 90°$), loops back, and passes rapidly through the $K\bar{K}$ threshold (see Fig. 19 and Au, Morgan, and Pennington, 1987). At ~1000 MeV $|T|^2$ reaches its minimum value ($\delta = 180°$) and then starts a new (inelastic) loop. The $f_0(980)$ then appears as a hole in the $\pi\pi$ intensity distribution. We shall return to the S-wave Argand diagram when discussing the fits to Crystal Barrel data.

Consider now the production of a resonance α in $\bar{p}p$ annihilation. In the isobar model, the resonance is assumed not to interact with the recoiling system. The coupling strength to $\bar{p}p$ is denoted by the (complex) constant β_α, while γ_{α_i} describes its decay strength into channel i (say $\pi\pi$ for $i = 1$ and $K\bar{K}$ for $i = 2$). Following Aitchison (1972) the amplitudes are given by the components of the vector,

$$\mathcal{T} = (1 - iK\rho)^{-1} P. \tag{88}$$

The K matrix now describes the propagation of the channel i through the resonances α while the vector P describes their production. P and K share the common poles m_α so that $\mathcal{T}$ remains finite at the poles. The vector P is given by

$$P_j(m) = \sum_\alpha \frac{\beta_\alpha \gamma_{\alpha j} m_\alpha \Gamma'_\alpha B_{\alpha_j}(m)}{m_\alpha^2 - m^2}, \tag{89}$$

where the sum runs over all resonances. For a single resonance feeding only one decay channel we again obtain from Eq. (88) a Breit-Wigner distribution of the form (82) with coupling strength β:

$$\mathcal{T} = \frac{\beta m_0 \Gamma_0 B(m)/\rho(m_0)}{m_0^2 - m^2 - i m_0 \Gamma(m)}. \tag{90}$$

Let us now assume a series of resonances with the same quantum numbers decaying into two final states. The amplitude for the first final state is given by Eq. (88):

$$\mathcal{T}_1 = \frac{(1 - iK_{22}\rho_2)P_1 + iK_{12}\rho_2 P_2}{1 - \rho_1\rho_2 D - i(\rho_1 K_{11} + \rho_2 K_{22})}, \tag{91}$$

with

$$D \equiv K_{11}K_{22} - K_{12}^2. \tag{92}$$

As an example, consider a single resonance, say $a_0(980)$ decaying to $\eta\pi$ and $K\bar{K}$. In this case $D \equiv 0$ and $B(m) \equiv 1$ (S wave). We then obtain from Eq. (91) the formula (Flatté, 1976)

$$\mathcal{T}(\eta\pi) = \frac{b g_1}{m_0^2 - m^2 - i(\rho_1 g_1^2 + \rho_2 g_2^2)}, \tag{93}$$

with

$$g_i \equiv \gamma_i \sqrt{m_0 \Gamma'_0} \Rightarrow \sum_{i=1}^{2} g_i^2 = m_0 \Gamma'_0, \tag{94}$$

and

$$b \equiv \beta \sqrt{m_0 \Gamma'_0}. \tag{95}$$

The phase-space factors are

$$\rho_1(m) = \frac{2p_\eta}{m} \text{ and } \rho_2(m) = \frac{2p_K}{m} = \sqrt{1 - \frac{4m_K^2}{m^2}}. \tag{96}$$

The $\mathcal{T}(K\bar{K})$ amplitude is obtained by interchanging the labels 1 and 2 in Eq. (93). Below $K\bar{K}$ threshold ρ_2 becomes imaginary. Compared to pure $\eta\pi$ decay this leads

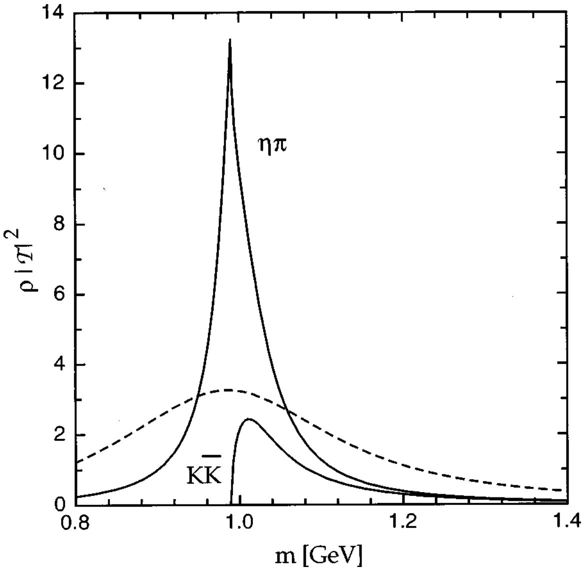

FIG. 20. $\eta\pi$ and $K\bar{K}$ mass distributions for the $a_0(980)$ resonance in $\bar{p}p\rightarrow\eta\pi X$ and $K\bar{K}X$ (in arbitrary units and assuming that no other resonance is produced in these channels). The dashed line shows the $\eta\pi$ mass distribution for the same width Γ_0' in the absence of $K\bar{K}$ coupling ($g_2=0$).

to a shift of the resonance peak and to a narrower and asymmetric distribution of the observed signal in the $\eta\pi$ channel. This is shown in Fig. 20 for $g_1=0.324$ GeV, $g_2=0.329$ GeV (hence $\Gamma_0'=0.46$ GeV). These parameters have been extracted from the $a_0(980)$ contribution to $\bar{p}p\rightarrow\eta\pi^0\pi^0$ and $K\bar{K}\pi$ (Sec. VIII.H). A width of 54.12 ± 0.36 MeV was determined directly from the $a_0(980)\rightarrow\eta\pi$ signal in the annihilation channel $\omega\eta\pi^0$ (Amsler *et al.,* 1994c), in good agreement with the observed width in Fig. 20. Also shown in Fig. 20 is the expected distribution for $\Gamma_0'=0.46$ GeV, assuming no $K\bar{K}$ decay. The observed width $\Gamma_0=\Gamma_0'\rho_1(m_0)$ increases to 0.31 GeV.

The standard procedure in the analysis of Crystal Barrel data is to replace the Breit-Wigner function (55) by $\mathcal{T}$ [Eq. (88)] and to fit the parameters g_{α_i}, β_α, and m_α. The resonance parameters m_R and Γ_R are then extracted by searching for the complex poles [Eq. (85)] of the matrix $\mathcal{T}$. A one-channel resonance appears as a pole in the second Riemann sheet and a two-channel resonance manifests itself as a pole in the second or third Riemann sheet (Badalyan *et al.,* 1982).

Some of the Crystal Barrel Dalitz plots have also been analyzed using the so-called N/D formalism (Chew and Mandelstam, 1960), which takes into account the direct production of three mesons and also the final-state interaction. In this formalism the amplitude $\mathcal{T}$ has the same denominator as, for example, Eq. (91), but the numerator allows for additional degrees of freedom (Bugg *et al.,* 1994).

VIII. ANNIHILATION AT REST INTO THREE PSEUDOSCALAR MESONS

Proton-antiproton annihilation at rest into three pseudoscalar mesons is the simplest process to search for scalar resonances $0^+\rightarrow0^-0^-$, the recoiling third pseudoscalar meson removing the excess energy. The annihilation rates for these processes in liquid hydrogen ($^1S_0$ atomic state) are reasonably large, since no angular momentum barrier is involved. Channels with three pseudoscalar mesons had been studied earlier, but essentially in the two-prong configuration and with limited statistics, e.g., $\pi^+\pi^-\pi^0$ with 3838 events (Foster *et al.,* 1968b), $\pi^+\pi^-\eta$ with 459 events (Espigat *et al.,* 1972), and $\pi^+\pi^-\eta'$ with 104 events (Foster *et al.,* 1968a). The samples collected by the Asterix collaboration at LEAR (May *et al.,* 1989; Weidenauer *et al.,* 1990) are larger but were collected from atomic P states. The $\pi^+\pi^-\pi^0$ final state revealed the existence of a tensor meson, $f_2(1565)$, produced from P states (May *et al.,* 1989, 1990). In the kaonic sector, data were collected in bubble chambers for the final states $\pi^\pm K^\mp K_S$ (2851 events) and $\pi^0K_SK_S$ (546 events) in the experiments of Barash *et al.* (1965) and Conforto *et al.* (1967). Branching ratios for annihilation into three mesons are listed in Table IX.

Annihilation with charged pions is dominated by $\rho(770)$ production, which complicates the spin-parity analysis of underlying scalar resonances in the $\pi\pi$ S wave. Both $^1S_0$ and $^3S_1$ atomic states contribute. All-neutral (zero-prong) channels are therefore simpler to analyze but more complex to select due to the large γ multiplicity. The channel $\pi^0\pi^0\pi^0$ with 2100 events had been reconstructed earlier with optical spark chambers (Devons *et al.,* 1973). The existence of a scalar resonance decaying to $\pi\pi$ with mass 1527 MeV and width 101 MeV was suggested in the $3\pi^0$ channel and in its $\pi^-\pi^-\pi^+$ counterpart in $\bar{p}n$ annihilation in deuterium (Gray *et al.,* 1983). This was actually the first sighting of $f_0(1500)$, which will be discussed below.

The sizes of the hitherto existing data samples were vastly increased by Crystal Barrel. We shall first review annihilation into three neutral nonstrange mesons. We start from 6γ final states and select the channels $\bar{p}p\rightarrow\pi^0\eta\eta$, $3\pi^0$, $\pi^0\pi^0\eta$, $\pi^0\eta\eta'$, and $\pi^0\pi^0\eta'$ by assuming total energy and total momentum conservation and constraining the 2γ masses to π^0,η, and η' decays (seven-constraint fits), excluding any other possible configuration: Events are accepted if the kinematic fit satisfies the assumed three-pseudoscalar hypothesis with a confidence level typically larger than 10%. Background from the other 6γ channels is suppressed by rejecting those events that also satisfy any other 6γ final-state hypothesis (including the strong $\omega\omega$, $\omega\rightarrow\pi^0\gamma$) with a confidence level of at least 1%. The absolute branching ratios for the 6γ channels are determined by normalizing on the branching ratio for $\bar{p}p\rightarrow\omega\omega$. These three-pseudoscalar channels have all been analyzed and we now review the salient features of their Dalitz plots. Results on kaonic channels are treated in Sec. VIII.G and VIII.H.

A. $\bar{p}p\rightarrow\pi^0\eta\eta$

The first evidence for two $I=0$ scalar mesons in the 1400-MeV mass region, now called $f_0(1370)$ and

TABLE IX. Branching ratios for $\bar{p}p$ annihilation at rest into three narrow mesons. Mesons in parentheses were not detected.

Channel	Final state			B		Reference
$\pi^0\pi^0\pi^0$	6γ	6.2	$\pm$	1.0	10^{-3}	Amsler *et al.* (1995f)‡
$\pi^+\pi^-\pi^0$	$\pi^+\pi^-(\pi^0)$	6.9	$\pm$	0.4	10^{-2}	Foster *et al.* (1968b)
$\pi^0\eta\eta$	6γ	2.0	$\pm$	0.4	10^{-3}	Amsler *et al.* (1995e)‡
$\pi^0\pi^0\omega$	7γ	2.00	$\pm$	0.21	10^{-2}	Amsler *et al.* (1993a)‡
	$\pi^+\pi^-6\gamma$	2.57	$\pm$	0.17	10^{-2}	Amsler *et al.* (1994d)‡
$\pi^+\pi^-\omega$	$2\pi^+2\pi^-(\pi^0)$	6.6	$\pm$	0.6	10^{-2}	Bizzarri *et al.* (1969)
$\omega\eta\pi^0$	7γ	6.8	$\pm$	0.5	10^{-3}	Amsler *et al.* (1994c)‡
$\pi^0\pi^0\eta$	6γ	6.7	$\pm$	1.2	10^{-3}	Amsler *et al.* (1994b)‡
	$\pi^+\pi^-6\gamma$	6.50	$\pm$	0.72	10^{-3}	Amsler *et al.* (1994d)‡
$\pi^+\pi^-\eta$	$\pi^+\pi^-2\gamma$	1.63	$\pm$	0.12	10^{-2}	Abele *et al.* (1997a)‡
	$\pi^+\pi^-6\gamma$	1.33	$\pm$	0.16	10^{-2}	Amsler *et al.* (1994d)‡
	$2\pi^+2\pi^-(\pi^0)$	1.38	$\pm$	0.17	10^{-2}	Espigat *et al.* (1972)
	$2\pi^+2\pi^-(\pi^0)$	1.51	$\pm$	$^{0.17}_{0.21}$	10^{-2}	Foster *et al.* (1968a)
$\pi^0\pi^0\eta'$	10γ	3.2	$\pm$	0.5	10^{-3}	Abele *et al.* (1997e)‡
	6γ	3.7	$\pm$	0.8	10^{-3}	Abele *et al.* (1997e)‡
$\pi^+\pi^-\eta'$	$\pi^+\pi^-6\gamma$	7.5	$\pm$	2.0	10^{-3}	Urner (1995)‡
	$3\pi^+3\pi^-(\pi^0)$	2.8	$\pm$	0.9	10^{-3}	Foster *et al.* (1968a)
$\pi^0\eta\eta'$	6γ	2.3	$\pm$	0.5	10^{-4}	Amsler *et al.* (1994f)‡
$\pi^0\pi^0\phi$	$8\gamma(K_L)$	9.7	$\pm$	2.6	10^{-5}	Abele *et al.* (1997c)‡
$\pi^+\pi^-\phi$	$2\pi^+2\pi^-(K_L)$	4.6	$\pm$	0.9	10^{-4}	Bizzarri *et al.* (1969)
$\pi^0K_SK_L$	$3\pi^0(K_L)$	6.7	$\pm$	0.7	10^{-4}	Amsler *et al.* (1993d) [a]‡
$\pi^0K_SK_S$	$2\pi^+2\pi^-(\pi^0)$	7.5	$\pm$	0.3	10^{-4}	[b]
$\pi^\pm K^\mp K_S$	$\pi^+\pi^-\pi^\pm K^\mp$	2.73	$\pm$	0.10	10^{-3}	[b]
$\pi^\pm K^\mp K_L$	$\pi^\pm K^\mp(K_L)$	2.91	$\pm$	0.34	10^{-3}	Abele *et al.* (1998d)‡
ωK_SK_S	$3\pi^+3\pi^-(\pi^0)$	1.17	$\pm$	0.07	10^{-3}	Bizzarri *et al.* (1971)
ωK^+K^-	$K^+K^-\pi^+\pi^-(\pi^0)$	2.30	$\pm$	0.13	10^{-3}	Bizzarri *et al.* (1971)

[a]Using $B(\pi^0\phi)$ from Table VI and Eq. (47).
[b]Average between Armenteros *et al.* (1965) and Barash *et al.* (1965).
‡Crystal Barrel experiment.

$f_0(1500)$, was obtained from a reduced sample of 2.3 $\times 10^4$ $\pi^0\eta\eta$ events (Amsler *et al.,* 1992c). The invariant-mass distributions are shown in Fig. 21. The two scalar states decaying to $\eta\eta$ are also observed when one η decays to $3\pi^0$ (10γ final state), a channel with entirely different systematics [Fig. 21(b)]. The distributions in Fig. 21(a) and (b) are nearly identical.

An amplitude analysis of the Dalitz plot distribution for the 6γ final state was performed with the method outlined in the previous section. However, Breit-Wigner functions of the form (55) were used to describe the resonances. The fit required $J^{PC}=0^{++}$ for both $\eta\eta$ resonances. The (Breit-Wigner) masses and widths were m $=1430$, $\Gamma=250$ MeV, and $m=1560\pm25$, $\Gamma=245\pm50$ MeV, respectively. Note that the width of the upper state appears smaller in Fig. 21(a,b), due to interference effects.

The final analysis of this channel was performed with a tenfold increase in statistics, namely, 3.1×10^4 $\pi^0\eta\eta$ events from zero-prong data and 1.67×10^5 $\pi^0\eta\eta$ events from a triggered data sample requiring online one π^0 and two η mesons (Amsler *et al.,* 1995e). The Dalitz plot is shown in Fig. 22(a). The horizontal and vertical bands are due to $a_0(980)$ decaying to $\eta\pi^0$. One also observes diagonal bands, which correspond to the two states' decaying to $\eta\eta$. A residual incoherent flat background of 5%, mainly due to $\pi^0\pi^0\omega\to7\gamma$ with a missing photon, was subtracted from the Dalitz plot before applying the amplitude analysis, this time with the full K-matrix formalism.

Since S-wave annihilation dominates in liquid, the channel $\pi^0\eta\eta$ proceeds mainly through the $^1S_0$ atomic state. The $\eta\pi$ S wave was parametrized by a 2×2 K matrix with poles from the $a_0(980)$ and $a_0(1450)$. The parameters were taken from the $\pi^0\pi^0\eta$ analysis (Sec. VIII.B), leaving the production constants β free. A contribution from the $a_2(1320)$ ($\eta\pi$ D wave) with fixed mass and width was also offered to the fit. The $\eta\eta$ S and D waves were described by one-channel K matrices. Annihilation from atomic P states was not included in the fit except for tensor mesons [e.g., the expected

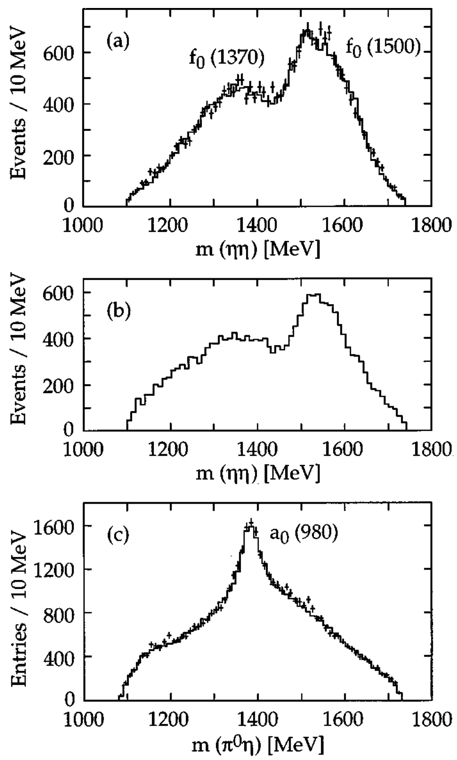

FIG. 21. Invariant-mass distributions for $\pi^0\eta\eta$: (a) $\eta\eta$ mass distribution for 6γ events showing the two new scalar mesons; (b) $\eta\eta$ mass distribution for one η decaying to $3\pi^0$ (10γ final state, not corrected for acceptance); (c) $\pi^0\eta$ mass distribution for 6γ events (two entries/event) showing the $a_0(980)$. The solid lines in (a) and (c) represent the best fit described in Amsler *et al.* (1992c).

$f_2(1565)$] decaying to $\eta\eta$. In fact, the fit demands a contribution from a tensor meson with mass ~ 1494 MeV and width ~ 155 MeV, produced mainly from P states.

The best fit was obtained with two poles for the $\eta\eta$ S wave. The resonance parameters (T-matrix poles) are

$$f_0(1370): m = 1360 \pm 35, \quad \Gamma = 300 - 600\,\text{MeV},$$

$$f_0(1500): m = 1505 \pm 15, \quad \Gamma = 120 \pm 30\,\text{MeV}. \tag{97}$$

A scalar state decaying to $\eta\eta$ has been observed by the GAMS collaboration in the reaction $\pi^- p \to \eta\eta n$ with 38-GeV pions (Binon *et al.,* 1983) and also with 300-GeV pions (Alde *et al.,* 1988b). The average mass and width are 1602 ± 16 MeV and 190 ± 28 MeV, respectively. This state also decays into $\eta\eta'$ (Binon *et al.,* 1984). Mass and width were obtained assuming a Breit-Wigner amplitude. The Crystal Barrel K-matrix mass and width of the $f_0(1500)$ are 1569 and 191 MeV, respectively, in accord with the Breit-Wigner parameters of Amsler *et al.* (1992c) and of the GAMS resonance. It is therefore generally accepted that the GAMS state, previously called $f_0(1590)$ by the Particle Data Group, and the Crystal Barrel $f_0(1500)$ are identical (Barnett *et al.,* 1996). The branching ratio for $\pi^0\eta\eta$ is given in Table IX and the products of resonance production and decay branching ratios are listed in Table X.

B. $\bar{p}p \to \pi^0\pi^0\eta$

This channel is relevant in the search for isovector 0^{++} states decaying to $\eta\pi$. The $\pi^0\pi^0\eta$ Dalitz plot (2.8×10^5 events) is shown in Fig. 22(b). Qualitatively, one observes the $a_0(980)$ and $a_2(1320)$ decaying to $\eta\pi$ and the $f_0(980)$ into $\pi\pi$. The strong interference patterns point to coherent contributions from a single $\overline{pp}$ atomic state ($^1S_0$).

An amplitude analysis based on the K-matrix formalism (and, alternatively, the N/D formalism) was performed, assuming pure S-wave annihilation (Amsler *et al.,* 1994b). The $\pi\pi$ S wave was described by two poles, one for the $f_0(980)$, coupling to $\pi\pi$ and $K\overline{K}$, and one for the $f_0(1370)$. Elastic $\pi\pi$ scattering data (Grayer *et al.,* 1974; Rosselet *et al.,* 1977) were included in the fit. The $\pi\pi$ D wave $f_2(1270)$ was also introduced but turned out to be negligible. The $\eta\pi$ D wave was described by one pole for the $a_2(1320)$. The $\eta\pi$ S wave was described by a one-pole 2×2 K matrix for $a_0(980)$ with couplings g_1 to $\eta\pi$ and g_2 to $K\overline{K}$. Since decay to $K\overline{K}$ was not measured, g_2 was obtained indirectly from the $\eta\pi$ line shape. The fit yielded $g_1 \sim 0.353$ GeV and

$$\frac{g_2^2}{g_1^2} \sim 0.88. \tag{98}$$

These amplitudes were, however, not sufficient to describe the data. A satisfactory fit was obtained by adding (i) a second pole to the $\eta\pi$ S wave, (ii) a second pole to the $\eta\pi$ D wave, and (iii) an $\eta\pi$ P wave. Note that this last has the quantum numbers $J^{PC} = 1^{-+}$, which do not couple to $q\overline{q}$ mesons. This wave was introduced to search for the $\hat{\rho}(1405)$ reported by Alde *et al.* (1988a).

Branching ratios are given in Table X. The branching ratio for $\pi^0\pi^0\eta$ (Table IX) is in excellent agreement with the one derived from the channel $\pi^0\pi^0\eta \to \pi^+\pi^-3\pi^0$ (Amsler *et al.,* 1994d). The main result was the observation of a new isovector scalar resonance in the $\eta\pi$ S wave:

$$a_0(1450): m = 1450 \pm 40, \quad \Gamma = 270 \pm 40\,\text{MeV}. \tag{99}$$

This resonance manifests itself as a depletion in the bottom right (or top left) corner of the Dalitz plot [Fig. 22(b)]. Evidence for the $a_0(1450)$ decaying to $\eta\pi$ is also reported in an analysis of the channel $\pi^+\pi^-\eta$, which requires, in addition, an amplitude for $\rho\eta$ production from $^3S_1$ (Abele *et al.,* 1997a).

The $\eta\pi$ D-wave contribution corresponds to a 2^{++} resonance around 1650 MeV, called $a_2'(1650)$ in Table X, with a width of about 200 MeV. This state could be the radial excitation of the $a_2(1320)$. The mass and width of the structure in the $\eta\pi$ P wave (exotic 1^{-+}) are not well defined. They vary from 1200 to 1600 MeV and from 400 to 1000 MeV, respectively, without significant changes in the χ^2. The 1^{-+} $\hat{\rho}(1405)$ reported by Alde *et al.* (1988a) is therefore not required by the $\pi^0\pi^0\eta$ data. We shall return to the $\eta\pi$ P wave in Sec. XI.A.

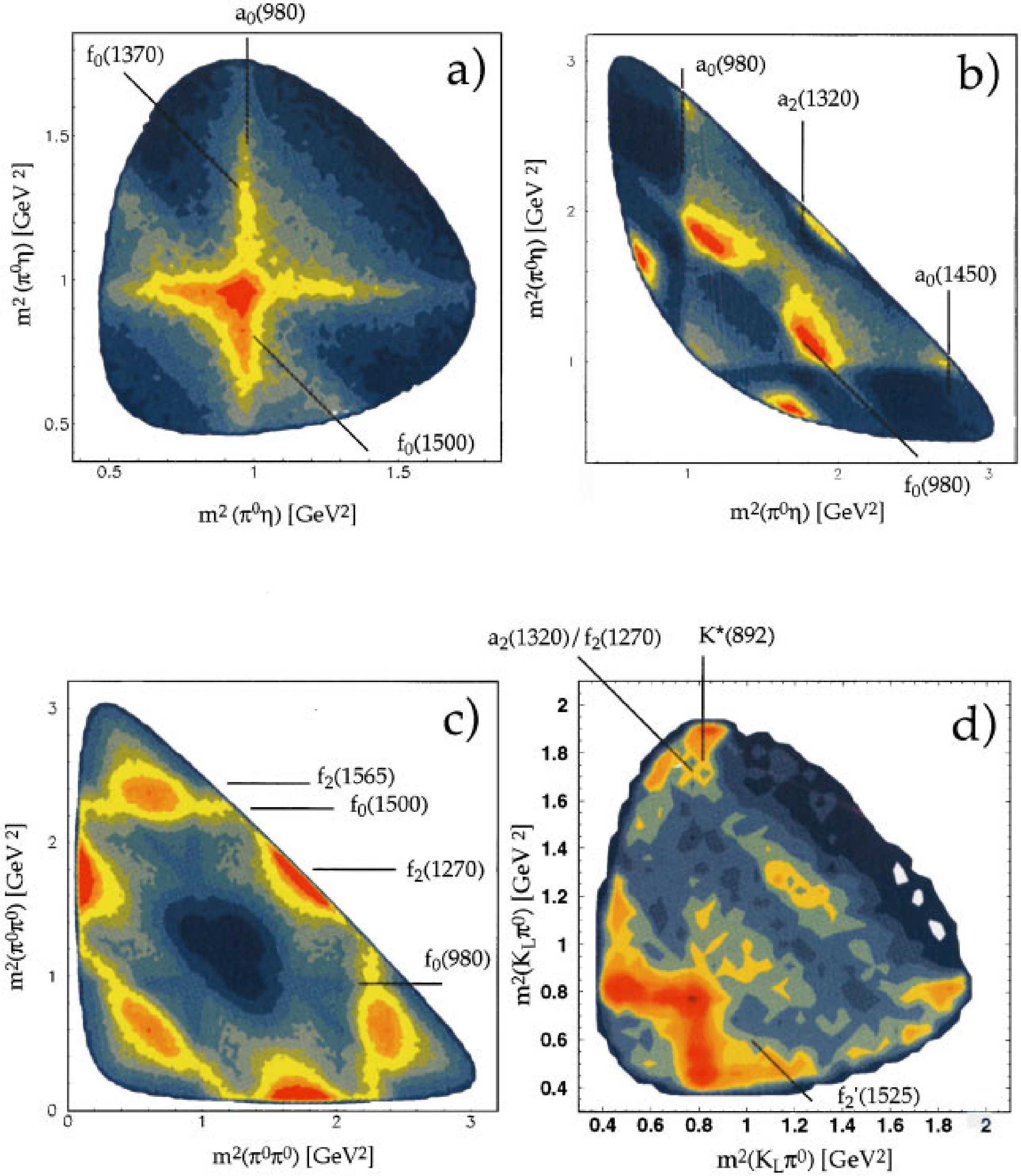

FIG. 22. (Color) Dalitz plots of three-pseudoscalar channels. Red and blue regions correspond to high and low event densities, respectively: (a) $\pi^0\eta\eta$ (198 000 events). The Dalitz plot is symmetrized across the main diagonal; (b) $\pi^0\pi^0\eta$ (symmetrized, 280 000 events); (c) $3\pi^0$ (712 000 events)-each event is entered six times for symmetry reasons; (d) $\pi^0 K_L K_L$ (37 358 events).

C. $\bar{p}p \rightarrow \pi^0\pi^0\pi^0$

The first analysis of this channel used a sample of only 5.5×10^4 events and reported an isoscalar 2^{++} meson at 1515 ± 10 MeV with width 120 ± 10 MeV, decaying to $\pi^0\pi^0$ (Aker *et al.,* 1991). This state was identified with $f_2(1565)$, which had been observed before in the final state $\pi^+\pi^-\pi^0$ in hydrogen gas (May *et al.,* 1989, 1990). P-wave annihilation from $^3P_1$ and $^3P_2$ was therefore allowed when fitting the $3\pi^0$ channel. Resonances in the $\pi\pi$ S wave were described by the $\pi\pi$ elastic-scattering amplitude, replacing the Breit-Wigner amplitude by

$$BW_0(m)=\frac{m}{p}\left(\frac{\eta(m)\exp[2i\delta(m)]-1}{2i}\right), \tag{100}$$

according to Eq. (86), where δ and η were taken from the Argand diagram of Au, Morgan, and Pennington (1987). This is an approximation assuming equal production strengths for all resonances in the $\pi\pi$ S wave, which is reasonable for the $3\pi^0$ channel, as I shall show below.

TABLE X. Branching ratios for $\bar{p}p$ annihilation at rest in liquid, determined from Dalitz plot analyses. The branching ratios include all decay modes of the final-state stable particles (e.g., π^0, η, η') but only the decay mode of the intermediate resonance leading to the observed final state.

Channel / Subchannel	Contributing resonances / Branching ratio
$\pi^0\eta\eta$	$a_0(980), f_0(1370), f_0(1500), a_2(1320), X_2(1494)$
$f_0(1370)\pi^0$	$\sim 3.5\times 10^{-4}$
$f_0(1500)\pi^0$	$(5.5\pm 1.3)\times 10^{-4}$
$a_2(1320)\eta$	$\sim 5.6\times 10^{-5}$
$X_2(1494)\pi^0$	$\sim 4.0\times 10^{-4}$ (dominantly P-wave annihilation)
$\pi^0\pi^0\eta$	$a_0(980), a_0(1450), a_2(1320), a_2'(1650), (\eta\pi)_P$ $(\pi\pi)_S \equiv f_0(400-1200)+f_0(980)+f_0(1370)$
$a_0(980)\pi^0$	$(8.7\pm 1.6)\times 10^{-4}$
$a_0(1450)\pi^0$	$(3.4\pm 0.6)\times 10^{-4}$
$(\pi\pi)_S\eta$	$(3.4\pm 0.6)\times 10^{-3}$
$(\eta\pi)_P\pi$	$\sim 1.0\times 10^{-4}$
$a_2(1320)\pi^0$	$(1.9\pm 0.3)\times 10^{-3}$
$a_2'(1650)\pi^0$	$\sim 1.3\times 10^{-4}$
$\pi^0\pi^0\pi^0$	$(\pi\pi)_S+f_0(1500), f_2(1270), f_2(1565)$
$(\pi\pi)_S\pi^0$	$\sim 2.6\times 10^{-3}$
$f_0(1500)\pi^0$	$(8.1\pm 2.8)\times 10^{-4}$
$f_2(1270)\pi^0$	$\sim 1.8\times 10^{-3}$
$f_2(1565)\pi^0$	$\sim 1.1\times 10^{-3}$
$\pi^0\eta\eta, \pi^0\pi^0\eta, 3\pi^0$	Coupled channels (S-wave annihilation only) $(\eta\eta)_S \equiv f_0(400-1200)+f_0(1370)$
$(\pi\pi)_S\pi^0$	$(3.48\pm 0.89)\times 10^{-3}$
$(\pi\pi)_S\eta$	$(3.33\pm 0.65)\times 10^{-3}$
$(\eta\eta)_S\pi^0$	$(1.03\pm 0.29)\times 10^{-3}$
$f_0(1500)(\rightarrow\pi^0\pi^0)\pi^0$	$(1.27\pm 0.33)\times 10^{-3}$
$f_0(1500)(\rightarrow\eta\eta)\pi^0$	$(0.60\pm 0.17)\times 10^{-3}$
$f_2(1270)(\rightarrow\pi^0\pi^0)\pi^0$	$(0.86\pm 0.30)\times 10^{-3}$
$f_2(1565)(\rightarrow\pi^0\pi^0)\pi^0$	$(0.60\pm 0.20)\times 10^{-3}$
$f_2(1565)(\rightarrow\eta\eta)\pi^0$	$(8.60\pm 3.60)\times 10^{-5}$ (may be more than one object)
$a_0(980)(\rightarrow\pi^0\eta)\pi^0$	$(0.81\pm 0.20)\times 10^{-3}$
$a_0(980)(\rightarrow\pi^0\eta)\eta$	$(0.19\pm 0.06)\times 10^{-3}$
$a_0(1450)(\rightarrow\pi^0\eta)\pi^0$	$(0.29\pm 0.11)\times 10^{-3}$
$a_2(1320)(\rightarrow\pi^0\eta)\pi^0$	$(2.05\pm 0.40)\times 10^{-3}$ [including $a_2'(1650)$]
$\pi^0\eta\eta'$	$f_0(1500)$
$f_0(1500)\pi^0$	$(1.6\pm 0.4)\times 10^{-4}$
$\pi^0\pi^0\eta'$	$(\pi\pi)_S, a_2(1320), a_0(1450)$
$(\pi\pi)_S\eta'$	$(3.1\pm 0.4)\times 10^{-3}$
$a_2(1320)\pi^0$	$(6.4\pm 1.3)\times 10^{-5}$
$a_0(1450)\pi^0$	$(1.16\pm 0.47)\times 10^{-4}$

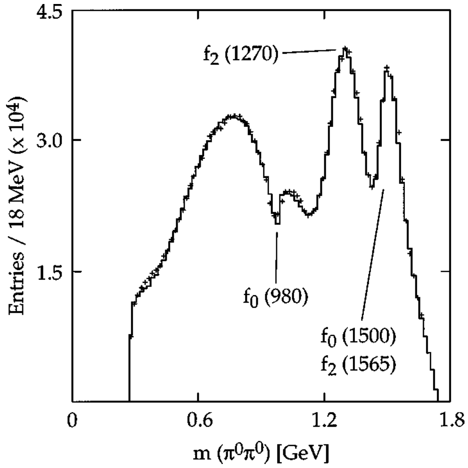

FIG. 23. $\pi^0\pi^0$ mass projection in $\bar{p}p \rightarrow 3\pi^0$ (three entries/event) with the fit (solid line) described in the text.

A statistical sample an order of magnitude larger then revealed a new feature (Amsler *et al.,* 1994e), which was consolidated by a reanalysis of the early Crystal Barrel data (Anisovich *et al.,* 1994): the presence in the Dalitz plot of a narrow homogeneously populated band from a scalar resonance, $f_0(1500)$, decaying to $2\pi^0$. The $3\pi^0$ Dalitz plot is shown in Fig. 22(c) and the $2\pi^0$ mass projection in Fig. 23.

Qualitatively, one observes the following features: the population along the $\pi\pi$ mass band marked $f_2(1270)$ increases at the edges of the Dalitz plot, indicating that one decay π^0 is preferably emitted along the flight direction of the resonance. This is typical of a spin-2 resonance decaying with the angular distribution $(3\cos^2\theta-1)^2$ from $^1S_0$ or $(1+3\cos^2\theta)$ from $^3P_1$. The blobs labeled $f_2(1565)$ at the corners correspond to an angular distribution $\sin^2\theta$ from another spin-2 resonance produced from $^3P_2$, together with constructive interference from the two $\pi\pi$ S waves. The $f_0(980)$ appears as a narrow dip in the $\pi\pi$ S wave. The new feature is the homogeneous narrow band marked $f_0(1500)$, which must be due to a spin-0 state.

The analysis of the full data sample was performed with the K-matrix formalism (Amsler *et al.,* 1995f). A 2×2 K matrix with three poles was sufficient to describe the $\pi\pi$ S wave. Elastic $\pi\pi$ scattering data up to 1200 MeV from Grayer *et al.* (1974) and Rosselet *et al.* (1977) were also included in the fit. The contributing scalar resonances are $f_0(980)$ and

$$f_0(1370):\quad m\simeq1330,\quad \Gamma\sim760\,\text{MeV},$$

$$f_0(1500):\quad m=1500\pm15,\quad \Gamma=120\pm25\,\text{MeV}. \tag{101}$$

A four-pole K matrix helps to constrain the $f_0(1370)$ parameters, giving

$$f_0(1370):\quad m=1330\pm50,\quad \Gamma=300\pm80\,\text{MeV}, \tag{102}$$

and the fourth pole corresponds to a 600-MeV broad structure around 1100 MeV [called $f_0(400-1200)$ by the Particle Data Group (Barnett *et al.,* 1996)], also reported by a recent reanalysis of $\pi\pi$ S-wave data (Morgan and Pennington, 1993; Kaminski, Lesniak, and Rybicki, 1997). The data are therefore compatible with three or four poles, and it is not obvious that $f_0(1370)$ and $f_0(400-1200)$ are not part of one and the same object.

A one-dimensional K matrix describes the $\pi\pi$ D wave. In addition to $f_2(1270)$ one finds

$$f_2(1565):\quad m\sim1530,\quad \Gamma\sim135\,\text{MeV}. \tag{103}$$

The fractional contribution of P waves is 46%. Without P waves the fit deteriorates markedly, but the $f_0(1370)$ and $f_0(1500)$ parameters remain stable. We shall return to $f_2(1565)$ in the discussion below. Branching ratios are given in Table X.

D. Coupled-channel analysis

A simultaneous fit was performed to the channels $\pi^0\eta\eta$, $\pi^0\pi^0\eta$, and $3\pi^0$ (Amsler *et al.*, 1995g) using the full data samples presented in the previous sections with, in addition, the $\pi\pi$ scattering data up to 1200 MeV. However, pure S-wave annihilation was assumed. A 3×3 K matrix with 4 poles was used to describe the $\pi\pi$ S-wave coupling to $\pi\pi$, $\eta\eta$, and the at that time unmeasured $K\bar{K}$ through the resonances $f_0(980)$, $f_0(1370)$, $f_0(1500)$, also taking into account the broad structure around 1100 MeV. Common β_α parameters [Eq. (89)] were introduced to describe the production of resonances associated with the same recoiling particle. For example, $f_0(1500)$ recoiling against π^0 is produced with the same strength in $\pi^0\eta\eta$ and $3\pi^0$. The $\eta\pi$ S wave was described by a 2×2 K matrix for $a_0(980)$ and $a_0(1450)$. The $\pi\pi$, $\eta\eta$, and $\eta\pi$ D waves were treated with one-dimensional K matrices, the latter including $a_2(1320)$ and $a_2'(1650)$ with pole parameters taken from the $\pi^0\pi^0\eta$ analysis of Sec. VIII.B.

The branching ratios are given in Table X. Note that the $\pi\pi$ S wave includes contributions from $f_0(400-1200)$, $f_0(980)$, and $f_0(1370)$ [but excluding $f_0(1500)$], which cannot be disentangled due to interferences. The fit is in good agreement with the single-channel analyses and constrains the resonance parameters. Hence a consistent description of all three annihilation channels was achieved with the following main features:

(1) The data demand three scalar resonances in the 1300–1600 MeV region:

$$a_0(1450):\quad m=1470\pm25,\quad \Gamma=265\pm30\,\text{MeV},$$

$$f_0(1370):\quad m=1390\pm30,\quad \Gamma=380\pm80\,\text{MeV},$$

$$f_0(1500):\quad m=1500\pm10,\quad \Gamma=154\pm30\,\text{MeV}. \tag{104}$$

(2) The broad scalar structure around 1100 MeV, $f_0(400-1200)$ has very different pole positions in sheets II and III, making a resonance interpretation of this state difficult.

(3) The production data demand a larger width ($\simeq100$ MeV) for $f_0(980)$ than the $\pi\pi$ scattering data alone [$\simeq50$ MeV, according to Morgan and Pennington (1993)].

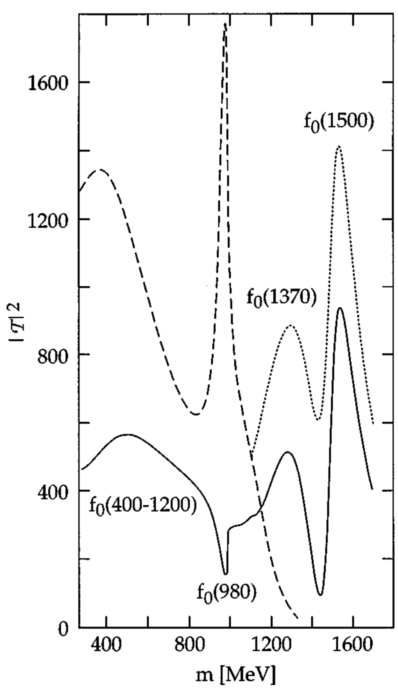

FIG. 24. Isoscalar S-wave production intensities $|\mathcal{T}|^2$ in $3\pi^0$ (solid curve), $2\pi^0\eta$ (dashed curve), and $2\eta\pi^0$ (dotted curve) before multiplying by the phase-space factor ρ. The vertical scale is arbitrary (from Spanier, 1994).

(4) A tensor meson is observed in the $\pi\pi$ D wave with mass 1552 and width 142 MeV, in accord with May *et al.* (1989, 1990), notwithstanding the absence of atomic P waves in the present analysis. A structure is also required in this mass range in the $\eta\eta$ D wave. This state is not compatible with $f_2'(1525)$, which is produced with a much lower rate, as we shall see in Sec. X.C.

The $\pi\pi$ scattering amplitude T [Eq. (86)] obtained from the fit to the elastic-scattering data and the Crystal Barrel data is shown in Fig. 19. Note that Crystal Barrel $K\bar{K}$ data are not yet included and therefore the third K-matrix channel also contains by default all other unmeasured inelasticities. Figure 24 shows the $I=0$ S-wave production intensity $|\mathcal{T}|^2$ [Eq. (88)] for the three annihilation channels. The maxima around 1300 and 1550 MeV correspond to the K-matrix poles for $f_0(1370)$ and $f_0(1500)$. It is instructive to compare the dip around 1000 MeV in the $\pi\pi$ S wave for the $3\pi^0$ channel to the peak in the $\pi^0\pi^0\eta$ channel, both due to $f_0(980)$. This is produced by interferences between the $\pi\pi$ S waves in $3\pi^0$ which have the opposite sign to the interference between the $\pi\pi$ and the $\eta\pi$ S waves in $\eta\pi^0\pi^0$. The $\pi\pi$ S wave in $\pi\pi$ scattering exhibits qualitatively the same behavior as in $\bar{p}p$ annihilation into $3\pi^0$, namely, sharp minima around 1000 and 1450 MeV. The ansatz (100) used in several Crystal Barrel analyses [e.g., in Aker *et al.* (1991)] for the $\pi\pi$ S wave is therefore a rough but reasonable approximation.

E. $\bar{p}p\rightarrow\pi^0\eta\eta'$

Another piece of evidence for the $f_0(1500)$ stems from $\pi^0\eta\eta'$ (Amsler *et al.,* 1994f). This channel was also

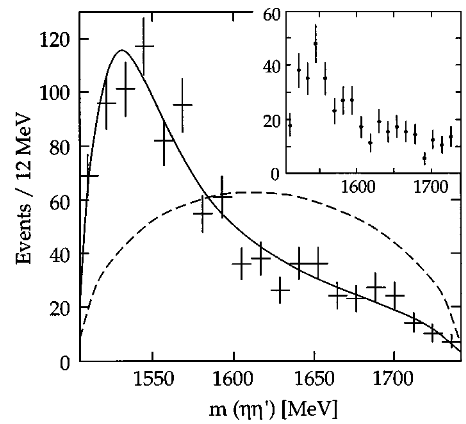

FIG. 25. $\eta\eta'$ mass projection in $\pi^0\eta\eta'$. The solid curve is the fit to the 6γ data with a scalar resonance close to threshold and the dashed curve shows the expected phase-space distribution. The inset shows the $\eta\eta'$ mass distribution from $\pi^0\eta(\rightarrow 2\gamma)\eta'(\rightarrow\eta\pi^+\pi^-)$.

reconstructed from the 6γ final state. Since η' decays to $\gamma\gamma$ with a branching ratio of only 2.1%, the data sample is small (977 events). Most of these events were collected with the online trigger requiring one π^0, one η, and one η'. The $\pi^0\eta\eta'$ Dalitz plot shows an accumulation of events at small $\eta\eta'$ masses. Figure 25 shows the $\eta\eta'$ mass projection. The $\eta\eta'$ mass spectrum from the same annihilation channel, but with $\eta'\rightarrow\eta\pi^+\pi^-$, has entirely different systematics but is identical (inset in Fig. 25). The enhancement at low masses is due to a scalar resonance, since the angular distribution in the $\eta\eta'$ system is isotropic. A maximum-likelihood fit was performed to the 6γ channel using a (damped) Breit-Wigner function according to Eqs. (55), (56), and a flat incoherent background. The resonance parameters are

$$f_0(1500):\quad m=1545\pm 25,\quad \Gamma=100\pm 40\,\text{MeV}. \qquad (105)$$

The branching ratio is given in Table X. The $f_0(1500)$ mass is somewhat larger than for $3\pi^0$ and $\pi^0\eta\eta$. However, Abele *et al.* (1996a) point out that a constant width in the denominator of the Breit-Wigner function yields a mass around 1500 MeV. This is a more realistic procedure, since the total width at the $\eta\eta'$ threshold remains finite due to the channels $\pi\pi$ and $\eta\eta$. However, this does not modify the branching ratio for $f_0(1500)$ $\rightarrow\eta\eta'$. We shall therefore ignore Eq. (105), when averaging below the $f_0(1500)$ mass and width.

F. $\bar{p}p\rightarrow\pi^0\pi^0\eta'$

With zero-prong data this final state is accessible through $\eta'\rightarrow 2\gamma$ or $\eta'\rightarrow\eta\pi^0\pi^0$, leading to six or ten photons, respectively (Abele *et al.,* 1997e). The branching ratios from both final-state configurations agree (Table IX). A sample of 8230 10γ events were kinematically fitted to $4\pi^0\eta$. The $\pi^0\pi^0\eta$ mass distribution (Fig. 26) shows a sharp signal from η' and a shoulder around 1400 MeV due to the E meson, which will be discussed in Sec. XII.

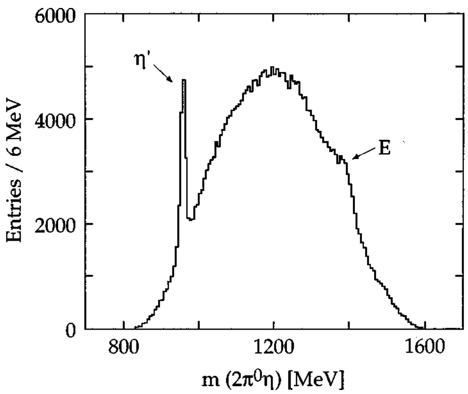

FIG. 26. $2\pi^0\eta$ mass distribution recoiling against $\pi^0\pi^0$ for events with ten reconstructed photons (six entries/event).

The $\pi^0\pi^0\eta'$ Dalitz plot was obtained by selecting events in the η' peak and subtracting background Dalitz plots from either side of the peak. It shows a broad accumulation of events in its center which can be described by a dominating $\pi\pi$ S wave and small contributions from $a_2(1320)$ and $a_0(1450)$ with branching ratios given in Table X. These resonances are included in the fit with fixed mass and width. The ratios of rates for $a_2(1320)$ and $a_0(1450)$ decays into $\eta\pi$ and $\eta'\pi$ can be predicted from SU(3) and compared with measurements. This will be discussed in Sec. X.A. An analysis of the 6γ Dalitz plot (3559 events) leads to similar results. Figure 27 shows that $a_0(1450)$ is required for a satisfactory description of this annihilation channel.

G. $\bar{p}p\rightarrow\pi^0K_LK_L$

The isoscalar $f_0(1500)$ meson has been observed to decay into $\pi^0\pi^0$, $\eta\eta$ and $\eta\eta'$. To clarify its internal structure it was essential to search as well for its $K\bar{K}$ decay mode. In a previous bubble-chamber experiment (Gray *et al.,* 1983) no $K\bar{K}$ signal had been observed in the 1500-MeV region in $\bar{p}p$ annihilation into $K\bar{K}\pi$, leading to the conclusion that the $f_0(1500)$ coupling to $K\bar{K}$ was suppressed (Amsler and Close, 1996; see also Amsler and Close, 1995). However, no partial-wave analysis was performed due to limited statistics.

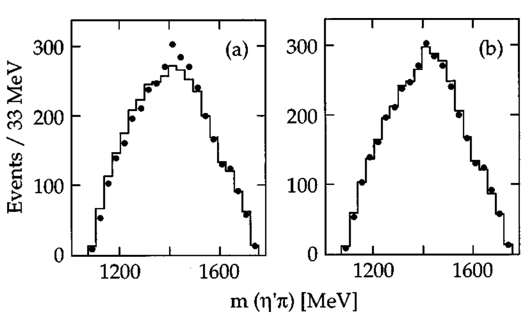

FIG. 27. $\eta'\pi^0$ mass projection in $\pi^0\pi^0\eta'\rightarrow 6\gamma$ for data (dots) and fits (histograms): (a) $(\pi\pi)$ S wave and $a_2(1320)$; (b) including the $a_0(1450)$ (best fit).

Crystal Barrel therefore searched for the $f_0(1500)$ in the annihilation channel $\pi^0K_LK_L$ (Abele *et al.,* 1996b; Dombrowski, 1996), which proceeds from the $^1S_0$ atomic state. All-neutral events were selected with three energy clusters in the barrel, and the channel $\bar{p}p\rightarrow\pi^0K_LK_L$ could be reconstructed by measuring the $\pi^0(\rightarrow 2\gamma)$ momentum and the direction of one of the K_L which interacts hadronically in the CsI barrel. The main background contribution was due to events with a reconstructed π^0 and one additional γ which happened to fulfill the $\pi^0K_LK_L$ kinematics but for which one or more γ's had escaped detection. This background ($\sim$17%) could be removed by subtracting a Dalitz plot constructed from 2γ pairs with invariant masses just below or above the π^0 mass.

Further background contributions were due to $\bar{p}p\rightarrow\omega K_LK_L$ where ω decays to $\pi^0\gamma$ and both K_L were not detected, and $\bar{p}p\rightarrow K_SK_L$ where one photon from $K_S\rightarrow\pi^0\pi^0\rightarrow 4\gamma$ and the K_L were undetected. These events could be removed with appropriate mass cuts. Background from final states like $\omega\eta$, $\omega\pi^0$, and $3\pi^0$ were studied by Monte Carlo simulation. The total residual background contamination was $(3.4\pm0.5)\%$.

The background-subtracted Dalitz plot is shown in Fig. 22(d). This plot was not symmetrized with respect to the diagonal axis, since one K_L was detected (vertical axis) whilst the other was missing (horizontal axis). The interaction probability as a function of K_L momentum was measured by comparing the intensities along the two K^* bands, $K^*\rightarrow K_L\pi^0$. The interaction probability was found to be flat with K_L momentum, but increasing slowly below 300 MeV/c (Dombrowski, 1996). The $\pi^0K_LK_L$ Dalitz plot shown in Fig. 22(d) is already corrected for detection efficiency and for K_L decay between the production vertex and the crystals. Its symmetry along the diagonal axis is nearly perfect, indicating that acceptance and backgrounds have been taken into account properly.

One observes signals from $K^*(892)$ decaying to $K\pi$ and $a_2(1320)/f_2(1270)$ decaying to $K\bar{K}$. The accumulation of events at the edge for small $K\bar{K}$ masses is due to the tensor $f_2'(1525)$, which is observed for the first time in $\bar{p}p$ annihilation at rest. These resonances and the broad $K_0^*(1430)$ were introduced in a first attempt to fit the Dalitz plot.[8] The K matrix for the $K\pi$ $(I=1/2)$ S wave was written as

$$K=\frac{am}{2+abp^2}+\frac{m_0\Gamma_0/\rho_0}{m_0^2-m^2}, \tag{106}$$

where the first term describes the low-energy $K\pi$ scattering (a is the scattering length and b the effective range) and the second term accounts for the $K_0^*(1430)$

[8]The absence of threshold enhancement from $a_0(980)$ or $f_0(980)$ at the upper right border of the Dalitz plot could be due to destructive interference between these states and/or to the loss of acceptance close to the $K\bar{K}$ threshold.

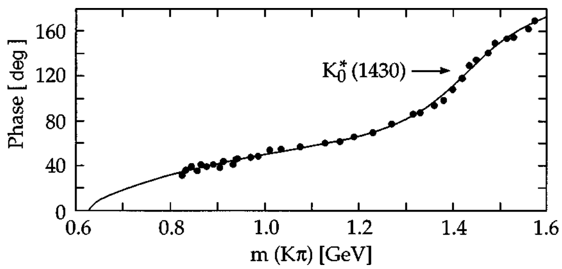

FIG. 28. The phase shift δ in elastic $K\pi$ scattering from Aston *et al.* (1988b). The curve shows the fit using prescription (106).

resonance. The parameters m_0, Γ_0, a, and b were determined by fitting the scattering amplitude T [Eq. (74)] to the $K\pi$ phase shifts (Aston, 1988b). The fit is shown in Fig. 28. Note that resonance occurs at $\delta\simeq 120°$. The corresponding mass and width (T-matrix pole) for the $K_0^*(1430)$ are $m=(1423\pm 10)$ MeV and (277 ± 17) MeV, respectively, in close agreement with Aston *et al.* (1988b), who used a different parametrization and found $m_0=1429\pm 6$ and $\Gamma_0=287\pm 23$ MeV.

A one-pole K matrix for a scalar resonance was added for the peak around 1450 MeV in the $K\bar{K}$ mass distribution (Fig. 29). The fit clearly fails to describe the $K\bar{K}$ mass spectrum (dashed line in Fig. 29). The second attempt assumed a K matrix with two scalar resonances, $f_0(1370)$ and $f_0(1500)$, in the $K\bar{K}$ amplitude. The fit now provided a satisfactory description of the Dalitz plot and the $K\bar{K}$ mass spectrum (solid line in Fig. 29). However, the isovector meson $a_0(1450)$ is also expected to decay to K_LK_L and one cannot distinguish between isovector and isoscalar mesons from the $\pi^0K_LK_L$ data alone. Therefore a Breit-Wigner function was added for the isovector meson $a_0(1450)$ with fixed mass and width taken from the coupled-channel analysis (Sec. VIII.D). The $f_0(1370)$ and $f_0(1500)$ poles are stable, nearly independent of the $a_0(1450)$ contribution. One finds

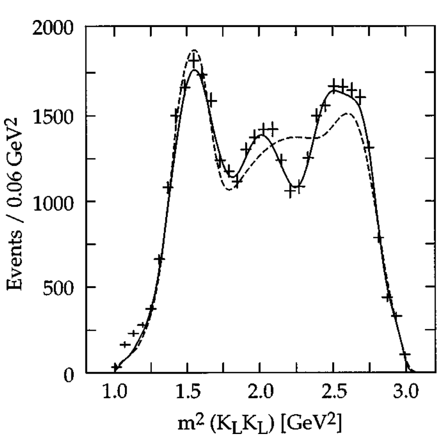

FIG. 29. $K\bar{K}$ mass projection in $\pi^0K_LK_L$. The dashed line shows the fit with one scalar resonance, the solid line the fit with two scalar resonances. The peak on the left is due to $f_2(1270)$ and $a_2(1320)$ and the peak on the right to $K^*(892)$ reflections. The central peak is due to interference from various amplitudes.

$$f_0(1370):\quad m=1380\pm 40,\quad \Gamma=360\pm 50\,\mathrm{MeV},$$
$$f_0(1500):\quad m=1515\pm 20,\quad \Gamma=105\pm 15\,\mathrm{MeV}, \tag{107}$$

in agreement with the resonance parameters measured in the other decay channels.

Due to uncertainties in the K_L interaction probability the branching ratio for $\pi^0K_LK_L$ could not be determined accurately. The branching ratios given in Table XI (Abele *et al.*, 1996b; Dombrowski, 1996) are therefore normalized to the known branching ratio for $\pi^0K_SK_S$ (Armenteros *et al.,* 1965; Barash *et al.,* 1965).[9]

The branching ratios for $\bar{p}p\to f_0(1370)$ and $f_0(1500)\to K_LK_L$ also vary with the $a_0(1450)$ contribution (Fig. 30). In Table XI the branching ratios for $f_0(1370)$ and $f_0(1500)$ are therefore derived from Fig. 30 assuming an $a_0(1450)$ contribution r_0 to the $\pi^0K_LK_L$ final state, derived from its measured contribution $r=(10.8\pm 2.0)\%$ to $\pi^\pm K^\mp K_L$ (next section)

$$r_0=\frac{r}{4}\,\frac{B(\bar{p}p\to\pi^\pm K^\mp K_S)}{B(\bar{p}p\to\pi^0K_SK_S)}=(9.8\pm 1.9)\%, \tag{108}$$

where we have used the branching ratios from Armenteros *et al.* (1965) and Barash *et al.* (1965).

H. $\bar{p}p\to\pi^\pm K^\mp K_L$

This channel selects only isospin-1 resonances decaying to $K\bar{K}$ and therefore permits a direct measurement of the contribution from isovector mesons to $K\bar{K}\pi$, in particular from $a_0(1450)$. Crystal Barrel studied the reaction $\bar{p}p\to\pi^\pm K^\mp K_L$ with a noninteracting K_L (Heinzelmann, 1996; Abele *et al.,* 1998d). This channel was selected from 7.7×10^6 triggered two-prong data by requiring exactly two clusters in the barrel from $\pi^\pm$ and $K^\mp$. Particle identification was achieved by measuring the ionization in the drift chamber (Fig. 31) and a one-constraint kinematic fit ensured momentum and energy conservation. The background contribution, mainly from $\pi^+\pi^-\pi^0$, was about 2%. The Dalitz plot (Fig. 32) was corrected for background and acceptance, as well as for the K_L interaction probability. The latter was determined by reconstructing the channel $\pi^0K_S(\to\pi^+\pi^-)K_L$ with and without missing K_L. The branching ratio

$$B(\bar{p}p\to\pi^\pm K^\mp K_L)=(2.91\pm 0.34)\times 10^{-3} \tag{109}$$

is in excellent agreement with the one given in Table XI for $\pi^\pm K^\mp K_S$ from bubble-chamber experiments (Armenteros *et al.,* 1965; Barash *et al.,* 1965).

The Dalitz plot shows clear signals from $K^*(892)$, $a_2(1320)$, and $a_0(980)$. The $K^*(892)$ and $a_2(1320)$ were parametrized by Breit-Wigner functions. The $a_0(980)$ was described by a 2×2 K matrix [Flatté for-

[9]The isospin contributions from $^1S_0$ to the $K^*\bar{K}$ system cannot be determined in this channel since the K^* bands interfere constructively for both $I=0$ and $I=1$.

TABLE XI. Branching ratios for $\overline{p}p$ annihilation at rest in liquid into kaonic channels. The branching ratios include only the decay mode of the intermediate resonance leading to the observed final state.

Channel / Subchannel	$\overline{p}p(I)$	Contributing resonances / Branching ratio
$\pi^0 K_L K_L$		$K^*(892), K_0^*(1430), a_2(1320), f_2(1270), f_2'(1525)$ $f_0(1370), f_0(1500), a_0(1450)$
Total [a]		$(7.5 \pm 0.3) \times 10^{-4}$
$K^*(892)\overline{K}$	$^1S_0(0,1)$	$(8.71 \pm 0.68) \times 10^{-5}$
$K_0^*(1430)\overline{K}$		$(4.59 \pm 0.46) \times 10^{-5}$ [b]
$a_2(1320)\pi^0$	$^1S_0(0)$	$(6.35 \pm 0.74) \times 10^{-5}$
$a_0(1450)\pi^0$		$(7.35 \pm 1.42) \times 10^{-5}$ [c]
$f_2(1270)\pi^0$	$^1S_0(1)$	$(4.25 \pm 0.59) \times 10^{-5}$
$f_2'(1525)\pi^0$		$(1.67 \pm 0.26) \times 10^{-5}$
$f_0(1370)\pi^0$		$(2.20 \pm 0.33) \times 10^{-4}$
$f_0(1500)\pi^0$		$(1.13 \pm 0.09) \times 10^{-4}$
$\pi^\pm K^\mp K_L$		$K^*(892), K_0^*(1430), a_2(1320)$ $a_0(980), a_0(1450), \rho(1450/1700)$
Total [a]		$(2.73 \pm 0.10) \times 10^{-3}$
$K^*(892)\overline{K}$	$^1S_0(0)$	$(2.05 \pm 0.28) \times 10^{-4}$
$K_0^*(1430)\overline{K}$		$(8.27 \pm 1.93) \times 10^{-4}$ [b]
$a_0(980)\pi$		$(1.97^{+0.15}_{-0.34}) \times 10^{-4}$
$a_2(1320)\pi$		$(3.99^{+0.31}_{-0.83}) \times 10^{-4}$
$a_0(1450)\pi$		$(2.95 \pm 0.56) \times 10^{-4}$
$K^*(892)\overline{K}$	$^1S_0(1)$	$(3.00 \pm 1.10) \times 10^{-5}$
$K_0^*(1430)\overline{K}$		$(1.28 \pm 0.55) \times 10^{-4}$ [b]
$\rho(1450/1700)\pi$		$(8.73^{+1.40}_{-2.75}) \times 10^{-5}$
$K^*(892)\overline{K}$	$^3S_1(0)$	$(1.50 \pm 0.41) \times 10^{-4}$
$\rho(1450/1700)\pi$		$(8.73 \pm 2.75) \times 10^{-5}$
$K^*(892)\overline{K}$	$^3S_1(1)$	$(5.52 \pm 0.84) \times 10^{-4}$
$a_2(1320)\pi$		$(1.42 \pm 0.44) \times 10^{-4}$

[a]From the corresponding K_S channels (Armenteros *et al.,* 1965; Barash *et al.,* 1965).
[b]Includes low-energy $K\pi$ scattering.
[c]Fixed by $\pi^\pm K^\mp K_L$ data.

mula (93)]. The $K\pi$ S wave $[K_0^*(1430)]$ was treated using the data from Aston *et al.* (1988b), as described in the previous section. In contrast to $\pi^0 K_L K_L$, both atomic states $^1S_0$ and $^3S_1$ contributed. The $I=0$ and $I=1$ contributions to $K^*(892)\overline{K}$ could be determined from the (destructive) interference pattern around the crossing point of the K^* bands in Fig. 32.

The fit, however, did not provide a satisfactory description of the Dalitz plot, and the fitted $a_2(1320)$ mass, 1290 MeV, was significantly lower than the table value, a problem that had been noticed earlier in bubble-chamber data (Conforto *et al.,* 1967). A substantial improvement in the χ^2 (Fig. 33) was obtained when introducing the $a_0(1450)$ as a second pole in the K matrix, together with $a_0(980)$, leading to the resonance parameters (T-matrix pole)

$$a_0(1450): m = 1480 \pm 30, \quad \Gamma = 265 \pm 15\,\text{MeV}, \qquad (110)$$

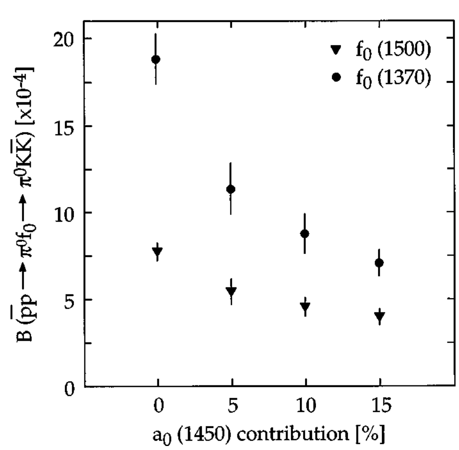

FIG. 30. Branching ratio for $f_0(1370)$ and $f_0(1500)$ decay into $K\overline{K}$ as a function of $a_0(1450)$ contribution to $\pi^0 K_L K_L$ (from Dombrowski, 1996).

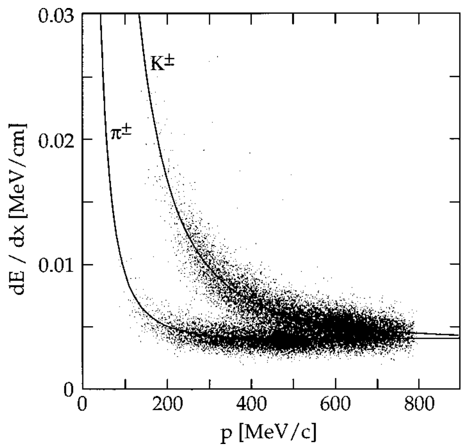

FIG. 31. dE/dx distribution in the jet drift chamber for two-prong events with a missing K_L. The curve shows the expected (Bethe-Bloch) dependence.

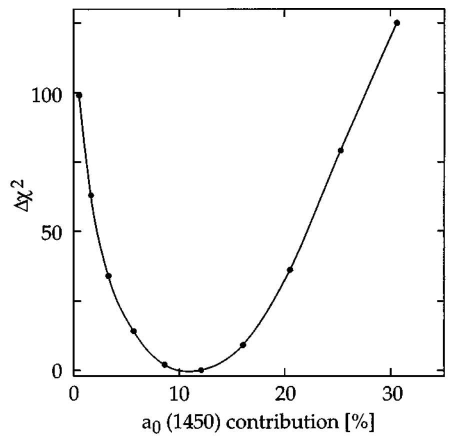

FIG. 33. χ^2 dependence on the fractional contribution from $a_0(1450)$ to $\pi^{\pm}K^{\mp}K_L$.

in agreement with the $\eta\pi$ decay mode. The $a_2(1320)$ mass now became compatible with the table value (Barnett *et al.,* 1996). We shall show below that the contribution to $\pi^{\pm}K^{\mp}K_L$ of $(10.8\pm 2.0)\,\%$ (Fig. 33) is consistent with predictions from the $\pi^0\pi^0\eta$ channel, using SU(3).

An even better fit was achieved by adding a broad structure in the $K\bar{K}$ P wave, presumably from the radial excitations $\rho(1450)$ and $\rho(1700)$, which could not, however, be disentangled by the fit.

For the $a_0(980)$ one finds for the T-matrix pole in the second Riemann sheet a mass of 987±3 MeV and a width of 86±7 MeV. Using the $\eta\pi$ decay branching ratio from the $\pi^0\pi^0\eta$ analysis (Table X) one also obtains the ratio

$$\frac{B(a_0(980)\rightarrow K\bar{K})}{B(a_0(980)\rightarrow \eta\pi)}=0.23\pm 0.05. \tag{111}$$

The ratio of couplings $g_2/g_1=g_{\eta\pi}/g_{K\bar{K}}$ can be tuned to satisfy Eq. (111) by integrating the mass distributions over the $a_0(980)$ distribution (Fig. 20). One gets $g_1=0.324\pm 0.015$ GeV and $g_2^2/g_1^2=1.03\pm 0.14$, in good agreement with the estimate from the line shape in the $\pi^0\pi^0\eta$ channel [Eq. (98)].

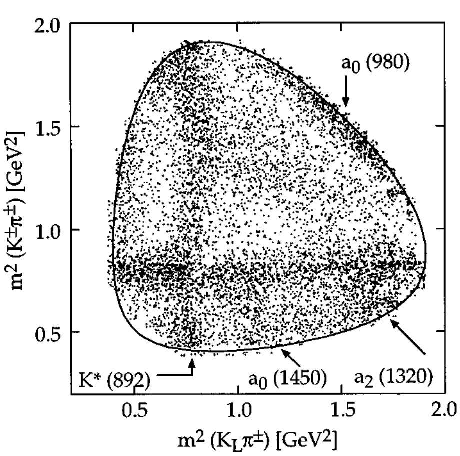

FIG. 32. $\pi^{\pm}K^{\mp}K_L$ Dalitz plot (11 373 events).

The branching ratios are given in Table XI. The intermediate $K^*\bar{K}$ is largest in the $(I=1)$ $^3S_1$ channel, a feature that was noticed before (Barash *et al.,* 1965; Conforto *et al.,* 1967) and that we have used in Sec. VI.A as a possible explanation for the $\pi\phi$ enhancement. The branching ratios are in fair agreement with those from Conforto *et al.* (1967) and those for $\pi^0K_LK_L$, except for the much larger $K\pi$ S wave in $\pi^{\pm}K^{\mp}K_L$.

I. Summary

Let us summarize the results presented in this section. Crystal Barrel studied the Dalitz plots for annihilation at rest into three neutral light pseudoscalar mesons: $3\pi^0$, $2\pi^0\eta$, $2\pi^0\eta'$, $2\eta\pi^0$, $\pi^0\eta\eta'$, $\pi^0\pi^0\eta'$, and $\pi^0K_LK_L$. Most of these channels were observed for the first time with very high statistics. A consistent description of the data was achieved from the $^1S_0$ initial state with the K-matrix formalism when introducing (i) four poles for the (isoscalar) $\pi^0\pi^0$ S wave, $f_0(980)$, $f_0(1370)$, $f_0(1500)$, and the broad structure $f_0(400-1200)$; (ii) two poles for the $\eta\pi^0$ S wave, $a_0(980)$ and $a_0(1450)$; (iii) a tensor meson in the $\pi\pi$ P wave, $f_2(1565)$. The $f_2'(1525)$ was observed with rates consistent with the predictions of the quark line rule. There was also evidence for the radial excitation of the $a_2(1320)$ around 1650 MeV. A charged $a_0(1450)$ was observed in the annihilation channel $\pi^{\pm}K^{\mp}K_L$. Its production rate was used to disentangle the contributions from $f_0(1370)$, $f_0(1500)$, and $a_0(1450)$ to $\pi^0K_LK_L$ and therefore fix the branching ratio for $f_0(1500)\rightarrow K\bar{K}$. The so-far-unknown couplings of $f_0(980)$ to $K\bar{K}$ and $\eta\pi$ were determined from a comparison of the channels $\pi^0\pi^0\eta$ and $\pi^{\pm}K^{\mp}K_L$.

IX. ANNIHILATION AT REST INTO FIVE PIONS

Resonances in $\rho^+\rho^-$ had been reported in $\bar{p}n$ annihilation in deuterium: A 2^{++} state was observed in bubble-chamber exposures in liquid deuterium (Bridges, Daftari, and Kalogeropoulos, 1987). An enhancement was also seen around 1500 MeV by the Asterix Collaboration at LEAR in gaseous deuterium, but no spin-parity analysis was performed (Weidenauer *et al.,* 1993). This state was interpreted as the $f_2(1565)$ in its $\rho\rho$ decay mode, the slightly lower mass being due to π rescattering with the recoil proton exciting the Δ resonance (Kolybashov, Shapiro, and Sokolskikh, 1989). The 2^{++} assignment was, however, disputed in favor of 0^{++} by a reanalysis of the bubble-chamber data (Gaspero, 1993).

The Crystal Barrel also searched for scalar mesons decaying to 4π. The $4\pi^0$ decay mode was investigated using $\bar{p}p$ annihilation into $5\pi^0$, leading to ten detected photons (Abele *et al.,* 1996c). The branching ratio for annihilation into $5\pi^0$ was found to be $(7.1\pm1.4)\times10^{-3}$. After removing the $\eta\to3\pi^0$ contribution, Abele *et al.* performed a maximum-likelihood analysis of a sample of 25 000 $5\pi^0$ events. The data demanded contributions from $\pi(1330)\to3\pi^0$ and from two scalar resonances decaying to $4\pi^0$. The mass and width of the lower state, presumably $f_0(1370)$, could not be determined precisely.

The upper state had a mass of $\sim$1505 MeV and width of $\sim$169 MeV and decayed into two $\pi\pi$ S-wave pairs and $\pi^0(1300)\pi^0$ with approximately equal rates. The branching ratio for $\bar{p}p\to f_0(1500)\pi^0\to5\pi^0$ was $(9.0\pm1.4)\times10^{-4}$. Using the 2π branching ratio from the coupled-channel analysis one finds

$$\frac{B(f_0(1500)\to4\pi)}{B(f_0(1500)\to2\pi)}=2.1\pm0.6, \tag{112}$$

$$\frac{B(f_0(1500)\to4\pi^0)}{B(f_0(1500)\to\eta\eta)}=1.5\pm0.5. \tag{113}$$

The $4\pi^0$ contribution in Eq. (112) was multiplied by 9 and the $2\pi^0$ contribution multiplied by 3 to take into account the unobserved charged pions. The ratio (112) is, in principle, a lower limit, which does not include $\rho\rho$. However, a reanalysis of the Mark III data on $J/\psi\to\gamma2\pi^+2\pi^-$ finds evidence for the $f_0(1500)$ decaying to 4π through two S-wave dipions with negligible $\rho\rho$ contribution (Bugg *et al.,* 1995). The ratio (113) is in agreement with the result for the former $f_0(1590)$ from Alde *et al.* (1987) in $\pi^-p\to4\pi^0n$: 0.8 ± 0.3.

A scalar resonance with mass 1374 ± 38 MeV and width 375 ± 61 MeV decaying to $\pi^+\pi^-2\pi^0$ was also reported by Crystal Barrel in the annihilation channel $\pi^+\pi^-3\pi^0$ (Amsler *et al.,* 1994d). The branching ratio for $\pi^+\pi^-3\pi^0$ was measured to be (9.7 ± 0.6)%. The 4π decay mode of the resonance was five times larger than the 2π, indicating a large inelasticity in the 2π channel. The relative decay ratio to $\rho\rho$ and two $\pi\pi$ S waves was 1.6 ± 0.2. However, the data do not exclude the admixture of a $f_0(1500)$ contribution.

X. THE NEW MESONS

We now discuss the properties of the mesons $a_0(1450)$, $f_0(1370)$, $f_0(1500)$, and $f_2(1565)$, reported in Secs. VIII and IX. It is instructive first to check the consistency within Crystal Barrel data and also to compare with previous measurements. The squares of the isospin Clebsch-Gordan coefficients determine the total branching ratios, including all charge modes. Note that two neutral isovector resonances [e.g., $a_2^0(1320)\pi^0$] do not contribute to $I=1$. Table XII gives the corresponding weights to $K\bar{K}$. For $K^*(892)$, $K_0^*(1430)$, $a_2(1320)$, and $a_0(1450)$ contributions to $K\bar{K}\pi$ the $\pi^0K_LK_L$ ratios in Table XI must be multiplied by a factor of 12, while those for $f_2(1270)$, $f_0(1370)$, $f_0(1500)$, and $f_2'(1525)$ must be multiplied by 4 (since K_S is not observed). For $\pi^\pm K^\mp K_L$ the resonance contributions in Table XI have to be multiplied by 3 for $K^*(892)$, $K_0^*(1430)$, by 3 for $a_0(980)$, $a_2(1320)$, $\rho(1450/1700)$ from $I=0$, and by 2 for $a_2(1320)$, $\rho(1450/1700)$ from $I=1$.

TABLE XII. Weights of the channels contributing to $\bar{p}p\to\pi K\bar{K}$. I refers to the $\bar{p}p$ isospin and i to the $K\pi$ or $K\bar{K}$ isospin.

Channel	$K\pi$ $i=1/2$ $I=0,1$	$i=1$ $I=1$	$K\bar{K}$ $i=0$ $I=1$	$i=1$ $I=0$
$\pi^\pm K^\mp K^0$	4	2	0	4
$\pi^0K^+K^-$	1	0	1	1
$\pi^0K^0\overline{K^0}$	1	0	1	1

Furthermore, the branching ratios must be corrected for all decay modes of the intermediate resonances to obtain the two-body branching ratios in Table XIII. We have used the following decay branching ratios (Barnett *et al.,* 1996): (28.2 ± 0.6)% for $f_2(1270)\to\pi^0\pi^0$, (4.6 ± 0.5)% for $f_2(1270)\to K\bar{K}$, (14.5 ± 1.2)% for $a_2(1320)\to\eta\pi$, (4.9 ± 0.8)% for $a_2(1320)\to K\bar{K}$, (0.57 ± 0.11)% for $a_2(1320)\to\eta'\pi$, and (88.8 ± 3.1)% for $f_2'(1525)\to K\bar{K}$. There are indications that the $a_2(1320)$ contribution to $\pi\pi\eta$ is somewhat too large. Otherwise the consistency is, in general, quite good and Crystal Barrel results also agree with previous data. This gives confidence in the following discussion on the new mesons.

A. a_0(1450)

We begin with the isovector meson $a_0(1450)$, which was observed in its $\eta\pi$, $\eta'\pi$, and $K\bar{K}$ decay modes. Averaging mass and width from the coupled channel and the $K\bar{K}$ analyses, one finds

$$a_0(1450):\quad m=1474\pm19,\quad \Gamma=265\pm13\,\text{MeV}. \tag{114}$$

The $a_0(1450)$ decay rates are related by SU(3) flavor, which can be tested with Crystal Barrel data. Following Amsler and Close (1996) we shall write for a quarkonium state

$$|q\bar{q}\rangle=\cos\alpha|n\bar{n}\rangle-\sin\alpha|s\bar{s}\rangle, \tag{115}$$

where

TABLE XIII. Branching ratios B for two-body $\overline{p}p$ annihilation at rest in liquid hydrogen (including all decay modes), calculated from the final states given in the last column.

Channel	B		Final state or Ref.
$f_2(1270)\pi^0$	3.1 ± 1.1	10^{-3}	$\pi^0\pi^0\pi^0$
$f_2(1270)\pi^0$	3.7 ± 0.7	10^{-3}	$\pi^0 K_L K_L$
	4.3 ± 1.2	10^{-3}	Foster *et al.* (1968b)
$f_2(1270)\omega$	3.26 ± 0.33	10^{-2}	Bizzarri *et al.* (1969)
$f_2(1270)\omega$	2.01 ± 0.25	10^{-2}	Amsler *et al.* (1993a)
$f_0(1500)\pi^0$	1.29 ± 0.11	10^{-2}	$\pi^0 K_L K_L$
$f_2'(1525)\pi^0$	7.52 ± 1.20	10^{-5}	$\pi^0 K_L K_L$
$a_2(1320)\pi$	3.93 ± 0.70	10^{-2}	$\pi^0\pi^0\eta$
$(^1S_0)$	3.36 ± 0.94	10^{-2}	$\pi^0\pi^0\eta'$
	1.55 ± 0.31	10^{-2}	$\pi^0 K_L K_L$
	$2.44 \pm ^{0.44}_{0.64}$	10^{-2}	$\pi^\pm K^\mp K_L$
	1.32 ± 0.37	10^{-2}	Conforto *et al.* (1967)
$a_2^\pm(1320)\pi^\mp$	5.79 ± 2.02	10^{-3}	$\pi^\pm K^\mp K_L$
$(^3S_1)$	4.49 ± 1.83	10^{-3}	Conforto *et al.* (1967)
$b_1^\pm(1235)\pi^\mp$	7.9 ± 1.1	10^{-3}	Bizzarri *et al.* (1969) [a]
$b_1^0(1235)\pi^0$	9.2 ± 1.1	10^{-3}	Amsler *et al.* (1993a) [a]
$a_2^0(1320)\omega$	1.70 ± 0.15	10^{-2}	Amsler *et al.* (1994c)
$K^*(892)\overline{K}$	7.05 ± 0.90	10^{-4}	$\pi^\pm K^\mp K_L$
$(^1S_0)$	1.05 ± 0.08	10^{-3}	$\pi^0 K_L K_L$
	1.5 ± 0.3	10^{-3}	Conforto *et al.* (1967)
$K^*(892)\overline{K}$	2.11 ± 0.28	10^{-3}	$\pi^\pm K^\mp K_L$
$(^3S_1)$	2.70 ± 0.37	10^{-3}	$\pi^0 K_S K_L$ [b]
	$\geqslant 2.51 \pm 0.22$	10^{-3}	Conforto *et al.* (1967)

[a]Assumes 100% b_1 decay to $\pi\omega$.
[b]Using $B(\pi^0\phi)$ from Table VI and Eq. (47).

$$|n\overline{n}\rangle \equiv (u\overline{u}+d\overline{d})/\sqrt{2}. \quad (116)$$

The mixing angle α is related to the usual nonet mixing angle θ (Barnett *et al.,* 1996) by the relation

$$\alpha = 54.7^\circ + \theta. \quad (117)$$

Ideal mixing occurs for $\theta = 35.3^\circ$ and -54.7°, for which the quarkonium state becomes pure $s\overline{s}$ or $n\overline{n}$, respectively.

The flavor content of η and η' are then given by the superposition [see also Eq. (21)]

$$|\eta\rangle = \cos\,\phi|n\overline{n}\rangle - \sin\,\phi|s\overline{s}\rangle,$$

$$|\eta'\rangle = \sin\,\phi|n\overline{n}\rangle + \cos\,\phi|s\overline{s}\rangle, \quad (118)$$

with $\phi = 54.7^\circ + \theta_p$, where θ_p is the pseudoscalar mixing angle, which we take as $\theta_p = (-17.3 \pm 1.8)^\circ$ (Amsler *et al.,* 1992b).

The partial decay width of a scalar (or tensor) quarkonium into a pair of pseudoscalar states M_1 and M_2 is given by

$$\Gamma(M_1,M_2) = \gamma^2(M_1,M_2) f_L(p) p. \quad (119)$$

The couplings γ can be derived from SU(3) flavor. The two-body decay momentum is denoted by p and the relative angular momentum by L. The form factor

$$f_L(p) = p^{2L} \exp\left(-\frac{p^2}{8\beta^2}\right) \quad (120)$$

provides a good fit to the decay branching ratios of the well-known ground-state 2^{++} mesons if β is chosen $\geqslant 0.5$ GeV/c (Amsler and Close, 1996). We choose $\beta = 0.5$ GeV/c, although the exponential factor can be ignored ($\beta \rightarrow \infty$) without altering the forthcoming conclusions. Replacing $f_L(p)p$ by prescription (28) also leads to a good description of decay branching ratios provided that $p_R > 500$ MeV/c, corresponding to an interaction radius of less than 0.4 fm (Abele *et al.,* 1997e).

The decay of quarkonium into a pair of mesons involves the creation of a $q\overline{q}$ pair from the vacuum. We shall assume for the ratio of the matrix elements for the creation of $s\overline{s}$ versus $u\overline{u}$ (or $d\overline{d}$) that

$$\rho \equiv \frac{\langle 0|V|s\overline{s}\rangle}{\langle 0|V|u\overline{u}\rangle} \simeq 1. \quad (121)$$

This assumption is reasonable, since from the measured decay branching ratios of tensor mesons one finds $\rho = 0.96 \pm 0.04$ (Amsler and Close, 1996). Similar conclusions are reached by Peters and Klempt (1995).

Let us now compare the Crystal Barrel branching ratios for the $a_2(1320)$ decays to $K\overline{K}$, $\eta\pi$ and $\eta'\pi$ with predictions from SU(3). One predicts for an isovector meson with the coupling constants γ given in the appendix of Amsler and Close (1996)

$$\frac{\Gamma(a_2^\pm(1320)\rightarrow K^\pm K^0)}{\Gamma(a_2^0(1320)\rightarrow \eta\pi^0)} = \frac{1}{2\cos^2\phi}\frac{f_2(p_K)p_K}{f_2(p_\eta)p_\eta} = 0.295 \pm 0.013, \quad (122)$$

$$\frac{\Gamma(a_2^0(1320)\rightarrow \eta'\pi^0)}{\Gamma(a_2^0(1320)\rightarrow \eta\pi^0)} = \tan^2\phi \frac{f_2(p_K)p_K}{f_2(p_\eta)p_\eta} = 0.029 \pm 0.004. \quad (123)$$

Both ratios are in excellent agreement with world data (Barnett *et al.,* 1996). The Crystal Barrel numbers to be compared with are taken from Tables X and XI for $I = 0$. One finds the ratios of branching ratios

$$\frac{B(a_2^\pm(1320)\rightarrow K^\pm K^0)}{B(a_2^0(1320)\rightarrow \eta\pi^0)} = 0.21^{+0.04}_{-0.06}, \quad (124)$$

$$\frac{B(a_2^0(1320)\rightarrow \eta'\pi^0)}{B(a_2^0(1320)\rightarrow \eta\pi^0)} = 0.034 \pm 0.009, \quad (125)$$

in fair agreement with SU(3) predictions. We now compare predictions and data for the $a_0(1450)$. From SU(3) one expects, using Eqs. (122) and (123) with $L=0$,

$$\frac{\Gamma(a_0^\pm(1450)\rightarrow K^\pm K^0)}{\Gamma(a_0^0(1450)\rightarrow \eta\pi^0)} = 0.72 \pm 0.03, \quad (126)$$

$$\frac{\Gamma(a_0^0(1450)\to\eta'\pi^0)}{\Gamma(a_0^0(1450)\to\eta\pi^0)}=0.43\pm0.06, \quad (127)$$

in agreement with the experimental results from Tables X and XI,

$$\frac{B(a_0^{\pm}(1450)\to K^{\pm}K^0)}{B(a_0^0(1450)\to\eta\pi^0)}=0.88\pm0.23, \quad (128)$$

$$\frac{B(a_0^0(1450)\to\eta'\pi^0)}{B(a_0^0(1450)\to\eta\pi^0)}=0.35\pm0.16. \quad (129)$$

This then establishes the $a_0(1450)$ as a $q\bar{q}$ isovector state in the scalar nonet.

The existence of the $a_0(1450)$ adds further evidence for the $a_0(980)$ being a non-$q\bar{q}$ state. The $f_0(980)$ and $a_0(980)$ have been assumed to be $K\bar{K}$ molecules (Weinstein and Isgur, 1990; Close, Isgur, and Kumano, 1993). This is motivated by their strong couplings to $K\bar{K}$—in spite of their masses close to the $K\bar{K}$ threshold—and their small $\gamma\gamma$ partial widths. For the $f_0(980)$, the 2γ partial width is $\Gamma_{\gamma\gamma}=(0.56\pm0.11)$ keV (Barnett *et al.*, 1996). The relative ratio for the $a_0(980)$ decay to $K\bar{K}$ and $\eta\pi$ has been determined by Crystal Barrel [Eq. (111)]. Using

$$\Gamma_{\gamma\gamma}B(a_0(980)\to\eta\pi)=0.24\pm0.08\,\text{keV} \quad (130)$$

(Barnett *et al.*, 1996), one then derives the partial width $\Gamma_{\gamma\gamma}=(0.30\pm0.10)$ keV. Thus the 2γ partial widths for the $f_0(980)$ and $a_0(980)$ appear to be similar, close to predictions for $K\bar{K}$ molecules (0.6 keV) and much smaller than for $q\bar{q}$ states (Barnes, 1985). However, not everybody agrees: In Törnqvist (1995) the $f_0(980)/f_0(1370)$ and the $a_0(980)/a_0(1450)$ are different manifestations of the same unitarized $s\bar{s}$ and $\bar{u}d$ states, while the broad structure around 1100 MeV is the $u\bar{u}+d\bar{d}$ state (Törnqvist and Roos, 1996). This then leaves the $f_0(1500)$ as an extra state. The nature of the $a_0(980)$ and $f_0(980)$, whether $q\bar{q}$ mesons, four-quark states, or $K\bar{K}$ molecules, will be clarified by the DAϕNE facility currently under construction at Frascati, by measuring the branching ratios for radiative ϕ decay to the $a_0(980)$ and $f_0(980)$ (Achasov and Gubin, 1997).

B. $f_0(1370)$ and $f_0(1500)$

From the single-channel analyses and the $K\bar{K}$ decay mode we find for $f_0(1370)$ and $f_0(1500)$ the average masses and widths

$$f_0(1370){:}\,m=1360\pm23\,\text{MeV},\quad \Gamma=351\pm41\,\text{MeV},$$

$$f_0(1500){:}\,m=1505\pm9\,\text{MeV},\quad \Gamma=111\pm12\,\text{MeV}. \quad (131)$$

The closeness of the $a_0(1450)$ and $f_0(1500)$ or even $f_0(1370)$ masses is conspicuous and points to a close-to-ideally mixed scalar nonet, one of the latter mesons being one of the $q\bar{q}$ isoscalars. However, the $f_0(1500)$ with a width of about 100 MeV is much narrower than the $a_0(1450)$, $f_0(1370)$, and $K_0^*(1430)$, with widths of typically 300 MeV. Theoretical predictions for the widths of scalar $q\bar{q}$ mesons, based on the $^3P_0$ model, agree that they should have widths of at least 250 MeV [for a discussion and references see Amsler and Close (1996)]. We therefore tentatively assign the $f_0(1370)$ to the ground-state scalar nonet.

If the $f_0(980)$ is indeed a molecule, then the (mainly) $s\bar{s}$ member of the scalar nonet still needs to be identified. We now show from their decay branching ratios that neither the $f_0(1370)$ nor the $f_0(1500)$ are likely candidates. To investigate the quark content of the $f_0(1500)$ we calculate its relative couplings to $\eta\eta$, $\eta\eta'$, and $K\bar{K}$ and search for a common value of the scalar mixing angle α. The ratios of couplings for a pseudoscalar mixing angle ϕ are (Amsler and Close, 1996)

$$R_1\equiv\frac{\gamma^2(\eta\eta)}{\gamma^2(\pi\pi)}=\frac{(\cos^2\phi-\sqrt{2}\tan\alpha\sin^2\phi)^2}{3},$$

$$R_2\equiv\frac{\gamma^2(\eta\eta')}{\gamma^2(\pi\pi)}=\frac{2(\cos\phi\sin\phi[1+\sqrt{2}\tan\alpha])^2}{3},$$

$$R_3\equiv\frac{\gamma^2(K\bar{K})}{\gamma^2(\pi\pi)}=\frac{(1-\sqrt{2}\tan\alpha)^2}{3}. \quad (132)$$

For $\eta\eta$ and $\pi\pi$ we use the branching ratios from the coupled-channel analysis (Table X) and multiply $\pi\pi$ by 3 to take into account the $\pi^+\pi^-$ decay mode. The branching ratio for $K\bar{K}$ is taken from Table XI and is multiplied by 4. The branching fractions are, including the 4π mode from Eq. (112) and ignoring a possible small $\rho\rho$ contribution to 4π,

$$\pi\pi{:}\quad (29.0\pm7.5)\,\%$$

$$\eta\eta{:}\quad (4.6\pm1.3)\,\%$$

$$\eta\eta'{:}\quad (1.2\pm0.3)\,\%$$

$$K\bar{K}{:}\quad (3.5\pm0.3)\,\%$$

$$4\pi{:}\quad (61.7\pm9.6)\,\%. \quad (133)$$

After correcting for phase space and form factor [Eq. (120)] we obtain

$$R_1=0.195\pm0.075,\ R_2=0.320\pm0.114,\ R_3=0.138\pm0.038. \quad (134)$$

Since $f_0(1500)$ lies at the $\eta\eta'$ threshold we have divided the branching ratios by the phase-space factor ρ integrated over the resonance and have neglected the form factor when calculating R_2.

Previously, the upper limit for R_3 was <0.1 (95% confidence level) from Gray *et al.* (1983), in which case no value for the mixing angle α could simultaneously fit R_1, R_2, and R_3 (Amsler and Close, 1996), therefore excluding the $f_0(1500)$ as a $q\bar{q}$ state. The (1σ) allowed regions of tan α are shown in Fig. 34 for the ratios (134).

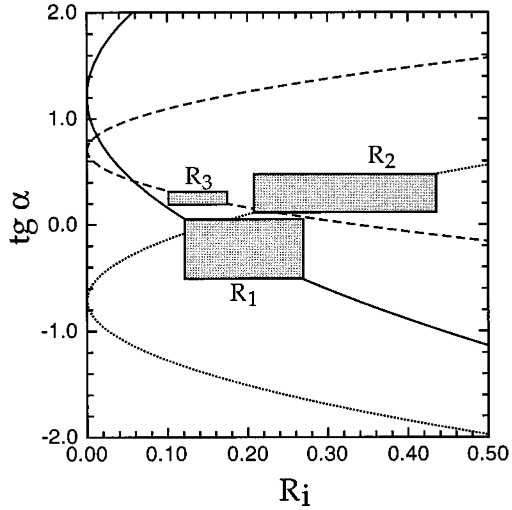

FIG. 34. Tangent of the nonet mixing angle α as a function of R_1 (solid), R_2 (dotted), and R_3 (dashed curve). The shaded areas show the experimentally allowed regions for $f_0(1500)$, assuming that this state is $q\bar{q}$.

The agreement between R_1 and R_3 is not particularly good. Remember, however, that branching ratios are sensitive to interference effects, and therefore caution should be exercised in not overinterpreting the apparent discrepancy in Fig. 34. On the basis of the ratios (134), one may conclude that the $f_0(1500)$ is not incompatible with a mainly $u\bar{u}+d\bar{d}$ meson ($\alpha=0$) structure. For a pure $s\bar{s}$ state ($\alpha=90°$) the ratios (134) would, however, become infinite. Therefore the $f_0(1500)$ is not the missing $s\bar{s}$ scalar meson.

Similar conclusions can be reached for the $f_0(1370)$, which has small decay branching ratios to $\eta\eta$ and $K\bar{K}$. Precise ratios R_i are difficult to obtain in this case, since the branching ratio to $\pi\pi$ in Table X also includes the low-energy $\pi\pi$ S wave, in particular $f_0(400-1200)$. Note that in the alternative analysis of Abele *et al.* (1996a), which uses some of the available $\pi^- p \to K\bar{K}n$ data, the $f_0(1370)$ mass and width are reported to be smaller, 1300 ± 15 MeV and 230 ± 15 MeV, respectively. The $\pi\pi\to K\bar{K}$ data alone already require a mass of $\simeq 1300$ MeV and a width of $\simeq 230$ MeV. This is surprising, since the authors of these experiments published quite different values (Barnett *et al.,* 1996). Moreover, some of the $\pi\pi\to K\bar{K}$ data are known to be inconsistent (Au, Morgan, and Pennington, 1987). In fact, a glance through the $f_0(1370)$ entry in "Review of Particle Physics" (Barnett *et al.,* 1996) shows a considerable uncertainty in mass and width from previous experiments. A coupled-channel analysis of Crystal Barrel data, also including the $\pi K\bar{K}$ data presented in Secs. VIII.G and VIIII.H will have to be performed to stabilize the $f_0(1370)$ mass and width, as well as its $K\bar{K}$ decay branching ratio.

This analysis shows that both $f_0(1370)$ and $f_0(1500)$ are compatible with isoscalar $u\bar{u}+d\bar{d}$ states, although the latter is much too narrow for the ground-state scalar nonet. This then raises the question of whether the $f_0(1500)$ could be the first radial excitation of $f_0(1370)$. This is unlikely, however, because (i) the splitting between the ground state and first radially excited state is expected to be around 700 MeV (Godfrey and Isgur, 1985); (ii) the next K_0^* lies at 1950 MeV (Barnett *et al.,* 1996); and, last but not least, first radials are expected to be quite broad (Barnes *et al.,* 1997).

The most natural explanation is that the $f_0(1500)$ is the ground-state glueball predicted in this mass range by lattice gauge theories. However, a pure glueball should decay to $\pi\pi$, $\eta\eta$, $\eta\eta'$, and $K\bar{K}$ with relative ratios 3 : 1 : 0 : 4, in contradiction with our ratios R_i. In the model of Amsler and Close (1996), the finite $\eta\eta'$ and the small $K\bar{K}$ rates can be accommodated by mixing the pure glueball G_0 with the nearby two $n\bar{n}$ and $s\bar{s}$ states. Conversely, the two isoscalar states in the $q\bar{q}$ nonet acquire a gluonic admixture. In first-order perturbation one finds[10]

$$|f_0(1500)\rangle = \frac{|G_0\rangle + \xi(\sqrt{2}|n\bar{n}\rangle + \omega|s\bar{s}\rangle)}{\sqrt{1+\xi^2(2+\omega^2)}}, \tag{135}$$

where ω is the ratio of mass splittings

$$\omega = \frac{m(G_0)-m(n\bar{n})}{m(G_0)-m(s\bar{s})}. \tag{136}$$

In the flux-tube simulation of lattice QCD the pure gluonium G_0 does not decay to $\pi\pi$ nor to $K\bar{K}$ in first order and hence the $f_0(1500)$ decays to $\pi\pi$ and $K\bar{K}$ through its $q\bar{q}$ admixture in the wave function. If G_0 lies between the two $q\bar{q}$ states, ω is negative and the decay to $K\bar{K}$ is hindered by negative interference between the decay amplitudes of the $n\bar{n}$ and $s\bar{s}$ components in Eq. (135). The ratio of couplings to $K\bar{K}$ and $\pi\pi$ is

$$\frac{\gamma^2(K\bar{K})}{\gamma^2(\pi\pi)} = \frac{(1+\omega)^2}{3}. \tag{137}$$

The cancellation is perfect whenever G_0 lies exactly between $n\bar{n}$ and $s\bar{s}$ ($\omega=-1$). We find with the measured R_3 two solutions, $\omega=-0.36$ or -1.64. Assuming that $f_0(1370)$ is essentially $n\bar{n}$ (with a small gluonic admixture), this leads to an $s\bar{s}$ state around 1900 MeV or 1600 MeV, respectively. Furthermore, the ratio of $\pi\pi$ partial widths for the $f_0(1500)$ and $f_0(1370)$, divided by phase space and form factor, is given by

$$\frac{\tilde{\Gamma}_{2\pi}[f_0(1500)]}{\tilde{\Gamma}_{2\pi}[f_0(1370)]} = \frac{2\xi^2(1+2\xi^2)}{1+\xi^2(2+\omega^2)} \sim 0.5, \tag{138}$$

using for the $f_0(1500)$ the branching ratios from Tables X and XI and the $4\pi/2\pi$ ratio (112). There is, however,

[10]We assume here that the quark-gluon coupling is flavor blind; see Amsler and Close (1996) for a generalization.

a large uncertainty in the ratio (138) due to the branching ratios of the $f_0(1370)$ decay, which cannot easily be disentangled from the $f_0(400-1200)$. This then leads to $|\xi|\sim 0.6$ and according to Eq. (135) to about 30% glue in $f_0(1500)$ for an $s\bar{s}$ state at 1600 MeV or about 60% glue for one at 1900 MeV.

The $f_0(1500)$ has also been observed in $\bar{p}p$ annihilation at higher energies (Armstrong *et al.,* 1993) and in other reactions, in particular in central production, decaying to $2\pi^+2\pi^-$ (Antinori *et al.,* 1995; Barberis *et al.,* 1997a). The VES Collaboration, studying $\pi^- p$ interactions on nuclei at 36 GeV/c, has reported a resonance, $\pi(1800)$, decaying to $\pi^-\eta\eta'$ (Beladidze *et al.,* 1992) and $\pi^-\eta\eta$ (Amelin *et al.,* 1996). The $\pi(1800)$ appears to decay into a resonance with mass 1460 ± 20 MeV and width 100 ± 30 MeV—in agreement with the $f_0(1500)$—with a recoiling π. They report an $\eta\eta'/\eta\eta$ ratio of 0.29 ± 0.07, which is in excellent agreement with the Crystal Barrel ratio for $f_0(1500)$ decays, 0.27 ± 0.10 (Table X). Note that if the $\pi(1800)$ is indeed a $q\bar{q}g$ (hybrid), as advocated by Close and Page (1995), then decay into gluonium is favored.

A reanalysis of J/ψ radiative decay to $2\pi^+2\pi^-$ finds evidence for the $f_0(1500)$ decaying to two S-wave dipions with a branching ratio in $J/\psi\to\gamma 4\pi$ of $(5.7\pm 0.8)\times 10^{-4}$ (Bugg *et al.,* 1995). This leads to an expected branching ratio of $(2.7\pm 0.9)\times 10^{-4}$ in $J/\psi\to\gamma 2\pi$, using the Crystal Barrel result (112). It is interesting to compare this prediction with data on $J/\psi\to\gamma\pi^+\pi^-$ from Mark III (Baltrusaitis *et al.,* 1987) where the $f_2(1270)$ is observed together with a small accumulation of events in the 1500-MeV region. Assuming that these are due to the $f_0(1500)$, one finds by scaling to $f_2(1270)$ a branching ratio in $J/\psi\to\gamma 2\pi$ of $\simeq 2.9\times 10^{-4}$, in agreement with the above prediction.

Summarizing, the $f_0(1500)$ has been observed in $\bar{p}p$ annihilation in several decay modes, some with very high statistics ($\sim$150 000 decays into $\pi^0\pi^0$) and also in other processes that are traditionally believed to enhance gluonium production, central production, and J/ψ radiative decay. The $K_0^*(1430)$ and $a_0(1450)$ define the mass scale of the $q\bar{q}$ scalar nonet. The $f_0(1500)$ is not the missing $s\bar{s}$ and is anyway too narrow for a scalar $q\bar{q}$ state. The most natural explanation for the $f_0(1500)$ is a ground-state glueball mixed with nearby scalar states. The missing element in this jigsaw puzzle is the $s\bar{s}$ scalar expected between 1600 and 2000 MeV. The analysis of in-flight annihilation data will hopefully provide more information in this mass range. The spin of the $f_J(1710)$ has not been determined unambiguously. If $J=0$ is confirmed, then the $f_J(1710)$ could be this state or, alternatively, become a challenger for the ground-state glueball (Sexton, Vaccarino, and Weingarten, 1995). A more detailed discussion of the $f_0(1500)$ and $f_J(1710)$ can be found in Close, Farrar, and Li (1997).

C. $f_2(1565)$

The $f_2(1565)$ with mass 1565 ± 20 MeV and width 170 ± 40 MeV was observed first by the Asterix Collaboration at LEAR in the final state $\pi^+\pi^-\pi^0$ in hydrogen gas (May *et al.,* 1989, 1990). A combined analysis of $\bar{p}p\to\pi^+\pi^-\pi^0$ in low-pressure gas, in gas at 1 atm and in liquid was performed by the Obelix collaboration (Bertin *et al.,* 1997a). Both the $f_0(1500)$ and $f_2(1565)$ were observed, albeit with somewhat smaller masses, 1449 ± 20 MeV and 1507 ± 15 MeV, respectively. The lower mass for the $f_2(1565)$, compared to the data of the Asterix Collaboration (May *et al.,* 1989, 1990), is not too surprising: A tensor meson was strongly favored by the data, and there was no reason to add a scalar contribution, since the $f_0(1500)$ was not known at that time.

The $f_2(1565)$ was reported by Aker *et al.* (1991) in the $3\pi^0$ final state in liquid. The $3\pi^0$ analysis gave a 60% P-state contribution to $3\pi^0$ in liquid with roughly equal intensities from $f_2(1565)$ of 9% each from $^1S_0$, $^3P_1$, and $^3P_2$. The full $3\pi^0$ data sample required 46% P-state annihilation (Amsler *et al.,* 1995f) and also required a tensor state around 1530 MeV (Sec. VIII.C). The $s\bar{s}$ tensor meson, $f_2'(1525)$, was observed in its $K\bar{K}$ decay mode (Sec. VIII.G). From the observed rate (Table XIII) and the known $f_2'(1525)$ decay branching ratios (Barnett *et al.,* 1996) it was found that the $f_2'(1525)$ could not account for much of the 2^{++} signal in $\pi\pi$ or $\eta\eta$. Hence the $f_2(1565)$ is not the $f_2'(1525)$.

The large P-state fraction in the $3\pi^0$ channel in liquid is not too surprising: the corresponding channel $\bar{p}p\to\pi^+\pi^-\pi^0$ in liquid proceeds mainly from the $(I=0)$ $^3S_1$ atomic state, while the $(I=1)$ $^1S_0$ is suppressed by an order of magnitude (Foster *et al.,* 1968b), as are normally P waves in liquid. On the other hand, the channel $\bar{p}p\to 3\pi^0$ proceeds only through the $(I=1)$ $^1S_0$ atomic state, while $^3S_1$ is forbidden. Indeed, the branching ratios for $3\pi^0$ is an order of magnitude smaller than for $\pi^+\pi^-\pi^0$ (Table IX). Hence, for $3\pi^0$, S- and P-wave annihilations compete in liquid.

A fraction of 50% P wave was also required in the Dalitz plot analysis of the $I=1$ final state $\pi^-\pi^0\pi^0$ at rest in liquid deuterium (Abele *et al.,* 1997f), which shows evidence for $f_0(1500)$ and $f_2(1565)$ production and requires in addition the ρ meson and two of its excitations, $\rho^-(1450)$ and $\rho^-(1700)$, decaying to $\pi^-\pi^0$.

However, the coupled-channel analysis described in Sec. VIII.D, ignoring P waves, still requires a tensor state at 1552 MeV. Neglecting P waves increases slightly the contribution from $f_0(1500)$ while decreasing the contribution from $f_2(1565)$, although the rates remain within errors (compare the two $\pi^0\pi^0$ branching ratios in Table X for the single- and coupled-channel analyses).

The alternative N/D analysis also reproduces the features of the $3\pi^0$ Dalitz plot without P-wave contributions, in particular the scalar state around 1500 MeV (Anisovich *et al.,* 1994). A tensor contribution with mass $\sim$1565 MeV and width $\sim$165 MeV is, however, still required, but most of the blob structure in Fig. 22(c) is taken into account by interferences in the low-energy $\pi\pi$ S wave.

An N/D analysis of Crystal Barrel data, together with former data from other reactions, also reports a tensor meson with mass 1534±20 MeV and width 180±60 MeV (Abele *et al.,* 1996a). These authors report strong $\rho\rho$ and $\omega\omega$ contributions and therefore assign this signal to the $f_2(1640)$ discovered by GAMS in $\pi^- p \to \omega\omega n$ (Alde *et al.,* 1990), also reported to decay into 4π by the Obelix Collaboration in $\bar{n}p \to 5\pi$ (Adamo *et al.,* 1992). It should be emphasized, however, that in Abele *et al.* (1996a) the inelasticity in the K matrix is attributed to $\rho\rho$ (and $\omega\omega$), although no 4π data are actually included in the fit. Given that mass and width of the tensor meson agree with the $f_2(1565)$, but disagree with the $f_2(1640)$, it seems more natural to assign the 2^{++} signal to the former. It is interesting to note that a $2^{++}\rho\rho$ molecule (Törnqvist *et al.,* 1991) or a 2^{++} baryonium state (Dover, 1986) decaying strongly to $\rho\rho$ (Dover, Gutsche, and Faessler, 1991) are predicted in this mass range. The $f_2(1565)$ could be one of these states.

In conclusion, there is a certain amount of model dependence when extracting the precise production and decay rates of the $f_2(1565)$. However, annihilation data require both a scalar and a tensor state around 1500 MeV, and the parameters and rates for the $f_0(1500)$ are reasonably stable, independent of an $f_2(1565)$ contribution. The Crystal Barrel data in gas will hopefully settle the issue of the fraction of P wave in $3\pi^0$ annihilations.

XI. SEARCH FOR HYBRIDS

The familiar $q\bar{q}$ color-neutral configuration is not the only one allowed by QCD. One expects multiquark mesons ($\bar{q}^2q^2$, $\bar{q}^3q^3$) and hybrid states ($q\bar{q}g$). For $\bar{q}^2q^2$ mesons one predicts a rich spectrum of isospin 0, 1, and 2 states in the 1–2-GeV region, none of which has been established so far. This casts doubt on whether multiquark states really bind or are sufficiently narrow to be observed. Bag model predictions for 0^+, 1^+, and 2^+ $\bar{q}^2q^2$ states have been presented by Jaffe (1977).

The flux-tube model implies that hybrids should lie in the 1.9-GeV region, the ground states being 0^{-+}, 1^{-+}, 2^{-+}, and 1^{--} (Isgur and Paton, 1985; Close and Page, 1995). Lattice QCD also predicts the lightest hybrid, a 1^{-+}, around 2000 MeV (Lacock, Boyle, and Rowland, 1997). These hybrids have distinctive decay patterns. They are expected to decay mainly into an S-wave and a P-wave meson [e.g., $f_1(1285)\pi$, $b_1(1235)\pi$], while the decay into two S-wave mesons is suppressed (Page, 1997). A 1^{-+} structure around 2 GeV decaying to $f_1(1285)\pi$ has been reported (Lee *et al.,* 1994). The 0^{-+} $\pi(1800)$ has been observed to decay into $f_0(980)\pi$ and $f_0(1370)\pi$ but not into $K^*\bar{K}$ nor $\rho\pi$ (Amelin *et al.,* 1995; Berdnikov *et al.,* 1994), in line with the prediction that a 0^{-+} hybrid should decay dominantly into an S-wave and a P-wave meson. We shall discuss the evidence for a 2^{-+} hybrid below, in connection with Crystal Barrel data.

However, the bag model predicts a 1^{-+} hybrid meson at a much lower mass, around 1.4 GeV (Barnes, Close, and deViron, 1983). A state with quantum numbers 1^{-+} does not couple to $q\bar{q}$, as can be verified from Eqs. (17) and (18), which also apply to $q\bar{q}$ states: For 1^{-+} Eq. (17) requires ℓ to be even and then Eq. (18) implies that $s=0$, thus excluding $J=1$. It is easy to show that the quantum numbers 0^{--}, 0^{+-}, and 2^{+-} do not couple to $q\bar{q}$ either. The discovery of a state with such quantum numbers would prove unambiguously the existence of exotic (non-$q\bar{q}$) mesons.

A. $\hat{\rho}(1405)$

A 1^{-+} hybrid around 1.4 GeV would decay to $\eta\pi$ and $\eta'\pi$, where the two pseudoscalars are in a relative P wave. This state would be isovector and hence could not be confused with a glueball. Both neutral and charged decays should be observed ($\eta\pi^0$ and $\eta\pi^{\pm}$). A candidate, $\hat{\rho}(1405)$ with mass 1406±20 MeV and width 180 ±20 MeV, has been reported in $\pi^- p \to \eta\pi^0 n$ at 100 GeV (Alde *et al.,* 1988a), but a reanalysis of the data claims ambiguous solutions in the partial-wave analysis (Prokoshkin and Sadovskii, 1995). More recently, the $\hat{\rho}(1405)$ with mass 1370^{+52}_{-34} MeV and width 385^{+76}_{-112} MeV has been reported in the partial-wave analysis of $\pi^- p \to \eta\pi^- p$ at 18 GeV (Thompson *et al.,* 1997). It is observed as an interference between the $L=1$ and $L=2$ $a_2(1320)\to\eta\pi$ amplitudes, leading to a forward/backward asymmetry in the $\eta\pi$ angular distribution.

Crystal Barrel searched for a resonance in the $\eta\pi$ P wave using the final state $\pi\pi\eta$. A weak 1^{-+} structure with poorly defined mass and width was reported by Amsler *et al.* (1994b) in the $\pi^0\pi^0\eta$ channel (Sec. VIII.B). This channel proceeds through the $I=0$ $\bar{p}p$ initial state $^1S_0$ (and $^3P_1$, $^3P_2$). It is conceivable that the production of $\hat{\rho}(1405)$ is suppressed from $^1S_0$ but enhanced from $^3S_1$. This initial state is accessible in deuterium with $\bar{p}n \to \pi^-\pi^0\eta$ (Abele *et al.,* 1998a). Here $I=1$ and $G=+1$ require $\ell+s$ to be odd [Eq. (19)] hence annihilation from $^3S_1$ or $^1P_1$. In deuterium the spectator proton may remove angular momentum and hence the inclusion of initial P waves becomes mandatory. The increasing complexity in the amplitude analysis is, however, compensated by the absence of 0^{++} isocalar mesons, which do not contribute to $\pi^-\pi^0\eta$.

Events with a single π^- and $\pi^0\eta\to 4\gamma$ were selected from the sample of 8.1 million one-prong triggered data in liquid deuterium. The single track requirement restricted the spectator proton momentum to less than 200 MeV/c, under which protons do not escape from the target. A three-constraint fit was applied to select $\pi^-\pi^0\eta$ with a missing proton. The missing proton momentum was then limited to 100 MeV/c. This procedure permitted the channel $\pi^-\pi^0\eta$ to be treated as quasifree, i.e., insensitive to final-state rescattering with the proton. The branching ratio for $\bar{p}n \to \pi^-\pi^0\eta$ was found to be $(1.41\pm 0.15)\%$.

The Dalitz plot from the resulting 52 567 events is shown in Fig. 35. Conspicuous is the strong production

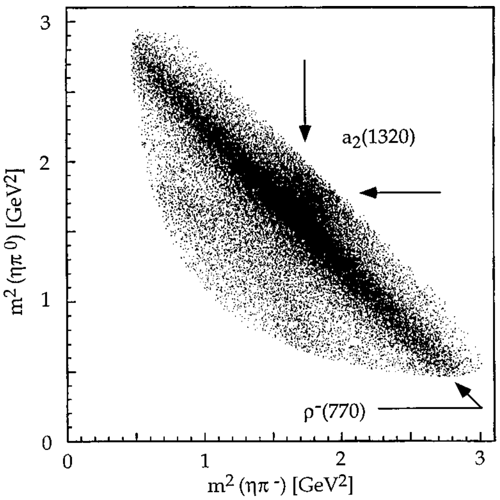

FIG. 35. Dalitz plot of $\bar{p}n \to \pi^- \pi^0 \eta$ (52 576 events).

of ρ^- and the accumulation of events in the $\eta\pi$ mass regions around 1300 MeV but only above the ρ band. This points to the presence of interferences between $a_2(1320)$ and some other amplitude. A partial-wave analysis was performed using Breit-Wigner amplitudes and introducing contributions from the $\rho^-(770)$, $\rho^-(1450)$, $a_2(1320)$ from $^3S_1$ and the $a_0(980)$, $a_0(1450)$ from $^1P_1$. The fit could not describe the observed interference pattern. The inclusion of a resonant $\eta\pi$ P wave from both $^3S_1$ and $^1P_1$ led, however, to a good description of the data. Contributions from the $\rho^-(1450)$, $a_0(980)$, and $a_0(1450)$ were found to be negligible. The Breit-Wigner mass and width of the 1^{-+} resonance are, respectively,

$$\hat{\rho}(1405): \quad m = 1400 \pm 28, \quad \Gamma = 310^{+71}_{-58} \text{ MeV}. \tag{139}$$

The resonance draws about 8% from $^3S_1$ and 3% from $^1P_1$. It interferes with both the $a_2(1320)$ and $\rho^-(770)$. The accumulation of events above the ρ (Fig. 35) leads to a forward/backward asymmetry in the $\eta\pi$ rest frame along the $a_2(1320)$ band.

These findings are consistent with the observation of an exotic 1^{-+} resonance in the 1400-MeV mass region. Mass and width are in good agreement with the results of Thompson *et al.* (1997). However, an adequate fit can also be obtained with a 1-GeV broad enhancement in the $\eta\pi$ P wave, coupling to the inelastic channel $f_1(1285)\pi$ and generating a cusp around threshold at 1420 MeV. This should be clarified by measuring the branching ratio for $f_1(1285)\pi\pi$ production in deuterium. If not a threshold effect, this meson could be a hybrid but also a four-quark state. A measurement of the partial width into $\eta'\pi$ would help to distinguish between the two alternatives (Close and Lipkin, 1987).

B. $\eta_2(1870)$

Two 2^{-+} isoscalars were reported by Crystal Barrel in $\bar{p}p$ annihilation into $3\pi^0\eta$ at 1.94 GeV/c (Adomeit *et al.,* 1996). The first state was observed in $\pi^0\pi^0\eta$ with mass and width

$$\eta_2(1645): \quad m = 1645 \pm 21, \quad \Gamma = 180^{+47}_{-33} \text{ MeV}. \tag{140}$$

Its dominant contribution to $\pi^0\pi^0\eta$ stems from $a_2(1320)\pi$. This state has been confirmed in central collisions in the reaction $pp \to pp2\pi^+2\pi^-$, where it is observed to decay into $a_2(1320)\pi$ (Barberis *et al.,* 1997a) and in $pp \to ppK\bar{K}\pi$, where it decays into $K^*\bar{K}$ (Barberis *et al.,* 1997b). The relative branching ratio for decay into $K^*\bar{K}$ and $a_2(1320)\pi$ is 0.07 ± 0.03, in accord with a mainly $u\bar{u} + d\bar{d}$ meson.

The second state was also observed in $\pi^0\pi^0\eta$ with mass and width

$$\eta_2(1870): \quad m = 1875 \pm 40, \quad \Gamma = 200 \pm 50 \text{ MeV}. \tag{141}$$

This is probably $\eta_2(1870)$, which was observed earlier by the Crystal Ball Collaboration in $\pi^0\pi^0\eta$ in $\gamma\gamma$ collisions (Karch *et al.*, 1992) and more recently in 4π in central production (Barberis *et al.,* 1997a). Crystal Barrel found for $\eta_2(1870)$ the dominant decay modes $a_2^0(1320)\pi^0$ and $f_2(1270)\eta$. The ratio of partial widths is

$$\frac{\Gamma(\eta_2(1870) \to a_2(1320)\pi)}{\Gamma(\eta_2(1870) \to f_2(1270)\eta)} = 4.1 \pm 2.3, \tag{142}$$

corrected for all a_2 and f_2 decay modes.

Assuming that the $\eta_2(1645)$ is mainly $u\bar{u} + d\bar{d}$, the 2^{-+} $q\bar{q}$ nonet contains the previously known $\pi_2(1670)$ and $\eta_2(1645)$, both made of u and d quarks. The nearly equal masses also points to ideal mixing in the 2^{-+} nonet, and therefore the $s\bar{s}$ state should mainly decay to $K^*\bar{K}$, while $a_2(1320)\pi$ and $f_2(1270)\eta$ should vanish in the limit of ideal mixing, in contrast to Crystal Barrel data. It appears therefore unlikely that the $\eta_2(1870)$ is the $s\bar{s}$ member of the 2^{-+} nonet. Unfortunately, the $K\bar{K}\pi$ data from Barberis *et al.* (1997b) do not extend sufficiently high in mass to provide information on the $K^*\bar{K}$ coupling of $\eta_2(1870)$.

Since this state is produced in $\gamma\gamma$ collisions (Karch *et al.,* 1992), it can hardly be a glueball. However, the ratio (142) is in good agreement with the predicted ratio of 6 for a 2^{-+} hybrid (Close and Page, 1995).

XII. E/ι DECAY TO $\eta\pi\pi$

The E meson, a 0^{-+} state, was discovered in the sixties in the $K\bar{K}\pi$ mass spectrum of $\bar{p}p$ annihilation at rest into $(K_SK^{\pm}\pi^{\mp})\pi^+\pi^-$. Its mass and width were determined to be 1425 ± 7 MeV and 80 ± 10 MeV, respectively, (Baillon *et al.,* 1967). Its quantum numbers have remained controversial, since other groups have claimed a 0^{-+} state [now called $\eta(1440)$] and a 1^{++} state [now called $f_1(1420)$] in this mass region from various hadronic reactions. A broad structure (previously called ι) was also observed in radiative J/ψ decay to $K\bar{K}\pi$ (Scharre *et al.,* 1980). Initially determined to be 0^{-+}, the E/ι structure was then found to split into three states, the first (0^{-+}) at 1416 ± 10 MeV decaying to $a_0(980)\pi$, the second, presumably the 1^{++} $f_1(1420)$, at 1443

± 8 MeV, and the third (0^{-+}) at 1490 ± 16 MeV, both decaying to $K^*\bar{K}$ (Bai *et al.,* 1990). The widths were not determined accurately. The Obelix Collaboration analyzed the $K\bar{K}\pi$ mass spectrum in $\bar{p}p$ annihilation at rest in liquid and also reported a splitting of the E meson into two pseudoscalar states at 1416 ± 2 MeV ($\Gamma=50\pm4$ MeV) and 1460 ± 10 MeV ($\Gamma=105\pm15$ MeV) (Bertin *et al.,* 1995). We shall refer to these pseudoscalar mesons as $\eta(1410)$ and $\eta(1460)$. When using gaseous hydrogen, one expects the production of 1^{++} mesons from $^3P_1$ recoiling against an S-wave dipion. Bertin *et al.* (1997b) indeed observed three states in the $K\bar{K}\pi$ mass spectrum in gas: $\eta(1410)$, $f_1(1420)$, and $\eta(1460)$.

In J/ψ radiative decay, ι decays to $K\bar{K}\pi$ through the intermediate $a_0(980)$ and hence a signal was also expected in the $a_0(980)\pi\to\eta\pi\pi$ mass spectrum. This was indeed observed by Mark III and DM2: Bolton *et al.* (1992) reported a signal in $a_0^\pm\pi^\mp$ at 1400 ± 6 MeV ($\Gamma=47\pm13$ MeV) and Augustin *et al.* (1990) in $\eta\pi^+\pi^-$ at 1398 ± 6 MeV ($\Gamma=53\pm11$ MeV). We shall tentatively assign these signals to $\eta(1410)$.

To clarify whether the structures observed in J/ψ radiative decay and in $\bar{p}p$ annihilation are compatible and, in particular, to confirm the quantum numbers of E (0^{-+} and not 1^{++}), Crystal Barrel searched for the $\eta\pi\pi$ decay mode of the E meson in the reaction $\bar{p}p\to(\eta\pi^+\pi^-)\pi^0\pi^0$ and $(\eta\pi^0\pi^0)\pi^+\pi^-$, leading to two charged particles and 6γ (Amsler *et al.,* 1995h; Urner, 1995). Since the rate for this reaction was expected to be rather small ($\sim10^{-3}$ of all annihilations), an online trigger required eight clusters in the barrel and at least two π^0 and one η. A seven-constraint kinematic fit then selected the channel $\pi^+\pi^-2\pi^0\eta$ while suppressing $\pi^+\pi^-2\eta\pi^0$ and $\pi^+\pi^-3\pi^0$. The branching ratio for $\pi^+\pi^-2\pi^0\eta$ was found to be $(2.09\pm0.36)\%$.

The final state $\pi^+\pi^-2\pi^0\eta$ includes a strong contribution from $\omega\eta\pi^0$ ($\omega\to\pi^+\pi^-\pi^0$), a channel that was studied in its 7γ decay mode (Amsler *et al.,* 1994c). Events compatible with $\omega\eta\pi^0$ were removed, leaving a sample of about 127 000 $\pi^+\pi^-2\pi^0\eta$ events. The evidence for $\eta(1410)$ decaying to $\eta\pi\pi$ is shown in the $\pi^0\pi^0\eta$ and $\pi^+\pi^-\eta$ mass distributions (Fig. 36). Some 9 000 $\eta(1410)$ decays into $\eta\pi\pi$ are observed in Fig. 36, an order of magnitude more than for E to $K\bar{K}\pi$ in the seminal work of Baillon *et al.* (1967).

A partial-wave analysis was performed using a maximum-likelihood optimization. The signal at 1400 MeV was described by the annihilation channels

$$\begin{aligned}\bar{p}p&\to\eta(1410)(\to\eta\sigma^0)\sigma^{+-},\\&\to\eta(1410)(\to a_0^0(980)\pi^0)\sigma^{+-},\\&\to\eta(1410)(\to\eta\sigma^{+-})\sigma^0,\\&\to\eta(1410)(\to a_0^\pm(980)\pi^\mp)\sigma^0,\end{aligned}\tag{143}$$

where σ^0 and σ^{+-} are shorthands for the $\pi^0\pi^0$ and $\pi^+\pi^-$ S waves. The latter were described by prescriptions of the form (100), which is reasonable since the $\pi\pi$ masses lie below 900 MeV. Background contributions, e.g., from $\eta\rho^0\sigma^0$ and $\eta'\rho^0$, were also included in the fit. Figure 37 shows, for example, the $a_0^\pm(980)$ angular distribution in the $\eta(1410)$ rest frame together with the best fit for a 0^{-+} state. The data exclude 1^{++}, hence the $\eta(1410)$ is definitively of pseudoscalar nature and is produced from the $^1S_0$ atomic state. It has mass and width

$$\eta(1410):\quad m=1409\pm3\,\text{MeV},\quad \Gamma=86\pm10\,\text{MeV}.\tag{144}$$

The width is somewhat larger than for $\eta\pi\pi$ in J/ψ decay (Augustin *et al.,* 1990; Bolton *et al.,* 1992) and for $K\bar{K}\pi$ in $\bar{p}p$ annihilation at rest (Bertin *et al.,* 1995).

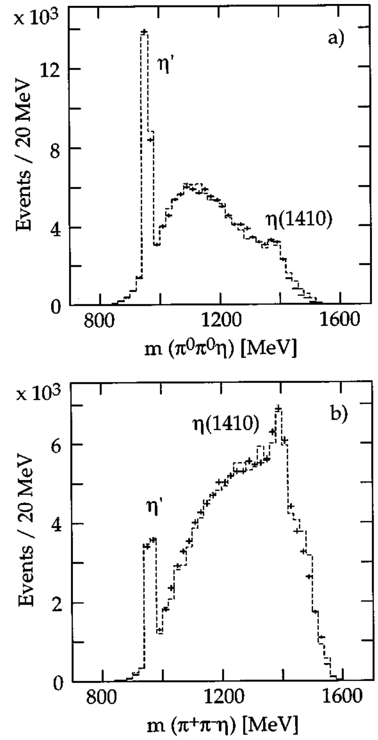

FIG. 36. Mass distributions in $\bar{p}p$ annihilation at rest into $\pi^+\pi^-\pi^0\pi^0\eta$, showing the η' and $\eta(1410)$ signals: (a) $\pi^0\pi^0\eta$; (b) $\pi^+\pi^-\eta$. The dashed line shows the result of the fit.

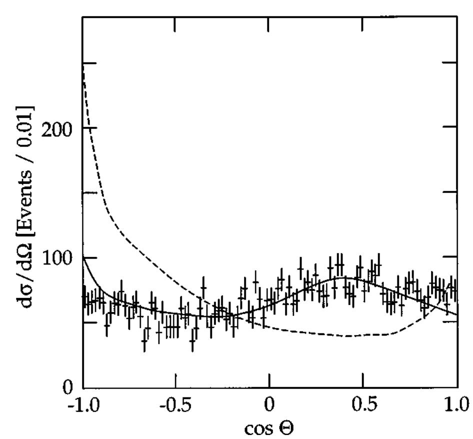

FIG. 37. Angular distribution of $a_0(980)^\pm$ in the $\eta(1410)$ rest frame. The data are shown with error bars. The solid curve shows the fit for a 0^{-+} state and the dashed curve the prediction for a 1^{++} state produced with the same intensity.

The branching ratio to $K\bar{K}\pi$ had been measured earlier (Baillon *et al.,* 1967)

$$B(\bar{p}p \to E\pi\pi, E \to K\bar{K}\pi) = (2.0 \pm 0.2) \times 10^{-3}, \quad (145)$$

while Crystal Barrel found for the $\eta\pi\pi$ mode

$$B(\bar{p}p \to \eta(1410)\pi\pi, \eta(1410) \to \eta\pi\pi) = (3.3 \pm 1.0) \times 10^{-3}. \quad (146)$$

The fit yielded $\eta\sigma$ and $a_0(980)(\to\eta\pi)\pi$ decay contributions with the relative rate

$$\frac{B(\eta(1410) \to \eta\sigma \to \eta\pi\pi)}{B(\eta(1410) \to a_0(980)\pi \to \eta\pi\pi)} = 0.78 \pm 0.16. \quad (147)$$

Assuming that 50% of the $K\bar{K}\pi$ mode proceeds through the $\eta(1410)$ decaying to $a_0(980)\pi$ (Baillon *et al.,* 1967) one can estimate from these branching ratios

$$\frac{B(a_0(980) \to K\bar{K})}{B(a_0(980) \to \eta\pi)} \sim 0.54 \pm 0.18, \quad (148)$$

somewhat larger than, but not in violent disagreement with, the result (111). Note that Alde *et al.* (1997) find a much higher ratio $\eta\sigma/a_0\pi$ [Eq. (147)] of 4.3±1.2 which would then increase the $K\bar{K}$-to-$\eta\pi$ ratio, Eq. (148), substantially.

The observation of the $\eta\pi^0\pi^0$ decay mode clearly establishes that the E meson is isoscalar $(C=+1)$. Note that the Crystal Barrel data do not exclude the presence of the other $I=0$ pseudoscalar, $\eta(1460)$, since the latter was observed in $K^*\bar{K}$ and not in $\eta\pi\pi$.

The first radial excitation of the η could be the $\eta(1295)$ decaying to $\eta\pi\pi$ (Barnett *et al.,* 1996). Hence one of the two pseudoscalars in the ι structure could be the radial excitation of the η'. The near equality of the $\eta(1295)$ and $\pi(1300)$ masses suggests an ideally mixed nonet of 0^{-+} radials. This implies that the second isoscalar in the nonet should be mainly $s\bar{s}$ and hence decay to $K^*\bar{K}$, in accord with observations for $\eta(1460)$. This scheme then favors an exotic interpretation for the $\eta(1410)$, perhaps gluonium mixed with $q\bar{q}$ (Close, Farrar, and Li, 1997) or a bound state of gluinos (Farrar, 1996). The gluonium interpretation is, however, not favored by lattice gauge theories, which predict the 0^{-+} state above 2 GeV (see Szczpaniak *et al.,* 1996). Bugg and Zou (1997) argue that the $s\bar{s}$ state expected around 1530 MeV is pushed down to 1410 MeV by a pseudoscalar glueball between 1750 and 2100 MeV. In this case, however, the nature of the $\eta(1460)$ remains unexplained.

XIII. SUMMARY AND OUTLOOK

Crystal Barrel collected 10^8 $\bar{p}p$ annihilations at rest in liquid hydrogen, three orders of magnitude more than previous bubble-chamber experiments. The results reviewed in this report were achieved thanks to the availability of pure, cooled, and intensive low-energy antiproton beams, which allowed a good spatial definition of the annihilation source, and thanks to the refinement of the analysis tools warranted by the huge statistical samples. The data processed so far concentrate on annihilations at rest into zero-prong events, i.e., only neutral events in the final state, that had not been investigated before. The data collected with the zero-prong trigger correspond to 6.3×10^8 annihilations.

The measurement of the branching ratio for annihilation into $\pi^0\pi^0$ leads, together with a cascade calculation of the antiprotonic atom, to a fraction of $(13\pm4)\%$ P wave in liquid hydrogen. Therefore S-wave dominance has been, in general, assumed to analyze Dalitz plots. The inclusion of P waves increases the number of fitting parameters and often leads to unstable fits. This limitation will be removed by analyzing simultaneously the high-statistics data in liquid and gaseous hydrogen.

The branching ratios for annihilation into two neutral light mesons ($\pi^0\eta$, $\pi^0\eta'$, $\eta\eta$, $\eta\eta'$, $\omega\eta$, $\omega\eta'$, $\eta\rho^0$, $\eta'\rho^0$) reveal the interplay of constituent quarks in hadrons. The nonplanar quark rearrangement graph must play an important role in the annihilation process. Using the OZI rule, the pseudoscalar mixing angle was determined to be $(-17.3\pm1.8)^\circ$.

However, the production of ϕ mesons is enhanced in nearly all channels compared to predictions by the OZI rule. The most significant deviation is found in the annihilation channel $\pi^0\phi$. After phase-space correction, the $\pi^0\phi/\pi^0\omega$ ratio is $(10.6\pm1.2)\%$ while OZI predicts 0.42%. Whether this enhancement can be explained by final-state interaction or by $s\bar{s}$ pairs in the nucleon is not clear yet. The analysis of data in P-state annihilations, in gas or at higher momenta, will be helpful in settling the nature of this phenomenon.

In electromagnetic processes, the radiative annihilations $\pi^0\gamma$, $\eta\gamma$ and $\omega\gamma$ were observed with rates consistent with predictions from the vector dominance model, but $\phi\gamma$ was enhanced. The branching ratio for $\omega\to\eta\gamma$, $(6.6\pm1.7)\times10^{-4}$, was measured independently of $\rho-\omega$ interference. This result solves the ambiguity in e^+e^- formation experiments, selecting the constructive $\rho-\omega$ interference solution. The $\eta\to3\pi^0$ Dalitz plot is not homogeneous but shows a negative slope of $\alpha=0.052 \pm0.020$, somewhat at variance with chiral perturbation theory. Crystal Barrel data also confirm the evidence for the direct decay $\eta'\to\pi^+\pi^-\gamma$, in addition to $\eta'\to\rho\gamma$.

Decisive progress has been achieved in understanding scalar mesons by studying annihilation into three pseudoscalars. An isovector state, $a_0(1450)$, with mass and width $(m,\Gamma)=(1474\pm19,\ 265\pm13)$ MeV has been observed to decay into $\eta\pi$, $\eta'\pi$, and $K\bar{K}$ with rates compatible with SU(3) flavor. The existence of the $a_0(1450)$ adds evidence for the $a_0(980)$ not being a $q\bar{q}$ structure, but perhaps a $K\bar{K}$ molecule. The ratio of $a_0(980)$ decay rates to $K\bar{K}$ and $\eta\pi$ was measured to be 0.23 ± 0.05. The nature of $a_0(980)$ [and $f_0(980)$], whether a $q\bar{q}$ meson, a four-quark state, or a $K\bar{K}$ molecule, will be clarified at DAϕNE, by studying radiative ϕ decay to $a_0(980)$ and $f_0(980)$.

An isoscalar state, $f_0(1370)$, with mass and width $(m,\Gamma)=(1360\pm23,\ 351\pm41)$ MeV has been observed to decay into $\pi\pi$, $\eta\eta$, $K\bar{K}$, and 4π. Obtaining accurate branching ratios for $f_0(1370)$ is difficult due to interferences with the broad structure $f_0(400-1200)$. The nature of this structure (meson or slowly moving background phase) is unclear. Whether $f_0(400-1200)$ is really distinct from $f_0(1370)$ is not entirely clear. Both questions will probably remain with us for some time. The states $a_0(1450)$, $f_0(1370)$, and $K_0^*(1430)$ are broad, consistent with expectations for $q\bar{q}$ scalar mesons, although there is some uncertainty in the mass, width, and $K\bar{K}$ decay branching ratio of $f_0(1370)$. A coupled-channel analysis of Crystal Barrel data including the $\pi K\bar{K}$ data will be helpful. The small coupling of $f_0(1370)$ to $K\bar{K}$ makes it an unlikely candidate for the $s\bar{s}$ meson, which is therefore still missing.

An additional isoscalar state, $f_0(1500)$, with mass $m=1505\pm9$ MeV and width $\Gamma=111\pm12$ MeV has been observed to decay into $\pi\pi$, $\eta\eta$, $\eta\eta'$, $K\bar{K}$, and 4π. The decay branching ratios are 29, 5, 1 , 3, and 62 %, respectively. These rates rule out this state as the missing $s\bar{s}$ state. Hence the $f_0(1500)$ is supernumerary and anyway too narrow to be easily accommodated in the scalar nonet. The likely explanation is that the $f_0(1500)$ is the ground-state glueball predicted by QCD, mixed with the two nearby $q\bar{q}$ isoscalars, $f_0(1370)$ and the higher-lying $s\bar{s}$ state. More information on this state will hopefully emerge in the mass range above 1600 MeV from Crystal Barrel in-flight data. It is, in particular, crucial to search for the $f_J(1710)$ and to establish its spin and its decay modes with high-statistics data, since the latter could be the missing $s\bar{s}$ scalar.

The tensor meson $f_2(1565)$ is dominantly produced from P states. It is, however, still required to fit the data when assuming pure S-wave annihilation: Its mass and width are $\simeq1552$ MeV and $\simeq142$ MeV, respectively. The systematic inclusion of P-wave annihilation at rest in all analyses is prevented by the large number of fit parameters. The simultaneous analysis of three neutral pseudoscalar data from Crystal Barrel in liquid and gaseous hydrogen might alleviate this problem, perhaps also modifying slightly some of the branching ratios obtained from liquid only.

The isovector $\hat{\rho}(1405)$ with exotic quantum numbers 1^{-+}, mass 1400 ± 28 MeV and width 310^{+71}_{-58} MeV was observed by Crystal Barrel in the $\eta\pi$ P wave. This meson could be a hybrid or a four-quark state. A measurement of the partial width into $\eta'\pi$ would help to distinguish between the two alternatives. However, flux-tube models and lattice gauge theories predict hybrids at higher masses. A study of the channel $f_1(1285)\pi$ in $\bar{p}n$ annihilation is required to assess whether the threshold for this reaction can mimic a 1^{-+} resonance at 1400 MeV.

The isoscalar partner of $\pi_2(1670)$ in the 2^{-+} nonet, $\eta_2(1645)$, has been observed in its $\pi^0\pi^0\eta$ decay mode. Its mass and width are 1645 ± 21 MeV and 180^{+47}_{-33} MeV, respectively. The other 2^{-+} isoscalar, $\eta_2(1870)$, also observed in $\pi^0\pi^0\eta$, has decay branching ratios to $a_2(1320)\pi$ and $f_2(1270)\eta$ compatible with those predicted for a hybrid state. The still missing $s\bar{s}$ state in the 2^{-+} nonet would decay mainly to $K^*\bar{K}$. It is therefore important to determine the $K^*\bar{K}$ branching ratio of $\eta_2(1870)$.

A 0^{-+} state, $\eta(1410)$, with mass $m=1409\pm3$ and width $\Gamma=80\pm10$ MeV has been observed to decay into $\eta\pi^0\pi^0$ and $\eta\pi^+\pi^-$. The neutral decay mode establishes this state as an isoscalar one and, together with other experiments, strengthens the evidence for two $I=0$ pseudoscalar states in the 1400–1500-MeV region, the lowest-lying state being perhaps a pseudoscalar glueball, notwithstanding the prediction from lattice gauge theories that pseudoscalar glueballs lie above 2 GeV. A further clue to the nature of $\eta(1410)$ could be obtained by searching for its $\eta'\pi^0\pi^0$ decay mode and measuring its branching ratio.

Radial excitations of $q\bar{q}$ mesons have begun to emerge. Crystal Barrel data show evidence for the two excitations of the ρ meson, $\rho(1450)$ and $\rho(1700)$, and for the radial excitation of the $a_2(1320)$ around 1650 MeV. It is essential to identify the $q\bar{q}$ radials in the 1500-MeV to 2000-MeV mass range and to measure their decay branching ratios into various channels, including $\eta\eta$, $\eta\pi\pi$, $K\bar{K}$, and $K\bar{K}\pi$. Except for the exotic 1^{-+}, hybrid mesons with the same quantum numbers as $q\bar{q}$ radials are also predicted in this mass range. Once radials have been established, supernumerary states will emerge. The distinct decay characteristics of hybrids into P- and S-wave mesons will then permit us to distinguish them from $q\bar{q}$ radial excitations.

The analysis of Crystal Barrel in-flight data will hopefully reveal further radial excitations, hybrid mesons, and higher-mass glueballs. For glueballs, more definitive progress will probably be achieved in radiative J/ψ decay at a high luminosity e^+e^- state factory or in central collisions at the forthcoming Compass experiment at CERN.

ACKNOWLEDGMENTS

The results presented in this review were obtained through the efforts of many physicists and technicians from the Crystal Barrel Collaboration and from the supporting institutions.[11] The author also wishes to thank C. Batty, F. Close, H. Genz, P. Giarritta, F. Heinsius, M. Heinzelmann, M. Locher, V. Markushin, L. Montanet, R. Ouared, S. Spanier, U. Wiedner, D. Wyler, and Č. Zupančič for reading the manuscript and for helpful discussions.

---

[11]Universities of California (Berkeley and Los Angeles), Bochum, Bonn, Hamburg, Karlsruhe, Mainz, Munich, Paris VI, Zürich, Carnegie Mellon University, Academy of Science (Budapest), Rutherford Appleton Laboratory, CERN, Queen Mary and Westfield College, Centre de Recherches Nucléaires (Strasbourg).

REFERENCES

Abele, A., *et al.*, 1996a, Nucl. Phys. A **609**, 562.

Abele, A., *et al.*, 1996b, "Observation of f_0 (1500) decay into $K_L K_L$," Phys. Lett. B **385**, 425.

Abele, A., *et al.*, 1996c, "A study of $f_0(1500)$ decays into $4\pi^0$ in $\overline{p}p \to 5\pi^0$ at rest," Phys. Lett. B **380**, 453.

Abele, A., *et al.*, 1997a, "$\rho-\omega$ interference in $\overline{p}p$ annihilation at rest into $\pi^+\pi^-\eta$," Phys. Lett. B **411**, 354.

Abele, A., *et al.*, 1997b, "Measurement of the $\omega \to \eta\gamma$ decay branching ratio," Phys. Lett. B **411**, 361.

Abele, A., *et al.*, 1997c, "Antiproton-proton annihilation at rest into $K_L K_S \pi^0 \pi^0$," Phys. Lett. B **415**, 280.

Abele, A., *et al.*, 1997d, "Antiproton-proton annihilation at rest into $K_L K^\pm \pi^\mp \pi^0$—manifestations of isospin interference," Phys. Lett. B **415**, 289.

Abele, A., *et al.*, 1997e, "Study of the $\pi^0\pi^0\eta'$ final state in $\overline{p}p$ annihilation at rest," Phys. Lett. B **404**, 179.

Abele, A., *et al.*, 1997f, "High-mass ρ meson states from $\overline{p}d$ annihilation at rest into $\pi^-\pi^0\pi^0\rho_{\rm spectator,}$" Phys. Lett. B **391**, 191.

Abele, A., *et al.*, 1997g, "Measurement of the decay distribution of $\eta' \to \pi^+\pi^-\gamma$ and evidence for the box anomaly," Phys. Lett. B **402**, 195.

Abele, A., *et al.*, 1998a, "Exotic $\eta\pi$ state in $\overline{p}d$ annihilation at rest into $\pi^-\pi^0\eta\rho_{\rm spectator}$," Phys. Lett B **423**, 175.

Abele, A., *et al.*, 1998b, "Momentum dependence of the decay $\eta \to \pi^+\pi^-\pi^0$," Phys. Lett. B **417**, 197.

Abele, A., *et al.*, 1998c, "Decay dynamics of the process $\eta \to 3\pi^0$," Phys. Lett. B **417**, 193.

Abele, A., *et al.*, 1998d, "$\overline{p}p$ annihilation at rest into $K_L K^\pm \pi^\mp$," Phys. Rev. D **57**, 3860.

Ableev, V. G., *et al.*, 1994, Phys. Lett. B **334**, 237.

Ableev, V. G., *et al.*, 1995, Nucl. Phys. A **585**, 577.

Achasov, N. N., and V. V. Gubin, 1997, Phys. Rev. D **56**, 4084.

Achasov, N. N., and G. N. Shestakov, 1978, Sov. J. Part. Nucl. **9**, 19.

Adamo, A., *et al.*, 1992, Phys. Lett. B **287**, 368.

Adiels, L., *et al.*, 1987, Z. Phys. C **35**, 15.

Adiels, L., *et al.*, 1989, Z. Phys. C **42**, 49.

Adomeit, J., *et al.*, 1996, "Evidence for two isospin zero $J^{PC} = 2^{-+}$ mesons at 1645 and 1875 MeV," Z. Phys. C **71**, 227.

Ahmad, S., *et al.*, 1985, Phys. Lett. B **157**, 333.

Aitchison, I. J. R., 1972, Nucl. Phys. **A189**, 417.

Aker, E., *et al.*, 1991, "Observation of a 2^{++} resonance at 1515 MeV in proton-antiproton annihilations into $3\pi^0$," Phys. Lett. B **260**, 249.

Aker, E., *et al.*, 1992, "The Crystal Barrel spectrometer at LEAR," Nucl. Instrum. Methods Phys. Res. A **321**, 69.

Alberico, V., *et al.*, 1998, Phys. Lett. B **432**, 427.

Alde, D., *et al.*, 1984, Z. Phys. C **25**, 225.

Alde, D., *et al.*, 1987, Phys. Lett. B **198**, 286.

Alde, D., *et al.*, 1988a, Phys. Lett. B **205**, 397.

Alde, D., *et al.*, 1988b, Phys. Lett. B **201**, 160.

Alde, D., *et al.*, 1990, Phys. Lett. B **241**, 600.

Alde, D., *et al.*, 1994, Z. Phys. C **61**, 35.

Alde, D., *et al.*, 1997, Phys. At. Nucl. **60**, 386.

Amelin, D. V., *et al.*, 1995, Phys. Lett. B **356**, 595.

Amelin, D. V., *et al.*, 1996, Phys. At. Nucl. **59**, 976.

Amsler, C., 1987, in *Advances in Nuclear Physics*, edited by J. W. Negele and E. Vogt (Plenum, New York), Vol. 18, p. 183.

Amsler, C., and J. C. Bizot, 1983, Comput. Phys. Commun. **30**, 21.

Amsler, C., and F. E. Close, 1995, Phys. Lett. B **353**, 385.

Amsler, C., and F. E. Close, 1996, Phys. Rev. D **53**, 295.

Amsler, C., and F. Myhrer, 1991, Annu. Rev. Nucl. Part. Sci. **41**, 219.

Amsler, C., *et al.*, 1992a, "P versus S-wave $\overline{p}p$ annihilation at rest in LH_2," Phys. Lett. B **297**, 214.

Amsler, C., *et al.*, 1992b, "The pseudoscalar mixing angle Θ_{PS} from η and η' production in $\overline{p}p$ annihilation at rest," Phys. Lett. B **294**, 451.

Amsler, C., *et al.*, 1992c, "Proton-antiproton annihilation into $\eta\eta\pi$—observation of a scalar resonance decaying into $\eta\eta$," Phys. Lett. B **291**, 347.

Amsler, C., *et al.*, 1993a, "Antiproton-proton annihklation at rest into $\omega\pi^0\pi^0$," Phys. Lett. B **311**, 362.

Amsler, C., *et al.*, 1993b, "Antiproton-proton annihilation at rest into two-body final states," Z. Phys. C **58**, 175.

Amsler, C., *et al.*, 1993c, "Radiative protonium annihilation into $\gamma\gamma$, $\gamma\pi^0$, $\gamma\eta$, $\gamma\omega$ and $\gamma\eta'$," Phys. Lett. B **311**, 371.

Amsler, C., *et al.*, 1993d, "Protonium annihilation into $K_L^0 K_S^0 \pi^0$ and $K_L^0 K_S^0 \eta$," Phys. Lett. B **319**, 373.

Amsler, C., *et al.*, 1994a, "Search for a new light gauge boson in decays of π^0 and η," Phys. Lett. B **333**, 271.

Amsler, C., *et al.*, 1994b, "Observation of a new $I^G(J^{PC}) = 1^-(0^{++})$ resonance at 1450 MeV," Phys. Lett. B **333**, 277.

Amsler, C., *et al.*, 1994c, "Study of $\overline{p}p$ annihilation at rest into $\omega\eta\pi^0$," Phys. Lett. B **327**, 425.

Amsler, C., *et al.*, 1994d, "Observation of a scalar resonance decaying to $\pi^+\pi^-\pi^0\pi^0$ in $\overline{p}p$ annihilation at rest," Phys. Lett. B **322**, 431.

Amsler, C., *et al.*, 1994e, in *Hadron '93*, Proceedings of the Hadron 93 Conference, edited by T. Bressani *et al.*, Nuovo Cimento A **107**, 1815.

Amsler, C., *et al.*, 1994f, "$\eta\eta'$ threshold enhancement in $\overline{p}p$ annihilation into $\pi^0\eta\eta'$ at rest," Phys. Lett. B **340**, 259.

Amsler, C., *et al.*, 1995a, "First observations of Pontecorvo reactions iwht a recoiling neutron," Z. Phys. A **351**, 325.

Amsler, C., *et al.*, 1995b, "First observation of the production of nueleon resonances in antiproton annihilation in liquid deuterium," Phys. Lett. B **352**, 187.

Amsler, C., *et al.*, 1995c, "Observation of radiative $\overline{p}p$ annihilation into a ϕ meson," Phys. Lett. B **346**, 363.

Amsler, C., *et al.*, 1995d, "η decays into three pions," Phys. Lett. B **346**, 203.

Amsler, C., *et al.*, 1995e, "High statistics study of $f_0(1500)$ decay into $\eta\eta$," Phys. Lett. B **353**, 571.

Amsler, C., *et al.*, 1995f, "High-statistics study of $f_0(1500)$ decay into $\pi^0\pi^0$," Phys. Lett. B **342**, 433.

Amsler, C., *et al.*, 1995g, "Coupled channel analysis of $\overline{p}p$ annihilation into $\pi^0\pi^0\pi^0$, $\pi^0\eta\eta$ and $\pi^0\pi^0\eta$," Phys. Lett. B **355**, 425.

Amsler, C., *et al.*, 1995h, "E decays to $\eta\pi\pi$ in $\overline{p}p$ annihilation at rest," Phys. Lett. B **358**, 389.

Amsler, C., *et al.*, 1996a, "Search for a new light gauge boson in π^0, η and η' decays," Z. Phys. C **70**, 219.

Andrews, D. E., Y. Fukushima, J. Harvey, F. Lobkowicz, E. N. May, C. A. Nelson, and E. H. Thorndike, 1977, Phys. Rev. Lett. **38**, 198.

Anisovich, V., *et al.*, 1994, "Observation of two $J^{PC}=0^{++}$ isoscalar resonances at 1365 and 1520 MeV," Phys. Lett. B **323**, 233.
Anisovich, A. V., V. V. Anisovich, and A. V. Sarantsev, 1997, Phys. Lett. B **395**, 123.
Antinori, F., *et al.*, 1995, Phys. Lett. B **353**, 589.
Armenteros R., and B. French, 1969, in *$\bar{N}N$ Interactions in High Energy Physics*, edited by E. H. S. Burhop (Academic, New York), Vol. 4, p. 237.
Armenteros, R., *et al.*, 1965, Phys. Lett. **17**, 170.
Armstrong, T., *et al.*, 1993, Phys. Lett. B **307**, 394,399.
Aston, D., *et al.*, 1988a, Phys. Lett. B **201**, 573.
Aston, D., *et al.*, 1988b, Nucl. Phys. B **296**, 493.
Atiya, M. S., *et al.*, 1992, Phys. Rev. Lett. **69**, 733.
Au, K. L., D. Morgan, and M. R. Pennington, 1987, Phys. Rev. D **35**, 1633.
Augustin, J.-E., *et al.*, 1990, Phys. Rev. D **42**, 10.
Badalayan, A. M., L. P. Kok, M. I. Policarpov, and Yu. A. Simonov, 1982, Phys. Rep. **82**, 31.
Bai, Z., *et al.*, 1990, Phys. Rev. Lett. **65**, 2507.
Baillon, P., *et al.*, 1967, Nuovo Cimento A **50**, 393.
Baker, C. A., *et al.*, 1988, Nucl. Phys. A **483**, 631.
Bali, G. S., K. Schilling, A. Hulsebos, A. C. Irving, C. Michael, and P. W. Stephenson, 1993, Phys. Lett. B **309**, 378.
Baltay, C., P. Franzini, G. Lütjens, J. C. Severiens, D. Tycko, and D. Zenello, 1966, Phys. Rev. B **145**, 1103.
Baltrusaitis, R. M., *et al.*, 1987, Phys. Rev. D **35**, 2077.
Barash, N., P. Franzini, L. Kirsch, D. Miller, J. Steinberger, T. H. Tan, R. Plano, and P. Yaeger, 1965, Phys. Rev. B **139**, 1659.
Barberis, D., *et al.*, 1997a, Phys. Lett. B **413**, 217.
Barberis, D., *et al.*, 1997b, Phys. Lett. B **413**, 225.
Barnes, T., 1985, Phys. Lett. **165B**, 434.
Barnes, T., F. E. Close, and F. de Viron, 1983, Nucl. Phys. B **224**, 241.
Barnes, T., F. E. Close, P. R. Page, and E. S. Swanson, 1997, Phys. Rev. D **55**, 4157.
Barnett, R. M., *et al.* (Particle Data Group), 1996, Phys. Rev. D **54**, 1.
Bassompierre, G., G. Binder, P. Dalpiaz, P. F. Dalpiaz, G. Gissinger, S. Jacquey, C. Peroni, M. A. Schneegans, and L. Tecchio, 1976, Phys. Lett. B **64**, 475.
Batty, C. J., 1989, Rep. Prog. Phys. **52**, 1165.
Batty, C. J., 1996, Nucl. Phys. A **601**, 425.
Beladidze, G. M., *et al.*, 1992, Sov. J. Nucl. Phys. **55**, 1535.
Benayoun, M., M. Feindt, M. Girone, A. Kirk, Ph. Leruste, J.-L. Narjoux, and K. Šafařik, 1993, Z. Phys. C **58**, 31.
Berdnikov, E. B., *et al.*, 1994, Phys. Lett. B **337**, 219.
Bertin, A., *et al.*, 1995, Phys. Lett. B **361**, 187.
Bertin, A., *et al.*, 1996, Phys. Lett. B **388**, 450.
Bertin, A., *et al.*, 1997a, Phys. Lett. B **408**, 476.
Bertin, A., *et al.*, 1997b, Phys. Lett. B **400**, 226.
Binon, F., *et al.*, 1983, Nuovo Cimento A **78**, 313.
Binon, F., *et al.*, 1984, Nuovo Cimento A **80**, 363.
Bityukov, S. I., *et al.*, 1987, Phys. Lett. B **188**, 383.
Bityukov, S. I., *et al.*, 1991, Z. Phys. C **50**, 451.
Bizzarri, R., M. Foster, Ph. Gavillet, G. Labrosse, L. Montanet, R. Salmeron, P. Villemoes, C. Guesquière, and E. Lillestol, 1969, Nucl. Phys. B **14**, 169.
Bizzarri, R., L. Montanet, S. Nilsson, Ch. d'Andlau, and J. Cohen-Ganouna, 1971, Nucl. Phys. B **27**, 140.
Blatt, J. M., and V. F. Weisskopf, 1952, in *Theoretical Nuclear Physics* (Wiley, New York), p. 361.
Blüm, P., 1996, Int. J. Mod. Phys. A **11**, 3003.
Bolton, T., *et al.*, 1992, Phys. Rev. Lett. **69**, 1328.
Bramon, A., R. Escribano, and M. D. Scadron, 1997, Phys. Lett. B **403**, 339.
Bridges, D., I. Daftari, and T. E. Kalogeropoulos, 1987, Phys. Rev. Lett. **57**, 1534.
Bugg, D. V., V. V. Anisovich, A. Sarantsev, and B. S. Zou, 1994, Phys. Rev. D **50**, 4412.
Bugg, D. V., A. V. Sarantsev, and B. S. Zou, 1996, Nucl. Phys. B **471**, 59.
Bugg, D. V., I. Scott, B. S. Zou, V. V. Anisovich, A. V. Sarantsev, T. H. Burnett, and S. Sutlief, 1995, Phys. Lett. B **353**, 378.
Bugg, D. V., and B. S. Zou, 1997, Phys. Lett. B **396**, 295.
Carbonell, J., G. Ihle, and J. M. Richard, 1989, Z. Phys. A **334**, 329.
Chamberlain, O., E. Segrè, C. E. Wiegand, and T. Ypsilantis, 1955, Phys. Rev. **100**, 947.
Chew, F. G., and S. Mandelstam, 1960, Phys. Rev. **119**, 467.
Chiba, M., *et al.,* 1987, in *Physics at LEAR with Low Energy Antiprotons*, Nuclear Science Research Conference Series No. 14, edited by C. Amsler *et al.* (Harwood, Academic, Chur, Switzerland), p. 401.
Chiba, M., *et al.*, 1988, Phys. Rev. D **38**, 2021; Chiba, M., *et al.*, 1989, Phys. Rev. D **39**, 3227.
Chung, S. U., J. Brose, R. Hackmann, E. Klempt, S. Spanier, and C. Strassburger, 1995, Ann. Phys. (Leipzig) **4**, 404.
Close, F. E., G. R. Farrar, and Z. Li, 1997, Phys. Rev. D **55**, 5749.
Close, F. E., N. Isgur, and S. Kumano, 1993, Nucl. Phys. B **389**, 513.
Close, F. E., and H. J. Lipkin, 1987, Phys. Lett. B **196**, 245.
Close, F. E., and P. R. Page, 1995, Nucl. Phys. B **443**, 233.
Conforto, B., *et al.*, 1967, Nucl. Phys. B **3**, 469.
Cooper, A. M., *et al.*, 1978, Nucl. Phys. B **146**, 1.
Day, T. B., G. A. Snow, and T. Sucher, 1960, Phys. Rev. **118**, 864.
Delcourt, B., J. Layssac, and E. Pelaquier, 1984, in *Physics at LEAR with Low Energy Antiprotons*, edited by U. Gastaldi and R. Klapisch (Plenum, New York), p. 305.
Devons, S., T. Kozlowsi, P. Nemethy, S. Shapiro, M. Dris, N. Horwitz, T. Kalogeropoulos, J. Skelly, R. Smith, and H. Uto, 1973, Phys. Lett. **47B**, 271.
Devons, S., T. Kozlowsi, P. Nemethy, S. Shapiro, N. Horwitz, T. Kalogeropoulos, J. Skelly, R. Smith, and H. Uto, 1971, Phys. Rev. Lett. **27**, 1614.
Dobroliubov, M. I., 1990, Sov. J. Nucl. Phys. **52**, 352.
Dobroliubov, M. I., and A. Yu. Ignatiev, 1988, Nucl. Phys. B **309**, 655.
Dolinsky, S. I., *et al.*, 1989, Z. Phys. C **42**, 511.
Dombrowski, S. v., 1996, Ph.D. thesis (University of Zurich).
Donoghue, J. F., B. R. Holstein, and D. Wyler, 1992, Phys. Rev. Lett. **69**, 3444.
Doser, M., *et al.*, 1988, Nucl. Phys. A **486**, 493.
Dover, C. B., 1986, Phys. Rev. Lett. **57**, 1207.
Dover, C. B., and P. M. Fishbane, 1989, Phys. Rev. Lett. **62**, 2917.
Dover, C. B., T. Gutsche, and A. Faessler, 1991, Phys. Rev. C **43**, 379.
Dover, C. B., T. Gutsche, M. Maruyama, and A. Faessler, 1992, Prog. Part. Nucl. Phys. **29**, 87.
Dover, C. B., and J. M. Richard, 1980, Phys. Rev. C **21**, 1466.
Ellis, J., M. Karliner, D. E. Kharzeev, and M. G. Sapozhnikov, 1995, Phys. Lett. B **353**, 319.

Espigat, P., C. Ghesquière, E. Lillestol, and L. Montanet, 1972, Nucl. Phys. B **36**, 93.
Farrar, G. R., 1996, Phys. Rev. Lett. **76**, 4111.
Flattè, S. M., 1976, Phys. Lett. B **63**, 224.
Foster, M., Ph. Gavillet, G. Labrosse, L. Montanet, R. A. Salmeron, P. Villemoes, C. Ghesquière, and E. Lillestol, 1986a, Nucl. Phys. B **8**, 174.
Foster, M., Ph. Gavillet, G. Labrosse, L. Montanet, R. A. Salmeron, P. Villemoes, C. Ghesquière, and E. Lillestol, 1968b, Nucl. Phys. B **6**, 107.
Gaspero, M., 1993, Nucl. Phys. A **562**, 407.
Gasser, J., and H. Leutwyler, 1985, Nucl. Phys. B **250**, 539.
Genz, H., 1983, Phys. Rev. D **28**, 1094.
Genz, H., 1985, Phys. Rev. D **31**, 1136.
Genz, H., M. Martinis, and S. Tatur, 1990, Z. Phys. A **335**, 87.
Gilman, F. G., and R. Kauffman, 1987, Phys. Rev. D **36**, 2761.
Godfrey, S., and N. Isgur, 1985, Phys. Rev. D **32**, 189.
Goldhaber, A. S., G. C. Fox, and C. Quigg, 1969, Phys. Lett. B **30**, 249.
Gortchakov, O., M. P. Locher, V. E. Markushin, and S. von Rotz, 1996, Z. Phys. A **353**, 447.
Gray, L., T. Kalogeropoulos, A. Nandy, J. Roy, and S. Zenone, 1983, Phys. Rev. D **27**, 307.
Grayer, G., *et al.*, 1974, Nucl. Phys. B **75**, 189.
Green, A. M., and J. A. Niskanen, 1987, Prog. Part. Nucl. Phys. **18**, 93.
Ghesquière, C., 1974, in *Antinucleon-Nucleon Interactions*, Proceedings of the Liblice Symposium, CERN Yellow Report No. 74-18, p. 436.
Hartmann, U., E. Klempt, and J. Körner, 1988, Z. Phys. A **331**, 217.
Heinzelmann, M., 1996, Diploma thesis (University of Zurich).
Hippel, F. V., and C. Quigg, 1972, Phys. Rev. D **5**, 624.
Isgur, N., and J. Paton, 1985, Phys. Rev. D **31**, 2910.
Jacob, M., and G. C. Wick, 1959, Ann. Phys. (N.Y.) **7**, 404.
Jaenicke, J., B. Kerbikov, and H.-J. Pirner, 1991, Z. Phys. A **339**, 297.
Jaffe, R. L., 1977, Phys. Rev. D **15**, 267.
Karch, K., *et al.*, 1992, Z. Phys. C **54**, 33.
Kambor, J., C. Wiesendanger, and D. Wyler, 1996, Nucl. Phys. B **465**, 215.
Kaminski, R., L. Lesniak, and K. Rybicki, 1997, Z. Phys. C **74**, 79.
Kerbikov, B. O., L. A. Kondratyuk, and M. G. Sapozhnikov, 1989, Sov. Phys. Usp. **32**, 739.
Klempt, E., 1990, Phys. Lett. B **244**, 122.
Kolybashov, V. M., I. S. Shapiro, and Yu. N. Sokolskikh, 1989, Phys. Lett. B **222**, 135.
Lacock, P., C. Michael, P. Boyle, and P. Rowland, 1997, Phys. Lett. B **401**, 308.
Landua, R., 1996, Annu. Rev. Nucl. Part. Sci. **46**, 351.
Layter, J. G., J. A. Appel, A. Kotlewski, W. Lee, S. Stein, and J. J. Thaler, 1973, Phys. Rev. D **7**, 2565.
Lee, J. H., *et al.*, 1994, Phys. Lett. B **323**, 227.
Locher, M. P., Y. Lu, and B. S. Zou, 1994, Z. Phys. A **347**, 281.
Markushin, V. E., 1997, Nucl. Phys. B (Proc. Suppl.) **56A**, 303.
May, B., *et al.*, 1989, Phys. Lett. B **225**, 450.
May, B., *et al.*, 1990, Z. Phys. C **46**, 191, 203.
Meijer Drees, R., *et al.*, 1992, Phys. Rev. Lett. **68**, 3845.
Morgan, D., and M. R. Pennington, 1993, Phys. Rev. D **48**, 1185.
O'Connell, H. B., B. C. Pearce, A. W. Thomas, and A. G. Williams, 1995, Phys. Lett. B **354**, 14.
O'Donnell, P. J., 1981, Rev. Mod. Phys. **53**, 673.
Okubo, S., 1963, Phys. Lett. **5**, 165.
Ore, A., and J. L. Powell, 1949, Phys. Rev. **75**, 1696.
Orfanidis, S. J., and V. Rittenberg, 1973, Nucl. Phys. B **59**, 570.
Page, P. R., 1997, Phys. Lett. B **402**, 183.
Pais, A., 1960, Ann. Phys. (N.Y.) **9**, 548.
Peters, K., and E. Klempt, 1995, Phys. Lett. B **352**, 467.
Pietra, C., 1996, Diploma thesis (University of Zurich).
Prokoshkin, Yu. D., and S. A. Sadovskii, 1995, Phys. At. Nucl. **58**, 606.
Prokoshkin, Yu. D., and V. D. Samoilenko, 1995, Sov. Phys. Dokl. **342**, 273.
Regenfus, C., 1997, Nucl. Instrum. Methods Phys. Res. A **386**, 60.
Reifenröther, J., *et al.*, 1991, Phys. Lett. B **267**, 299.
Rosselet, L., *et al.*, 1977, Phys. Rev. D **15**, 574.
Scharre, D. L., *et al.*, 1980, Phys. Lett. B **97**, 329.
Schmid, B., 1991, Ph.D. thesis (University of Zurich).
Sedlák, J., and V. Šimák, 1988, Sov. J. Part. Nucl. **19**, 191.
Sexton, J., A. Vaccarino, and D. Weingarten, 1995, Phys. Rev. Lett. **75**, 4563.
Spanier, S., 1994, Ph.D. thesis (University of Mainz).
Spanier, S., 1996, Yad. Fiz. **59**, 1352.
Spanier, S., 1997, Workshop on *The Strange Structure of the Nucleon*, CERN, unpublished.
Szczepaniak, A., E. S. Swanson, C. R. Ji, and S. R. Cotanch, 1996, Phys. Rev. Lett. **76**, 2011.
Thompson, D. R., *et al.*, 1997, Phys. Rev. Lett. **79**, 1630.
Törnqvist, N. A., 1991, Phys. Rev. Lett. **67**, 556.
Törnqvist, N. A., 1995, Z. Phys. C **68**, 647.
Törnqvist, N. A., and M. Roos, 1996, Phys. Rev. Lett. **76**, 1575.
Urner, D., 1995, Ph.D. thesis (University of Zurich).
Vandermeulen, J., 1988, Z. Phys. C **37**, 563.
Weidenauer, P., *et al.*, 1990, Z. Phys. C **47**, 353.
Weidenauer, P., *et al.*, 1993, Z. Phys. C **59**, 387.
Weinstein, J., and N. Isgur, 1990, Phys. Rev. D **41**, 2236.
Wyler, D., 1998, private communication.
Zemach, Ch., 1964, Phys. Rev. B **133**, 1201.
Zemach, Ch., 1965, Phys. Rev. B **140**, 97, 109.